Super-Resolution Microscopy to analyze replication and gliding motility in *Toxoplasma gondii*

von Yuan Song

Inaugural-Dissertation zur Erlangung der Doktorwürde

(Dr. rer. biol. vet.)

der Tierärztlichen Fakultät der Ludwig-Maximilians-Universität München

Super-Resolution Microscopy to analyze replication and gliding motility in *Toxoplasma gondii*

von Yuan Song

aus Shandong (China)

München 2025

Aus dem Veterinärwissenschaftlichen Department der Tierärztlichen Fakultät der Ludwig-Maximilians-Universität München

Lehrstuhl für Experimentelle Parasitologie

Arbeit angefertigt unter der Leitung von:

Univ.-Prof. Dr. Markus Meißner

Mitbetreuung durch: Dr. Francisco Javier Periz Coloma

Gedruckt mit Genehmigung der Tierärztlichen Fakultät der Ludwig-Maximilians-Universität München

Dekan: Univ.-Prof. Dr. Reinhard K. Straubinger, Ph.D.

Berichterstatter: Univ.-Prof. Dr. Markus Meißner

Korreferent/en: Univ.-Prof. Dr. Dušan Palić

Tag der Promotion: 26. Juli 2025

For my parents and friends

Table of Contents

TABLE OF CONTENTS

TABLE OF CONTENTS

LIST OF ABBREVIATIONS

ABBREVIATIONS

AA	Acrylamide
ABPs	actin-binding proteins
ADF	Actin depolymerising factor
AID	Auxin-inducible degron
AKMT	Apical complex lysine (K) methyltransferase
AMA1	Apical membrane antigen 1
Amp	Ampicillin
APEX2	ascorbate peroxidase 2
APR	Apical polar ring
APS	Ammonium persulfate
BioID	Biotin identification
BLAST	Basic local alignment search tool
bp	Base pair
BSA	bovine serum albumin
C. elegans	*Caenorhabditis elegans*
Cas9	CRISPR associated protein 9
CbEm	Chromobody-emeraldFP
CDPKs	Calcium-dependent protein kinases
CO_2	Carbon dioxide
Cre	Causes recombination
CRISPR	Clustered regularly interspaced short palindromic repeats
CW	Continuous wave

LIST OF ABBREVIATIONS

C-terminal	Carboxyl terminal
C_2H_6	Ethane
Da	Dalton
DAB	diaminobenzidine
dd	Destabilisation domain
ddH_2O	Double destilled water
DHFR	Dihydrofolate reductase
DiCre	Dimerisable recombinase
DMEM	Dulbecco's modified eagle's medium
DMSO	Dimethyl sulfoxide
DNA	Deoxyribunucleic acid
dNTP	Deoxynucleodtide 5'-triphosphate
DTT	Dithiothreitol
DSB	Double-strand break
E. coli	*Escherichia coli*
EDTA	Ethylene diamine tetra acetic acid
ER	Endoplasmic reticulum
EM	Electron microscopy
EtOH	Ethanol
ExM	Expansion microscopy
FA	Formaldehyde
FACS	Fluorescence-activated cell sorting
F-actin	Filamentous actin
FH	Formin homology
Fig	Figure

LIST OF ABBREVIATIONS

FRMs	Formins
FRM1	Formin 1
Fw	Forward
g	Gravity
G-actin	Globular actin
G1	gap phase 1
GA	Glutaraldehyde
GAC	Glideosome-associated connector
GAPs	Gliding-associated proteins
GAP45	Gliding-associated protein 45
GFP	Green fluorescent protein
GOI	Gene of interest
gRNA	Guide RNA
h	Hour(s)
HA	Human influenza hemagglutinin
HCl	Hydrochloric acid
HFFs	Human foreskin fibroblasts
IFA	Immunofluorescence assay
IMC	Inner membrane complex
Immunogold EM	Immunogold labeling electron microscopy
kb	Kilobase
kDa	Kilo Dalton
KO	Knock out
LB	Lysogeny broth
LINC	Linker of nucleoskeleton and cytoskeleton

LIST OF ABBREVIATIONS

LoxP	Locus of crossover (x)in P1
M	Molar
MA	Methacrylic acid
mAID	Minimal auxin-inducible degron
Mb	Megabases
MDa	Mega Dalton
mg	Milligram
MIC	Micronemal protein
MLC1	Myosin light chain 1
mm	Millimeter
mM	Millimolar
MORN1	Membrane occupation and recognition nexus protein 1
M-phase	Mitosis phase
mRNA	Messenger ribonucleic acid
MyoA	Myosin A
MyoH	Myosin H
NaCl	Sodium chloride
NaOH	Sodium hydroxide
NCBI	National Center for Biotechnology Information
NEB	New England Biolabs
NHEJ	Non-homologous end joining
N-terminal	Amino terminal
obj	objective
ORF	Open reading frame

LIST OF ABBREVIATIONS

PAM	Protospacer adjacent motif
PBS	Phosphate buffered saline
PCR	Polymerase chain reaction
PFA	Paraformaldehyde
pH	Potential of hydrogen
PA	Phosphatidic acid
PAGE	Polyacrylamide gel electrophoresis
PCRs	Preconoidal rings
PM	Plasma membrane
POI	Protein of interest
PSF	point-spread function
PV	Parasitophorous vacuole
PVM	Parasitophorous vacuole membrane
Rapa	Rapamycin
RB	Residual body
Rh	Rhoptry
ROI	Regions of interest
RONs	Rhoptry neck proteins
RoPs	Rhoptry bulb proteins
rpm	Revolutions per minute
RT	Room temperature
Rv	Reverse
s	Second(s)
S. pombe	*Schizosaccharomyces pombe*
SAGs	Surface antigens

LIST OF ABBREVIATIONS

sCas9	Split Cas9
SD	Standard deviation
SDS-PAGE	Sodium dodecyl sulphate polyacrylamide gel elecrophoresis
SEM	Scanning electron microscopy
SIM	Structured-illumination microscopy
SMLM	Single-molecule localization microscopy
S-phase	Synthesis phase
spp.	Species pluralis
STED	Stimulated emission depletion microscopy
SUN	Sad1/ UNC-84
T. gondii or Tg	*Toxoplasma gondii*
TAE	Tris-acetate-EDTA
TBS	Tris-buffered saline
TEM	Transmission electron microscopy
TEMED	Tetramethylethylendiamin
TgSLP1	*Toxoplasma gondii* SUN-like protein 1
TgSLP2	*Toxoplasma gondii* SUN-like protein 2
TRIS	Tris(hydroxymethyl)aminomethane
TX-100	Triton X-100
V	Volts
w/v	Weight / volume
WHO	World Health Organization
WT	Wildtype
YFP	Yellow fluorescent protein

LIST OF FIGURES

LIST OF FIGURES

LIST OF TABLES

1 Introduction

1.1 Apicomplexa

The existence of human parasites has been documented as early as 3000 B.C. (Cox 2002). Throughout evolutionary history, prolonged coevolution between parasitic organisms and their hosts has led to significant adaptive specialization in parasites (Vilcinskas 2016). Parasites are defined as organisms that obtain essential nutrients and energy from their host organisms to maintain their metabolic functions and survival. Throughout this parasitic relationship, they may excrete toxic metabolites or induce structural damage to host tissues through mechanical or biochemical mechanisms (Poulin 2007).

As the sole major taxonomic group comprising exclusively parasitic organisms, Apicomplexa represents a eukaryotic phylum encompassing over 6,000 described species. This unique characteristic renders it a particularly intriguing yet poorly understood group from a biodiversity perspective (Morrison 2009; Adl et al. 2007). A defining characteristic of apicomplexans is the absence of photosynthetic capability; they have apicoplast, a non-photosynthetic secondary plastid (Sato 2011). The majority of characterized apicomplexan species are obligate intracellular parasites. These organisms have evolved specialized apical complex structures and secretory organelles for gliding motility and invasion (Morrison 2009).

The Apicomplexa phylum includes many species that present considerable dangers to both the poultry and livestock industries, including *Eimeria* spp., *Babesia* spp., *Plasmodium* spp., *Cryptosporidium* spp., and *Toxoplasma gondii*. These pathogens not only cause substantial economic losses but also play critical roles in both medical and veterinary fields (Black and Boothroyd 2000; Stelzer et al. 2019). For instance, coccidiosis, caused by *Eimeria* spp., is a

disease with significant economic impact globally, leading to reduced productivity and high mortality rates in domestic poultry and livestock (Chapman et al. 2013). Similarly, *Babesia* spp., responsible for babesiosis, affect many hosts, including domestic and wild mammals, as well as humans. This disease has emerged as a zoonotic threat, as evidenced by human babesiosis cases (Michel, Mathis, and Ryser-Degiorgis 2014). Transmission primarily occurs through the bite of ixodid ticks, often resulting in clinical manifestations such as anemia, hyperbilirubinuria, hemoglobinuria, and, in severe cases, organ failure (Hildebrandt, Gray, and Hunfeld 2013).

In addition to these, *Plasmodium* spp., the etiological agents of malaria, represent one of the most severe global health challenges. Malaria is transmitted through the bites of infected female *Anopheles* mosquitoes (Alkema et al. 2021). According to recent data, the World Health Organization (WHO) reported that more than 260 million individuals across 83 malaria-endemic countries were infected in 2023, while the number of 2022 was 11 million less (WHO, 2024).

Furthermore, *Cryptosporidium* spp. are recognized as a leading cause of diarrheal disease worldwide, particularly affecting kids and immunocompromised individuals, particularly in developing countries (O'Leary, Sleator, and Lucey 2021). Notably, zoonotic transmission of *Cryptosporidium* often occurs through contaminated water supplies, making waterborne epidemics and large-scale outbreaks a significant public health concern (Hassan et al. 2021). Overall, these apicomplexan pathogens highlight the critical need for continued research and intervention strategies to mitigate their impact on both animal and human health.

1.2 *Toxoplasma gondii*

1.2.1 Research History

T. gondii is the sole species within the genus *Toxoplasma*. A summary of key milestones in *T. gondii* research is provided in Table I-1.

Table I-1. Concise historical timeline of *Toxoplasma gondii* research.

Year	Milestone	Reference
1908	*Toxoplasma gondii* first identified in *C. gundi* and a rabbit; named for its crescent shape and host.	(Nicolle 1908; Splendore 1908)
1939	Recognized as a human pathogen after isolation from a fatal congenital toxoplasmosis case; confirmed zoonotic potential through experimental transmission.	(Wolf, Cowen, and Paige 1939)
1948	Development of the methylene blue dye test, a serological assay for detecting *T. gondii* in humans and animals, facilitating global epidemiological studies.	(Sabin and Feldman 1948)
1954–1965	Identification of key transmission routes, including ingestion of infected pork, vertical transmission, and fecal-oral transmission.	(Weinman and Chandler 1954; Hutchison 1965)

1960–1970	Discovery of the oocyst as the environmentally resistant and infective stage in feline feces, elucidating aspects of the life cycle.	(Jacobs, Remington, and Melton 1960; Sheffield and Melton 1970).
1988–1995	Advances in genetic manipulation, including gene knockout and complementation, enhancing functional studies of *T. gondii*.	(Burg et al. 1988; Soldati et al. 1995; Donald and Roos 1994; Ferguson 2009)
2002	Application of proteomic approaches, including 2D electrophoresis, mass spectrometry, and bioinformatics, to analyze *Toxoplasma gondii* expressed sequence tags (ESTs).	(Cohen et al. 2002)

Collectively, these significant research advancements and established methodologies have provided a robust foundation for contemporary investigations, along with a diverse array of sophisticated tools that facilitate further exploration of *Toxoplasma gondii* biology and pathogenesis.

1.2.2 Pathogenesis and health risk

T. gondii is a pathogen that could infect almost all eukaryotic organisms and disseminating across tissues in warm-blooded hosts. As a globally successful protozoan parasites, epidemiological estimates indicate that nearly one-third of the global human population harbors *Toxoplasma gondii* infection (Montoya

2002). The global average, however, may not provide a faithful account of endemicity in particularly highly endemic regions. In Benin, for example, overall infection rates have been reported to reach 87.7% in certain communities (Rodier et al. 1995), and in Brazil, to reach 74.7% (Porto et al. 2008). In Germany and Iran, the infection rates reached levels of up to 59% (Molan et al. 2019; Fiedler et al. 1999; Youssefi et al. 2007).

In immunocompetent individuals, infections with *Toxoplasma gondii* are largely subclinical or asymptomatic. Clinical diseases are mainly manifested in three types of patient: the immunosuppressed host such as an AIDS patient, the fetus affected by congenital transmission of the parasite and presenting at birth or during its life with symptoms of the disease, and immunocompetent adult showing severe ocular disease due to *T. gondii* infection. For instance, Congenital Toxoplasmosis is acquired when the parasite crosses the placental barrier during a maternal infection, potentially resulting in spontaneous abortion or a spectrum of neonatal diseases. These conditions often involve severe neurological and ocular pathologies, including hydrocephalus and retinochoroiditis, among others. Such outcomes highlight the significant health risks associated with *Toxoplasma* infection, particularly in vulnerable populations (Caldas and De Souza 2018; Pinto-Ferreira et al. 2019; Holland 1999).

Geographically distinct subpopulations of *Toxoplasma gondii* parasites exhibit population genetic structures within different geographical regions (Sibley et al. 2009). In Europe most strains belong to one of three clonal lineages, denoted as Type I–III. Sexual recombination among these three predominant clonal lineages is exceptionally rare in natural populations (Howe and Sibley 1995). All 3 lineages have been isolated from human infections, prompting investigations into potential correlations between strain genotypes and disease

manifestations. Some studies suggested that type II strains were predominantly associated with toxoplasmosis, particularly in cases of AIDS-related and congenital infections, which often presented with severe complications such as encephalitis and pneumonitis (Howe et al. 1997; Honore et al. 2000; Howe and Sibley 1995; Dardé 2004). Nevertheless, virulent strains, particularly those of type I or atypical alleles, were associated with severe disease (Xiao and Yolken 2015; Grigg et al. 2001; Boothroyd and Grigg 2002) and congenital infection (Fuentes et al. 2001). These findings suggest that no definitive correlation exists between specific strain types and the occurrence of cerebral infections, highlighting the complexity of strain-specific pathogenicity in *Toxoplasma gondii*.

Beyond that, *Toxoplasma gondii* is also a significant meat safety hazard, especially in products such as mutton, with potential for zoonotic transmission to humans (Abu Samraa et al. 2007).

As a zoonotic parasite of considerable medical and veterinary significance, *T. gondii* has been the focus of extensive research for more than 100 years. However, no safe and effective antiparasitic drug or human toxoplasmosis vaccine is available yet (Konstantinovic et al. 2019; Kur, Holec-Gąsior, and Hiszczyńska-Sawicka 2009). Thus, additional research and development is critical to meet this ongoing public health challenge.

1.2.3 Life cycle

Unlike many other parasites, *Toxoplasma gondii* has a complex life cycle that includes both sexual and asexual stages of reproduction in different hosts. Sexual stage replication in *Toxoplasma gondii* occurs only in cats, the definitive host species. Asexual stage replication occurs in intermediate hosts that comprise almost all warm-blooded animals, including humans (Figure I-1). *T.*

gondii has 3 infectious phases: tachyzoites disseminate rapidly and proliferate within nucleated cells of intermediate hosts; bradyzoites replicate slowly within tissue cysts of intermediate hosts; and sporozoites are found in the oocysts shed by the definitive host (Deng et al. 2021). Even when no definitive host are present, *Toxoplasma gondii* can continue to cycle between intermediate hosts with the dissemination of bradyzoites. This adaptive ability contributes to the global dissemination and prevalence of this parasite (Attias et al. 2020; Hazards et al. 2018).

Foodborne transmission accounts for most instances of toxoplasmosis infection. As intermediate hosts, humans can acquire the infection through the consumption of animal products (e.g., milk, pork, mutton, beef, and poultry) derived from other intermediate hosts (Jones and Dubey 2010). Additionally, exposure to sporulated oocysts from feline feces in the environment or through contaminated water and produce represents another significant transmission route. These pathways underscore the multifaceted nature of *Toxoplasma* transmission and its implications for public health (Dubey 2016; Opsteegh et al. 2015).

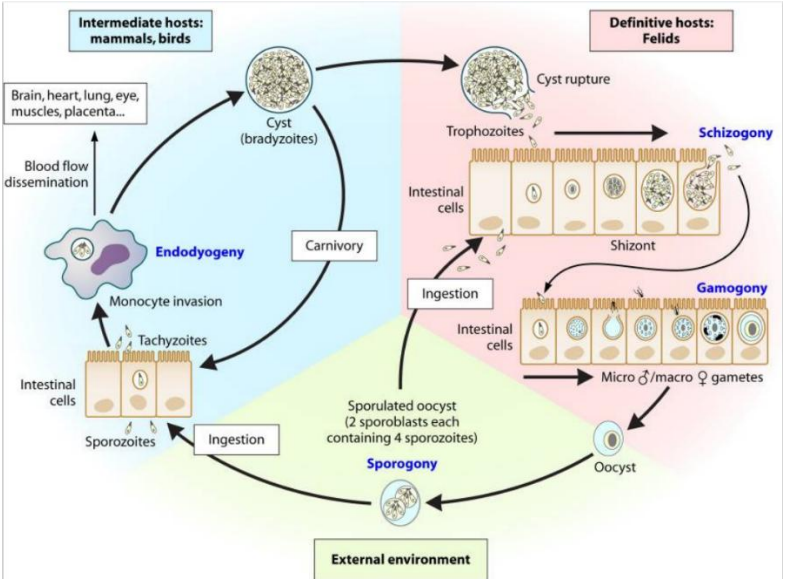

Figure I-1. The life cycle of *Toxoplasma gondii*.

This process involves multiple distinct stages. Felids, functioning as definitive hosts, contract *T. gondii* through consumption of infected intermediate carriers (rodents, avian species) or from environmental contamination. After consumption, the cyst wall is digested within the stomach and gastrointestinal tract. This process results in the release of either tachyzoites or bradyzoites. These invasive forms subsequently invade the intestinal epithelial cells. Then parasites undergo multiple schizogonic cycles, producing merozoites. These merozoites subsequently develop into microgamonts and macrogametes, which fusion to form oocysts. These oocysts are then released with feline feces.

Following environmental release, excreted oocysts initiate sporogenic development, acquiring infectivity through this process. Sporulated oocysts could directly infect intermediate hosts, including most warm-blooded animals and humans, through contamination of water, soil, grass, or vegetables. Additionally, humans may be infected by consuming raw meat or unpasteurized milk containing tissue cysts with bradyzoites or tachyzoites from infected food animals. In cases of maternal infection during pregnancy, tachyzoites can cross the placental barrier, leading to congenital transmission and potentially severe fetal complications. (Attias et al. 2020; Robert-Gangneux and Dardé 2012). Image copied from Robert-Gangneux and Dardé with license number 1600241-1.

1.2.3.1 Asexual replication

In intermediate hosts, *T. gondii* exhibits two distinct developmental phases: tachyzoite and bradyzoite forms. The former phase functions as a rapidly proliferating form, during which the parasite disseminates throughout the host's tissues, leading to acute infection. In contrast, the bradyzoite phase corresponds to chronic infection, characterized by cystogenesis. These parasitic cysts exhibit preferential tropism, predominantly colonizing neural tissues and striated musculature. The cysts could be ingested by other hosts, leading to the release of bradyzoites, which subsequently revert to tachyzoites. Alternatively, within the same host, cysts can convert back to tachyzoites under immunosuppressive conditions (Figure I-1) (Dubey, Lindsay, and Speer 1998; Skotarczak 2016; Pinto-Ferreira et al. 2019). The asexual or lytic cycle primarily drives for the clinical symptom severity (Tenter, Heckeroth, and Weiss 2000; Black and Boothroyd 2000).

1.2.3.2 Sexual reproduction

The life cycle of *T. gondii* also includes a sexual reproductive phase, which strictly confined to definitive host, typically felids (cats). When a feline definitive host ingests tissue cysts from intermediate hosts, such as mice or birds, the cysts reach the stomach and intestines, where the cyst wall is degraded by the acidic environment and digestive enzymes, releasing bradyzoites or sporozoites. These invasive forms then invade the intestinal epithelium, initiating several rounds of schizogony to produce merozoites. These merozoites differentiate into two distinct forms: female macrogametes display an oval-shaped configuration (8 × 6 µm), and elongated male microgamonts (6 × 2 µm). Following fertilization, unsporulated oocysts are generated and prior to

environmental release through fecal discharge (Figure I-1) (Attias et al. 2020; Dubey, Lindsay, and Speer 1998; Frenkel, Dubey, and Miller 1970).

Each oocyst eventually generates 2 sporocyst structures, each with 4 sporozoites. The excretion process could persist for one to two weeks, during which the freshly released oocysts in feces become infectious within 48 hours. Due to the protection provided by their thick, impermeable walls, oocysts can survive in harsh environmental conditions, such as in water or dry environments, for several months. Under more favorable conditions, their survival can extend to several years, highlighting their resilience and contributing to the parasite's widespread transmission (Hill and Dubey 2002; Freppel et al. 2019).

1.2.3.3 Lytic cycle of *Toxoplasma gondii*

These obligate intracellular parasites employ a conserved mechanism for migration and invasion, known as the lytic cycle. This cycle initiates through host cell invasion, followed by iterative proliferation phases in a unique compartment known as the parasitophorous vacuole (PV). Subsequently, the host cell is lysed, releasing tachyzoites to migrate and invade nearby cells, starting new cycles of replication (Fig. I-2). In *Toxoplasma gondii*, the intracellular replication cycle has a replication time ranging from 6 - 8 hours under in vitro conditions, resulting in the production of 64 to 256 progeny parasites. These progeny are then primed for egress and subsequent infection of new host cells (Radke and White 1998).

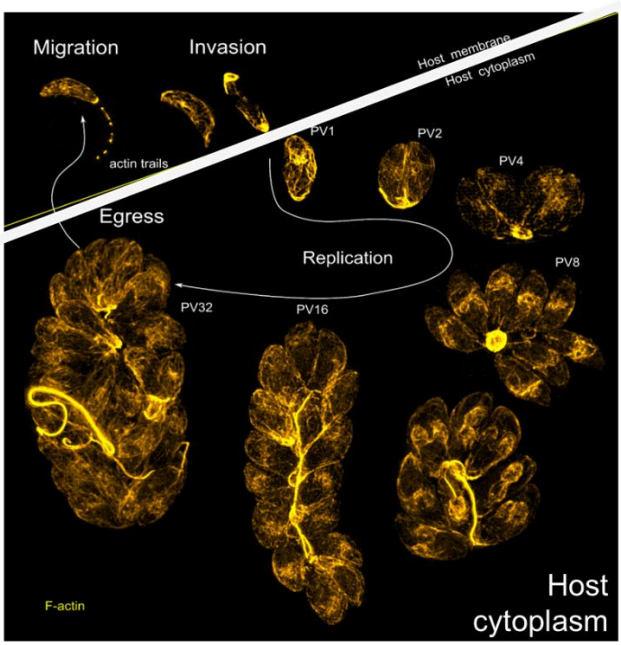

Figure I-2. Image of lytic cycle of *Toxoplasma gondii*.

Extracellular parasites initiate host cell invasion by forming a PV. Within this protective structure, proliferation occurs via endodyogeny. After egress, the parasites initiate another round of the lytic cycle. Actin-chromobodies were utilized to label parasites, revealing a dynamic filamentous actin (F-actin) network during the lytic cycle. The model, developed by Dr. Javier Periz and adapted from referenced studies, demonstrates the presence of independent F-actin structures within the PV, as detected through the expression of actin-chromobodies (Periz et al. 2019). Image copied from Dr. Javier Periz.

1.2.4 Ultrastructure of tachyzoite

During the lytic process, *T. gondii* exists as tachyzoites, characterized by dimensions of about 6 × 2 µm. The ultrastructural features of tachyzoites were first elucidated through electron microscopy (EM) over seven decades ago (Gustafson, Agar, and Cramer 1954). Morphologically, tachyzoites exhibit a

crescent-shaped or banana-like appearance, with a distinctly cuspate apical part contrasting with a blunt posterior region. This unique morphology is integral to their invasive capabilities and intracellular lifestyle (Dubey, Lindsay, and Speer 1998).

As illustrated in Figure I-3 (Sanchez and Besteiro 2021), the tachyzoite is enclosed by a trilaminar membrane structure, formed by the plasma membrane (PM) and a double-membraned compartment termed the inner membrane complex (IMC). The interspace of PM-IMC houses the motor complex, the motility apparatus of *Toxoplasma gondii* (Mann and Beckers 2001)(see Section 1.2.5). Tachyzoite cytoskeletal architecture includes 22 subpellicular microtubules (Mtbs) emanating from the conoid. These Mtbs elongate to approximately 2/3 of the tachyzoite's longitudinal axis. The cytoplasm, supported by a network of microtubules, provides structural flexibility and facilitates cell deformability in the tachyzoite. Positioned between IMC and the Mtbs is an alveolin network, formed by intermediate filament-like proteins. This network envelops the whole parasite except for the apical and posterior poles (Pacheco et al. 2020).

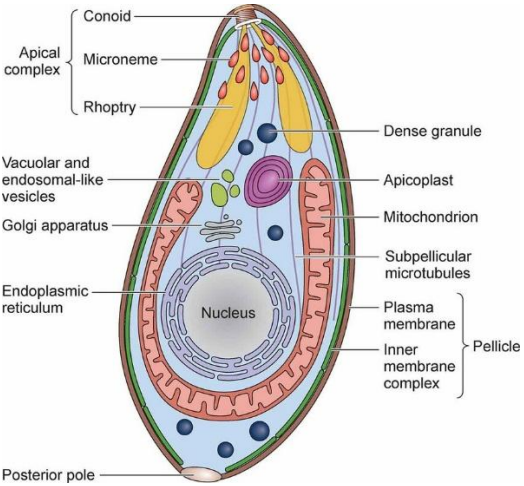

Figure I-3. Schematic ultrastructure of tachyzoite.

The schematic illustrates the ultrastructure of a tachyzoite, highlighting key organelles and structural components. The pellicle consists of the outermost PM (depicted in brown) and the underlying IMC (shown in green). At the apical region, the conoid (represented as a brown ring), along with the micronemes (in orange) and rhoptries (in yellow), forms the apical complex, a structure that is essential for parasite's invading. 22 Mtbs (grey lines) spanning from the conoid, spanning approximately two-thirds of the tachyzoite's length. Dense granules (in dark blue) and the mitochondrion (in pink) are distributed throughout the parasite's cytoplasm. In the mid-region of the tachyzoite, organelles such as vacuolar and endosomal-like vesicles (in green) are present. The apicoplast (in purple) and Golgi complex (in grey) are positioned anterior to the nucleus. The endoplasmic reticulum (ER) forms a reticular framework encircling the nucleus. (Sanchez and Besteiro 2021)

The phylum Apicomplexa is named after its defining feature, the apical complex. This specialized structure comprises the conoid complex, micronemes, and rhoptries, with hundreds of proteins precisely localized, as evidenced by proteomic and organellar protein localization studies. Functioning as a critical structural and signaling hub in *T. gondii*, the apical complex orchestrates essential processes such as gliding, invading and egress. This is mediated through the coordinated protrusion-retraction cycles of the conoid and the

regulated expression of micronemal and rhoptry proteins (discussed in detail in Sections 1.2.5 and 1.2.7). Furthermore, the apical complex undergoes initial assembly prior to other cellular structures in developing daughter cells, serving as an organizational center for the assembly of the cytoskeletal and membrane framework during parasite replication (elaborated in Section 1.2.6)(Hu et al. 2006; Long et al. 2017; Barylyuk et al. 2020; Sibley 2010).

The anterior terminus of the conoid complex houses the preconoidal rings (PCRs), characterized by an external periphery of approximately 220 nm and an internal diameter of around 160 nm. Due to their proximity and diminutive size, these 2 preconoidal rings can only be resolved using advanced super-resolution microscopy (SRM), like expansion microscopy (ExM) and electron microscopy (EM) (Figure I-4)(Munera Lopez et al. 2022). Positioned beneath the preconoidal rings (PCRs) is the conoid, a frustoconical structure comprising 14 distinct tubulin polymer fibers. These fibers are assemblage in a spiral configuration and exhibit active motility during parasite's invasion (Nagayasu et al. 2016; Munera Lopez et al. 2022). Adjacent to the conoid lies the apical polar ring (APR); within the conoid, 2 intra-conoid Mtbs is housed (Munera Lopez et al. 2022).

As a dynamic organelle, the conoid extends outward from the APR according to elevated intracellular Ca^{2+} levels. Figure I-4 depicts a tachyzoite in this protruded state. Several proteins localized at the conoid, including the glideosome-associated connector (GAC), formin 1 (FRM1), and Myosin H (MyoH), play important roles in regulating gliding, migration, and egress in *Toxoplasma gondii* (elaborated in Section1.3.2) (Koreny et al. 2021; Graindorge et al. 2016; Jacot et al. 2016; Dos Santos Pacheco et al. 2022).

The specialized organelles localized at the apical complex are named micronemes and rhoptries. They are necessary for the parasite's survival of, playing critical roles in invasion, replication, and egress, as detailed in subsequent sections. Micronemes are small, rod-shaped organelles, measuring approximately 40 by 100 nm, and are predominantly situated at the apical part of the parasite. Each tachyzoite possesses 50 to 100 micronemes, which are indispensable for successful progression through the parasite's developmental cycle. (Carruthers, Giddings, and Sibley 1999; Venugopal and Marion 2018).

In contrast to micronemes, rhoptries are larger, club-shaped organelles, measuring 2 to 3 µm in length. Each *Toxoplasma gondii* tachyzoite possesses eight to twelve rhoptries. Each rhoptry comprises two distinct regions: the rhoptry neck, which is located closest to the conoid; and the rhoptry bulb, which constitutes the posterior portion of the organelle. Rhoptries secrete proteins RONs (rhoptry neck proteins) and ROPs (rhoptry bulb proteins) are required for parasite's invading and modulation of host cellular functions (Boothroyd and Dubremetz 2008; Suarez et al. 2019).

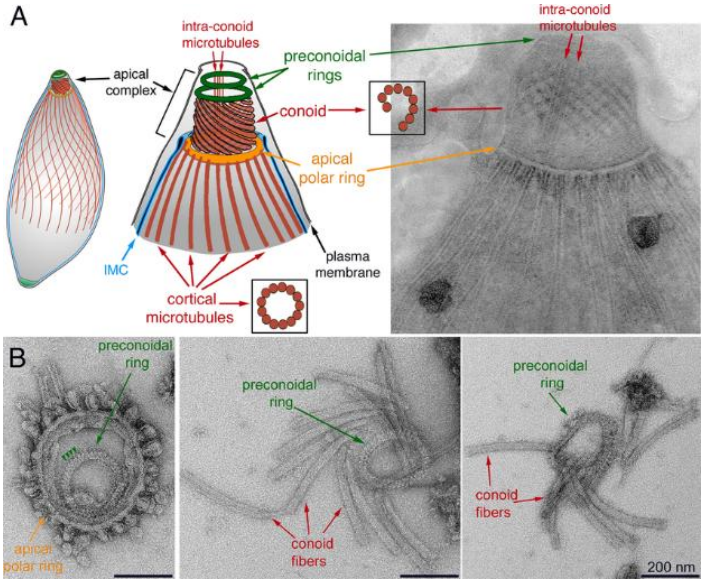

Figure I-4. Structure of the apical complex of tachyzoites.

The apical complex of *Toxoplasma gondii* is illustrated through schematic representations and transmission electron microscopy (TEM) images. **(A)** The schematic (left) and corresponding TEM image (right) depict the apical complex, which includes two preconoidal rings, 14 conoid fibers, an apical polar ring, and two intra-conoid Mtbs. **(B)** TEM data of the apical cytoskeleton, following treatment with detergents and proteases, reveal the structure after the removal of specific cellular components. An end-on view of the apical cytoskeleton shows the PCRs situated within the apical polar ring, with most Mtbs and conoid fibers separated (left). The middle and right panels display the preconoidal rings still linked to the disassembled conoid fibers. These images highlight the intricate organization and structural resilience of the apical complex. (Munera Lopez et al. 2022). © 2022 Munera Lopez et al. CC BY 4.0 license.

1.2.5 Gliding and invasion

The ability to glide is an important biological function for parasites, especially for obligate intracellular protozoan parasites that depend on host cells for their survival. Many intracellular parasites rely on host-mediated machinery to

invade, such as *Leishmania*, which utilizes phagocytosis, and *Trypanosoma cruzi*, which induces host cell uptake (Sibley 2004). Unlike eukaryotic cells, bacteria, viruses, or other parasites that depend on substantial changes in the shape (amoeboid movement) or force-producing structures like cilia or flagella, apicomplexans utilize a specific way of adhesion-based motility termed 'gliding'. This active process enables them to penetrate host cells without relying on host machinery, distinguishing their invasion strategy from other pathogens (Tardieux and Baum 2016).

Gliding motility in apicomplexan parasites is closely associated with its highly organized outer pellicle structures: IMC, PM, microtubules and filament-based cytoskeleton between PM-IMC (Morrissette and Sibley 2002; Pražák et al. 2024). This structurally stable yet non-dynamic knot enables the parasite to maintain its shape while retaining flexibility (Hanssen et al. 2013; Cyrklaff et al. 2007; Kan et al. 2014). Beneath the plasma membrane, *Toxoplasma gondii* possesses a specialized motility apparatus known as the glideosome, which incorporates the microtubules, actin, actomyosin and other components (This will be discussed in detail in Section 1.2.5.1). The glideosome, driven by actin polymerization, facilitates substrate-dependent gliding motility, enabling the parasite to traverse host tissue barriers, execute active cellular invasion, and lyse and released from old host cells (Tardieux and Baum 2016; Soldati, Foth, and Cowman 2004).

APR is a stable, multilayered structure, while the conoid exhibits dynamic extension and retraction through the APR. The mechanical forces associated with conoid extrusion facilitate the directional flux of filamentous actin enter the PM-IMC space and along the apico-basal axis, thereby regulating parasite motility and invading (Ren et al. 2024). In *Cryptosporidium parvum* and *T. gondii*, F-actin is localized at the PCRs. The extrusion of the conoid facilitates

the flow of F-actin into the pellicular space (Martinez et al. 2023; Pražák et al. 2024)

The integration of the apical complex and the glideosome underpins the remarkable efficiency of apicomplexan invasion. For example, *Plasmodium* sporozoites demonstrate locomotory velocities exceeding those of human cells by 10-fold (Münter et al. 2009). Invasive stages like *Plasmodium* and *Babesia* merozoites just need a few seconds to achieve cellular invasion. Similarly, *Toxoplasma gondii* is capable of targeting and invading host cells in less than 30 seconds through a conserved mechanism. Despite these insights, the precise spatial and structural organization of the myosin motor system that drives efficient parasite motility remains incompletely understood (Frénal et al. 2017; Leung et al. 2014; Martinez et al. 2023).

Toxoplasma gondii tachyzoites display three types of motility trails on 2D coated glass surfaces, presumably reflecting three types of gliding motility: clockwise twirling, counterclockwise circular gliding, and helical gliding, the latter characterized by a 180° rotation along its vertical axis during movement (Håkansson et al. 1999). In 2D helical moving (Tosetti et al. 2019; Pavlou et al. 2020), *T. gondii* initiates substrate adherence through apical pole anchorage. The adhesion site subsequently expands along the parasite's length, during progressive motility, parasite's apical part detaches from the substrate, causing the adhesion zone to contract until an ultimate posterior focalization. Upon reaching the posterior end, a new apical adhesion site forms, initiating a new cycle. Unlike *Plasmodium* sporozoites, the adhesion site of tachyzoites remains fixed relative to the substrate (Stadler et al. 2022). 2D traction force analysis demonstrated vectorially aligned tractive forces along the tachyzoite's anteroposterior axis, with negligible lateral force components. When coupled with microtubular forces, they could contribute to the unidirectional parasite

motility (Pavlou et al. 2020). The helical motility pattern likely originates through two biomechanical mechanisms: dynamic reorganization of microtubule cytoskeletal architecture altering three-dimensional force vectors, or generation of torque forces within the parasite's cytosolic matrix (Tardieux and Baum 2016).

In contrast, when observed within a three-dimensional (3D) gel matrix, *Toxoplasma gondii* tachyzoites display irregular, corkscrew-like trajectories (Tardieux and Baum 2016). Within this 3D environment, the adhesion site adopts a circular configuration, and the resulting motility pattern is likely more physiologically relevant, reflecting the parasite's movement within host tissues (Leung et al. 2014). 3D traction force analysis demonstrates that *T. gondii* generates biomechanical forces exhibiting rhythmic patterns. These centripetal force vectors converge at a defined pericellular locus within the extracellular matrix. These constrictions are not a consequence of the parasite mechanically pushing through gaps. They are caused by parasite-generated pulling forces on the substrate, which induce visible constrictions in the parasite's PM (Stadler et al. 2022). The ring of inward-directed force likely corresponds to a circumferential attachment zone between the parasite and the matrix, through which the parasite propels itself forward. This motility is powered by the parasite's myosin motors, which translocate F-actin in an opposite direction (Martinez et al. 2023).

For host cell adhesion, surface antigens (SAGs) play an important role in guiding the initial orientation and attachment of *Toxoplasma gondii* to the host cell membrane (Carruthers and Boothroyd 2007). The invasion process is further guided by the precisely timed expression of proteins from apical complex organelles, including micronemes, rhoptries, and dense granules. Microneme expression starts before the completion of previous lytic cycle and continues

until the next host cell attachment (Bisio and Soldati-Favre 2019; Dubois and Soldati‐Favre 2019). Upon release, microneme proteins such as AMA1 and MIC2 interact with the glideosome, which is localized beneath the plasma membrane. These proteins subsequently integrate into the tachyzoite plasma membrane, where they recognize and combined with specific receptors on the host cell membrane (Kato 2018). Microneme exocytosis is thought to regulate the secretion of rhoptry proteins, triggering the release of RONs and ROPs. This secretion process begins prior to invasion and concludes concurrently with the generation of the PV (Dubremetz 2007).

For instance, the micronemal protein MIC2 functions as a transmembrane adhesin, featuring multiple conserved extracellular domains that facilitate receptor binding, as well as a short cytosolic domain that interacts with the actinomyosin-based glideosome via aldolase (Huynh and Carruthers 2006; Jewett and Sibley 2003). The transmembrane adhesin complexes mediate critical interfacial stabilization during gliding motility. This mechanotransduction system counterbalances actomyosin-driven retrograde flow by establishing transient substrate anchors. Molecular coupling to the glideosome motor complex amplifies traction force, powering unidirectional zoite propulsion. Parasites deficient in MIC2 exhibit impaired generation of inward-directed forces and fail to form plasma membrane (PM) constrictions, resulting in defective surface attachment and an inability to complete host cell egress. This underscores the critical role of MIC2 in coordinating mechanical forces crucial for parasite gliding and invading (Gras et al. 2017; Stadler et al. 2022).

Apical membrane antigen 1 (AMA1) is a microneme-secreted protein that becomes widely distributed on parasite's surface before invading (Alexander et al. 2005; Besteiro et al. 2009). AMA1 directly interacts with RON2, forming a high-affinity complex in vitro. Rons such as RON2, RON4, RON5, and RON8 are

expressed and released to the host cell cytoplasm, where RON2 subsequently integrates into the host cell membrane. This integration facilitates the assembly of a RON complex, which interacts with other RON proteins and host cell actin filaments, playing a crucial role in parasite invasion (Besteiro et al. 2009; Lamarque et al. 2011; Tyler and Boothroyd 2011; Tonkin et al. 2011).

Apicomplexan pathogens orchestrate host cell invasion via microneme- and rhoptry-derived proteins, which assemble into a circumferential molecular adhesion complex at the parasite-host interface. This structure, known as the tight junction (TJ), remains stationary due to anchoring to the host cytoskeleton, providing a stable surface enabling parasite generates force for invasion (Tardieux and Baum 2016; Stadler et al. 2022). RON4, along with AMA1, is considered a key component of the MJ. Upon released to the host cell, RON4 associates with RON2, which binds to the host PM and functions as a ligand for AMA1 binding (Baum and Cowman 2011; Bargieri et al. 2013). Successful host cell invasion requires the parasite to engage its actomyosin motor with the MJ complex, ensuring efficient force application through proper anchorage to the host membrane and cytoskeleton.

During invading process, the TJ, in coordination with the parasite's glideosome, translocates from the apical to the basal end as the tachyzoite actively penetrates the host cell (Lebrun et al. 2005; Cova, Lamarque, and Lebrun 2022; Frénal et al. 2017; Sweeney et al. 2010). Micronemal proteins function as adhesins, generating the traction force necessary for invasion. However, following successful entry, adhesion protein are digested by rhomboid proteases (ROMs) within their transmembrane domains, facilitating detachment from host receptors and enabling complete internalization (Bargieri et al. 2014; Tardieux and Baum 2016). An excess of surface adhesins disrupts this process, resulting in unproductive host cell attachment, impaired migration

ability, defective tight junction assembly, and inefficient invading process. Notably, ROM-deficient parasites maintain cellular viability, with preserved MIC2 clearance from the membrane of invaded mutant organisms. This observation implies the existence of alternative pathways mediating adhesin shedding (Shen, Buguliskis, et al. 2014; Rugarabamu et al. 2015).

If *Toxoplasma gondii* tachyzoites encounter resistance during invasion or the TJ is not firmly fixed to the surface of host cell, the parasite continues to exert force on the junction. This lead to the retrograde displacement of the junction along the tachyzoite's surface, accompanied by the host cell membrane, ultimately facilitating the generation of a functional PV and enabling the tachyzoite to envelop itself within it (Bichet et al. 2014).

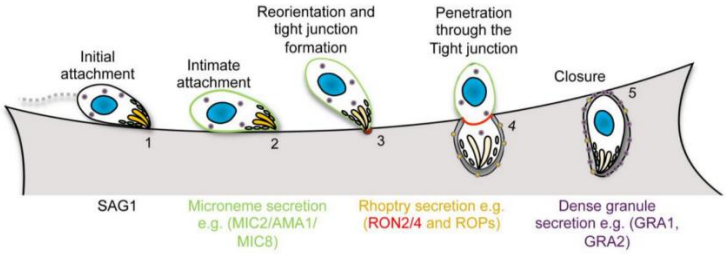

Figure I-5. Schematic overview process of *Toxoplasma gondii* invasion process.

(1) Initial Attachment: *Toxoplasma gondii* identifies and adheres to the host cell surface through the continuous expression of surface antigens (SAGs). **(2)** Microneme Secretion and Protrusion: Micronemal proteins, including MIC2, AMA1, and MIC8 (green), are expressed and localized to the parasite surface. These adhesins play a critical role in facilitating tight attachment via interaction with receptors on host cell. Concurrently, the parasite undergoes apical protrusion. **(3)** Reorientation and Moving Junction Formation: Prior to host cell penetration, the protozoan undergoes apical reorientation. RONs (shown in red and yellow) are discharged to the cytosolic part of host cell. These proteins undergo

trafficking to reaccumulate at the host-parasite interface. Here, RONs react with AMA1, forming the TJ (highlighted in red), a critical structure for host cell entry. **(4)** Rhoptry Bulb Protein Secretion and PV Formation: ROPs (yellow) are released and integrated with developing parasitophorous vacuole (PV), which serves as the intracellular niche for the parasite. **(5)** Dense Granule Secretion and PV Modulation: Simultaneously, dense granule proteins (shown in purple) are secreted, contributing to the modification and regulation of the PV environment to support intracellular survival and replication (Whitelaw 2017). Image copied from Dr. Whitelaw Jamie Adam.

Additionally, evidence suggests that endocytosis is a critical process for gliding motility, contributing to the establishment of retrograde membrane flow. This process aligns with the proposed 'fountain-flow model' in apicomplexan parasites, which functions alongside the glideosome-driven motility mechanism. As the name suggests, this model describes a dynamic membrane flow resembling a fountain, characterized by high membrane turnover rates that actively support cell migration (Tanaka et al. 2017). The apicomplexan fountain-flow model relies on microneme secretion to initiate retrograde membrane flow, after which excess membrane components and proteins are recycled and redistributed to various organelles to complete the cycle (Gras et al. 2019).

1.2.5.1 Gliding motor complex

The tachyzoites could be easily cultured and continuously propagated in mammalian cell culture. Over decades of research, *Toxoplasma gondii* has also developed a well-established and comprehensive genetic toolkit, solidifying its status as the leading model organism for studying gliding motility in apicomplexan functional biology (Lourido 2019; Ferguson 2009). In addition to actin and actomyosin, the glideosome, or gliding motor complex, comprises

several essential components, including glideosome-associated proteins (GAPs), the GAC, formin 1 (FRM1), and myosin H (MyoH), among others (Periz et al. 2019; Meissner, Schlüter, and Soldati 2002; Harding et al. 2016; Jacot et al. 2016; Tosetti et al. 2019; Graindorge et al. 2016).

1.2.5.1.1 Actin

Actin, an important factor of the cytoskeleton and a protein involved in numerous protein-protein interactions, is of high abundance and evolutionarily conserved proteins among most organisms (Dominguez and Holmes 2011). It serves as critical factors in a wide range of structural homeostasis and dynamic cellular activities, including myofibril shortening and cytoskeletal architecture stabilization (Pollard and Cooper 2009).

In contrast to its widespread presence in eukaryotes, apicomplexan genomes typically encode only a single actin gene, reflecting its role as the structural core of the glideosome. The sequence identity between apicomplexan actin and canonical actins (found in opisthokonts and plants) is less than 80%, making apicomplexan actin the least conservative member in this otherwise conserved family (Kumpula and Kursula 2015).

The actin contains 2 primary phases: globular (G-actin) consisting of individual soluble units, and filamentous (F-actin), which is polymerized and insoluble. In apicomplexans, actin was initially thought to predominantly exist in the G-actin form (Dobrowolski, Niesman, and Sibley 1997). However, subsequent studies have suggested that F-actin may exist as very short filaments, typically less than 100 nm in length, functioning as linear tracks for myosin motor proteins (Schatten, Sibley, and Ris 2003; Pospich et al. 2017).

Actin interacts with a diverse array of proteins known as actin-binding proteins (ABPs). In higher eukaryotes, the number of ABPs exceeds 100 (Dominguez 2004), whereas apicomplexan actins are associated with only approximately 10 ABPs and notably lack the ARP2/3 (Actin-related protein) complex (Gordon and Sibley 2005). Unlike canonical ABPs, apicomplexan ABPs exhibit distinct amino acid sequences and functional properties (Sattler et al. 2011; Wesseling, Smits, and Schoenmakers 1988; Skillman et al. 2011; Vahokoski et al. 2014). These proteins can bind to G-actin as nucleotide-exchange factors or interact with F-actin to facilitate nucleation, filament stabilization, or generation of higher level structures (Kumpula and Kursula 2015).

Given the limited repertoire of ABPs in apicomplexans, the switching of G-actin and F-actin is regulated not only by ABPs but also by additional binding factors through polymerization and depolymerization processes (Lee and Dominguez 2010; Dominguez and Holmes 2011). For instance, profilin promotes nucleotide substitution in actin monomers while enhancing formin-mediated filament assembly rates (Kovar et al. 2006). Cyclase-associated proteins (CAPs) function as enzymatic regulators of G-actin, binding directly to soluble monomers to drive nucleotide replacement reactions (Kumpula and Kursula 2015). Actin-depolymerizing factors (ADFs) play multifaceted roles, including filament shortening, polymerization enhancement, filament stabilization, nucleation mediation, and actin helix depolymerization and cleavege (Van Troys et al. 2008; Andrianantoandro and Pollard 2006; McGough et al. 1997; Galkin et al. 2011). In *Toxoplasma gondii*, actin nucleation and rapid filament assembly are primarily mediated by three formins (FRM1, FRM2, and FRM3) (Daher et al. 2010) (for details, see Section 1.2.5.1.5).

In apicomplexan parasites, the apicoplast is a crucial, vital organelle unique to apicomplexan parasites derived from endosymbiosis. Actin has been identified

as crucial for parasite maturation, apicoplast maintenance, and inheritance (Andenmatten et al. 2013b; Whitelaw 2017; Das et al. 2017).

The detection of filamentous actin (F-actin) has historically been challenging in apicomplexan parasites, hindering the elucidation of its functional roles. However, the advent of actin chromobodies (Cb) has revolutionized the visualization of F-actin, even in live imaging (Tosetti et al. 2019; Periz et al. 2017). Utilizing actin chromobodies fused to EmeraldFP, our laboratory identified F-actin in the cytosol of *Toxoplasma gondii*, revealing an extensive F-actin network which interconnects *T. gondii* in the PV. This network facilitates vesicle exchange between parasites and supports their organization, replication, and egress (Periz et al. 2017; Periz et al. 2019; Das et al. 2021).

As a highly dynamic structure, actin is proposed to form in the cytosol and exhibit bidirectional movement, from apical to posterior pole or in the opposite way. Additionally, actin flows from the cytosol to the parasite periphery, adopting a retrograde pattern along the surface, likely associated with the inner membrane complex (Das et al. 2021; Del Rosario et al. 2019).

Actin is also hypothesized to exist and flow between the PM and the IMC, serving as a critical component of the glideosome (Frenal et al. 2017; Tosetti et al. 2019). During migration and invading process, F-actin accumulates at the basal complex of *Toxoplasma gondii*. The presence of F-actin meshwork surrounding nucleus during cell entry led to the hypothesis that actin may protect the nucleus and facilitate its passage through the TJ via a force transduction system (Del Rosario et al. 2019).

1.2.5.1.2 Myosin A

Myosin A (MyoA), which binds to actin, serves as the primary force-generating motor protein mediating the substrate-adherent gliding mechanism of *Toxoplasma gondii* (Meissner, Schlüter, and Soldati 2002). Genetic depletion of MyoA does not disrupt conoid extrusion; however, it leads to the aberrant accumulation of F-actin localized at the apical region and severely compromises parasite motility (Dos Santos Pacheco et al. 2022; Egarter et al. 2014).

MyoA belongs to the class XIV unconventional small myosin family. While *Plasmodium* expresses 6 myosin genes, *Toxoplasma gondii* expresses 11, with 4 of these genes exhibiting overlap between the two species (Douglas, Moon, and Frischknecht 2024).

Initially, MyoA was regarded t to be attached to the PM. However, Bergman et al. later demonstrated that the Myosin A tail domain-interacting protein (MTIP) is localized at the IMC of *P.* sporozoites, suggesting that MyoA may also be linked to the IMC in apicomplexans (Bergman et al. 2003; Gaskins et al. 2004). Structurally, MyoA comprises head domain and neck domain but lacks a discernible tail architecture. Instead, its neck region associates with myosin light chains. The unique myosin light chain, MLC, features an elongated N-terminal sequence. This distinctive structural motif functionally compensates for the absent tail domain through establishment of critical membrane associations with the inner membrane complex (Bosch et al. 2006; Heaslip et al. 2010; Herm-Götz et al. 2002; Martinez et al. 2023). Another light chain of *Toxoplasma gondii* is ELC1 has also been described necessary for rapid directional movement mediated through conventional F-actin networks (Nebl et al. 2011; Bookwalter et al. 2014). Another essential light chain in *Toxoplasma gondii*, ELC1, has been identified as critical for rapid motility along canonical actin

filaments (Nebl et al. 2011; Bookwalter et al. 2014). In other apicomplexans, such as *Plasmodium falciparum*, filamentous actin (F-actin) has been observed in association with densities corresponding to myosin heads, with their tails oriented toward the IMC (Pražák et al. 2024).

In contrast to conventional myosins, which generate force through a piston-like mechanism, Myosin A (MyoA) employs a distinct mechanism involving electrostatic interactions and a unique N-terminal extension. These features enable rapid transitions during the power stroke, facilitating efficient force production (Moussaoui et al. 2020; Robert-Paganin et al. 2019). MyoA is also hypothesized to drive migration and invading process by translocating apically released adhesins in a rearward direction toward the basal end of the parasite (Herm ‐ Götz et al. 2002).

Recent studies have further proposed that MyoA exhibits perimitochondrial localization during terminal phases of apicomplexan cell replication. It also serves as a key factor of mitochondrial morphology and inheritance of *T. gondii* (Oliveira Souza, Yang, and Arrizabalaga 2024).

1.2.5.1.3 Glideosome associated proteins

Following the consensus that the glideosome of *Toxoplasma gondii* is driven by actin filaments and Myosin A (MyoA), which interacts with actin, additional proteins associated with these key structures have been investigated for their roles in motility. Gaskins et al. identified two glideosome-associated proteins (GAPs), GAP45 and GAP50, which form a complex with MyoA and the MLC1, thereby refining the definition of the glideosome to include actin, MyoA, and GAPs (Gaskins et al. 2004).

As a membrane-associated protein, GAP45 may contains little globular folded structure. It serves as the anchoring point for the MyoA-MLC1 complex, recruiting it to the IMC (Whitelaw 2017; Frénal et al. 2010). It also functions as a linker of the PM and IMC through its myristoylated and palmitoylated residues, maintaining the structural spacing between these two membranes (Gilk et al. 2009; Egarter et al. 2014).

Further researches have demonstrated that GAP40 is a polytopic IMC protein that may participate in connecting and stabilizing subpellicular microtubules, while GAP50 is an integral membrane glycoprotein located at the outer side of the IMC. Both proteins are essential for IMC biogenesis and contribute to its structural integrity (Frénal et al. 2010; Harding et al. 2016).

1.2.5.1.4 Glideosome-associated connector

The glideosome-associated connector (GAC) is a 280 kDa protein that is unique and highly conserved across apicomplexan parasites, playing an important role in parasite motility (Jacot et al. 2016; Hung et al. 2022).

GAC is structurally and functionally modular, with distinct domains contributing to its role in motility. The central region of GAC is responsible for conoid targeting and has been observed localizing at the apical pole during *Toxoplasma gondii* invasion. This localization is dependent on AKMT, an apical lysine methyltransferase that ensures proper positioning (Jacot et al. 2016; Tosetti et al. 2019). The C-terminal domain interacts with microneme-secreted adhesin MIC2, both in vivo and in vitro, forming an adhesion complex essential for host cell attachment (Lamarque et al. 2014; Jacot et al. 2016). Meanwhile, the N-terminus combined with actin and stabilizes actin filaments, facilitating the rearward translocation of F-actin within the parasite (Jacot et al. 2016). Through interactions with transmembrane adhesins and phosphatidic acid, GAC bridges

F-actin to the plasma membrane. This complex could thereby convert myosin-driven force into substrate-adherent propulsive forces, ultimately driving parasite motility (Kumar et al. 2023).

During gliding motility and invasion, GAC is proposed to serve as a dynamic connector of F-actin and the adhesion complex, potentially acting in a spring-like manner (Vahokoski et al. 2014; Kumpula et al. 2019). It is hypothesized that GAC clusters or accumulates along the waves of F-actin and adhesins, modulating the force transmission required for movement (Jacot et al. 2016; Tosetti et al. 2019; Hung et al. 2022).

Given the limited PM-IMC space, where the actomyosin system has occupied a substantial portion, GAC must align parallel to F-actin and the PM to accommodate this confined environment. This lateral binding configuration may contribute to actin filament stabilization. However, it remains unclear whether all the coiled-coil domains of GAC interact with actin at the same time or sequential control occurs in coordination with MyoA-driven actin translocation (Hung et al. 2022).

1.2.5.1.5 Formins

In *Toxoplasma gondii*, formins (FRMs) serve as key regulators of actin nucleation and polymerization. All FRMs contain a formin homology 2 (FH2) structure. It facilitates actin polymerization by binding to filament end, promoting the formation of linear, unbranched actin structures (Pruyne et al. 2002; Martinez et al. 2023). During F-actin polymerization, the proline-enriched FH1 domain recruits profilin-bound G-actin, accelerating polymerization (Paul and Pollard 2009).

FRM1 is stably anchored to the conoid, displaying a ring-like localization in both the mother cell and developing daughter cells. It functions as a critical factor of motility by generating F-actin, which supports egress, gliding, and invasion. Conditional depletion of FRM1 leads to the concurrent disruption of actin filament polymerization initiation, conoid protrusion, and apicomplexan gliding mechanism (Tosetti et al. 2019; Dos Santos Pacheco et al. 2022).

FRM2 is localized to the Golgi complex and transiently overlaps with the apicoplast in non-dividing *Toxoplasma gondii*. In contrast, for replicating individual, FRM2 accumulates at the apicoplast periphery during elongation and division, aligning with the positions of the two centrosomes, suggesting a role in apicoplast inheritance. FRM3 is predominantly localized at the basal end, the residual body (RB), and the apex of emerging daughter cells during division, indicating a function in cell-cell communication (Tosetti et al. 2019; Dos Santos Pacheco et al. 2022).

1.2.5.1.6 Myosin H

Myosin H, a class XIV myosin, is a critical component of a microtubule-associated complex on the conoid, facilitated by three α-tubulin suppressor domains at its tail. MyoH has been implicated in parasite invasion, motility, and egress (Graindorge et al. 2016). During F-actin polymerization at the preconoidal rings, MyoH translocates F-actin to the apical polar ring, anchoring it in place and thereby enabling conoid protrusion (Dos Santos Pacheco et al. 2022).

MyoH also plays a crucial role in the extension of the TJ from the parasite's apical tip to the terminus of the IMC. Additionally, it functions as a translocator for the transposition of the GAC in coordination with MyoA. Both MyoH and MyoA facilitate the moving of F-actin along the pellicle, leading to filament

accumulation at the basal pole, independent of microneme secretion or GAC activity. This mechanism is central to the generation of mechanical force which is indispensable for migration (Jacot et al. 2016; Meissner, Schlüter, and Soldati 2002).

Disruption of MyoH through gene knockout results in severe defects in parasite motility, impaired conoid extrusion, and abnormal leakage of F-actin into the cytoplasm, further underscoring its essential role in *Toxoplasma gondii* pathogenesis (Graindorge et al. 2016; Dos Santos Pacheco et al. 2022).

1.2.5.2 Linear model

The prevailing model of *Toxoplasma gondii* motility, known as the linear model or glideosome model, describes the parasite's migration mechanism. This model postulates that the PM and IMC are connected by glideosome-associated proteins (GAPs), which span the entire parasite surface except for the apical and basal pole. A 30-nm-wide space exists between the PM and IMC, where the motor complex consists of Myosin A (MyoA), filamentous actin (F-actin), GAPs, and the glideosome-associated connector (GAC) (Fig. I-6). During the initiation of migration and invasion, apical eompex organelles secreted proyeins from the apical pole, triggering the actin motor. In conjunction with FRM1, MyoH, MyoA, and GAC, F-actin is stabilized and translocated from the preconoidal rings to the basal pole along the pellicle, where it interacts with transmembrane adhesins, including micronemal proteins. GAC further facilitates the directional translocation of F-actin toward the posterior end, ensuring that as the motor complex moves in one direction, the parasite propels itself in the opposite direction (Frenal et al. 2017; Venugopal and Marion 2018; Dos Santos Pacheco et al. 2022; Graindorge et al. 2016; Tardieux and Baum 2016).

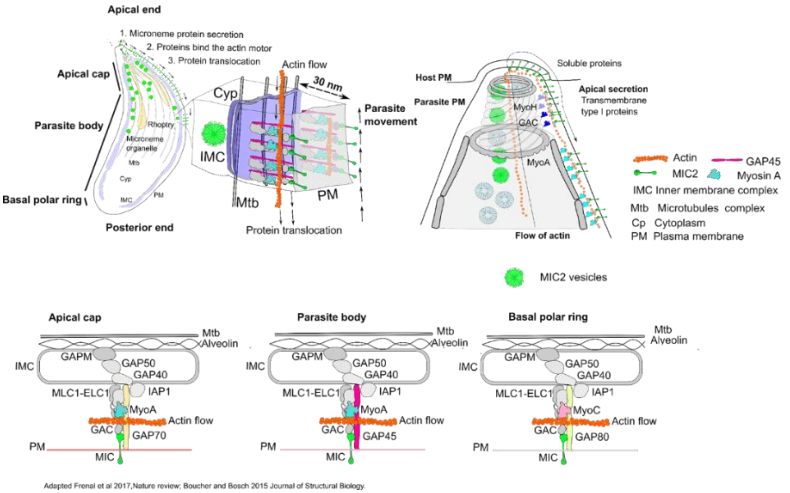

Figure I-6. Schematic diagram of the linear model.

Top Left and Top Right Panels: Expanded view of the apical complex, illustrating the interaction between secreted organelles and actin filaments. The secreted organelles bind to actin, facilitating movement as actin undergoes dynamic flow. **Bottom Row:** Structural representation of the linear model, depicting the organization of the apical cap (GAP70), the body (GAP45), and the basal part (GAP80). The model was developed by Dr. Javier Periz and adapted from referenced studies (Frenal et al. 2017; Boucher and Bosch 2015). Image copied from Dr. Javier Periz.

1.2.5.3 Related data

Although this model is currently the most widely accepted, recent advancements in the literature, the development of conditional knockout (KO) techniques, and the application of advanced microscopy methods suggest that it requires re-evaluation. Experimental results from our laboratory demonstrate that the genetic knockout of Myosin A (MyoA), Myosin C (MyoC), or actin does not completely abolish invasion and migration (Egarter et al. 2014; Andenmatten et al. 2013a). Some data also indicates that cytosolic F-actin

connected with not only microtubules (Mtbs), but also parasite periphery (Fig. I-7, upper left and upper right). Furthermore, Myo A patterned distribution recycled in anterior and posterior end of the parasite, with accumulation and internalization somewhere (Fig. I-7, lower left). The F-actin localization and Myo A distribution suggests a role of the motor in parasite plasticity. Preliminary data using expansion microscopy suggest that the IMC can be permeable during the shape changes observed in migration and invasion (Fig. I-8) (Periz et al. 2017).

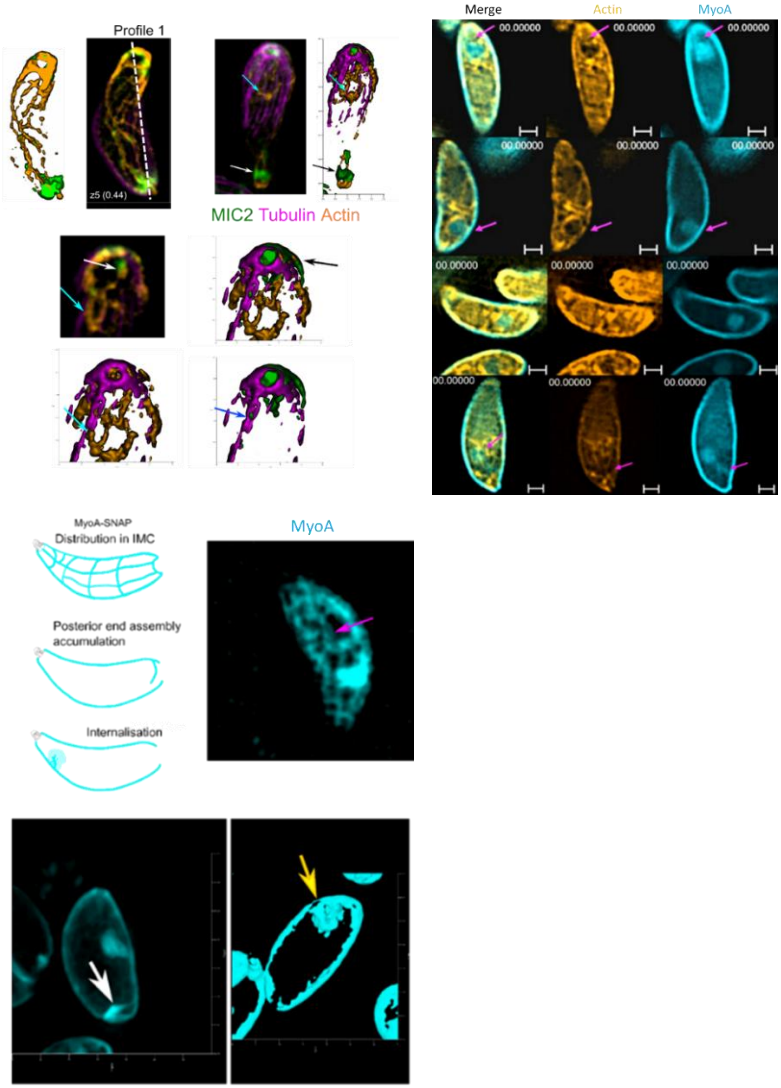

Figure I-7. Images not fit to the linear model.

Upper left panel: Cytosolic filamentous actin (F-actin; cyan arrows) exhibits interactions with microtubules (Mtbs; blue arrow). MIC2 is indicated with white arrows. **Upper right panel**: F-actin (yellow) is also observed to associate with the peripheral structures (MyoA) of the parasite (magenta arrows). **Lower left panel**: MyoA displays a distinct spatial distribution pattern. Single-molecule localization microscopy (SMLM) was employed to visualize actin chromobody-emerald GFP (orange), SirTubulin (magenta), microneme 2-HALO (green), and myosin A-SNAP (cyan). These findings highlight the intricate spatial organization of cytoskeletal components and their potential roles in parasite motility and structural dynamics. Images developed by Dr. Javier Periz. (Periz et al. 2019).

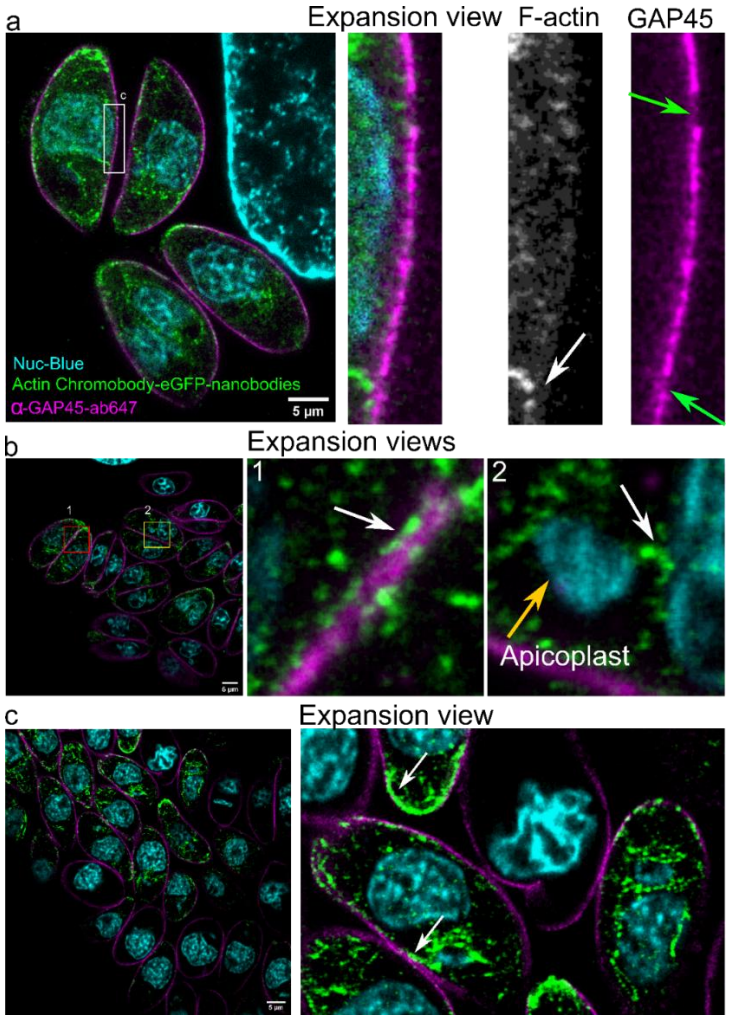

Figure I-8. Actin and GAP45 distribution by pre-labeling Expansion Confocal-STED microscopy (Ex-ConSTEDM).

(a) Actin is localized beneath, yet in close proximity to, GAP45, a marker for the inner membrane complex (IMC) space. Expansion microscopy reveals potential pores facilitating communication between the IMC and the parasite cytoplasm. The white arrow indicates actin labeled with actin chromobody-emerald GFP. **(b)** In two-stage parasitophorous

vacuoles (PVs), cytosolic actin exhibits associations with both GAP45 (red square) and the apicoplast (yellow square). Expansion view 1: The white arrow highlights cytosolic actin associated with GAP45. Expansion view 2: Actin (white arrow) is shown in association with the apicoplast (yellow arrow). **(c)** In large PVs, actin displays a cytosolic distribution (white arrow). Actin is labeled with actin chromobody-emerald GFP (green). GAP45 (magenta) was visualized with a primary rabbit antibody and an Abberior 635 secondary antibody. The nucleus (cyan) was labeled with NucBlue (Periz et al. 2017). Images copied from Dr. Javier Periz.

1.2.6 Replication

After invasion, the secreted ROPs localize to the PVM. Concurrently, the expression of dense granule proteins induces modifications to the PVM and facilitates the formation of an intricate network of Mtbs and F-actin within the PV lumen (Attias et al. 2020). Subsequently, tachyzoites initiate replication within the non-fusogenic, protective environment of the PV (Portes et al. 2020).

Within the PV, tachyzoites replicate via a distinctive process termed endodyogeny (Sheffield and Melton 1968), wherein the daughter cells develop internally in the maternal cell, rather than the mother cell undergoing binary fission. The critical stages of this replication process are illustrated in Figure I-9 (Gissot 2022). Tachyzoites exhibit a unique cell cycle characterized by closed mitosis, consisting of three primary phases: the growth gap phase (G1), the DNA synthesis phase (S), and mitosis (M), with the apparent absence of a distinct G2 phase (Gubbels et al. 2008).

The replication process of *T. gondii* initiates during the G1 phase, marked by the replication and division of centrosomes and Golgi complex. Next is DNA synthesis phase (S phase), during which the apicoplast elongates, and the ER and mitochondria undergo division (Hartmann et al. 2006; Nishi et al. 2008). Upon completion of apicoplast duplication, the APR and conoid complexes of daughter cells begin to assemble. Subsequently, the inner membrane complexes (IMCs) of daughter cells bud and elongate from the apical to basal

end. Concurrently, specialized secretory organelles, including rhoptries and micronemes, are newly synthesized, initiating after nuclear segregation at the conclusion of the S/M phase (Nishi et al. 2008). However, research results indicated that some components of daughter cells are recycled from the mother cell (Periz et al. 2019).

During the final budding stage, the membrane occupation and recognition nexus protein 1 (MORN1) assembles circumferential scaffolding at the basal end, facilitating the physical separation of the daughter cells (Lorestani et al. 2010). Simultaneously, the cytoskeletal architecture and apical complex of maternal cell undergo degradation, and the PM of maternal cell is fused into the developing plasma membranes of the daughter cells. The residual components of the maternal cell are transformed into a residual body (RB), which remains connected to the developing daughter cells (Periz et al. 2017; Anderson-White et al. 2012; Gubbels et al. 2020). Through repeated cycles of this process, a rosette-like cluster of *Toxoplasma gondii* parasites is formed (Attias et al. 2020).

Under optimal conditions, the entire replication cycle is completed within 6–7 h (Anderson-White et al. 2012). *T. gondii* is able to independently undergo nuclear division and generate new parasite bodies through budding enables the parasite to achieve an optimal population size, thereby facilitating adaptation to diverse host-cell environments (Chen and Gubbels 2015).

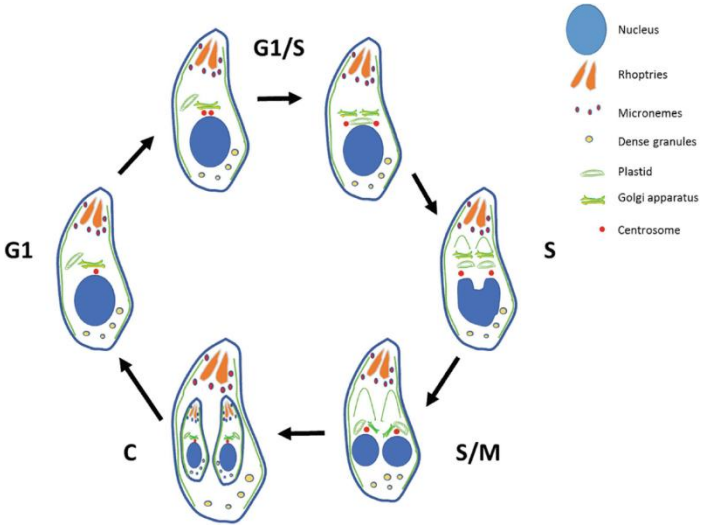

Figure I-9. Replication process of *T. gondii.*

The cell cycle of tachyzoites initiates with the division of the centrosome (depicted in red), which occurs at the G1/S transition, following by diving of the Golgi apparatus (shown in green and yellow). Then the apicoplast elongates in the S phase. When the parasite progresses into the S/M stage, the apicoplast (represented as a green oval) undergoes division. Concurrently, the inner membrane complexes (IMCs; illustrated as green lines) of the daughter cells begin to bud near the centrosome as nuclear division commences. Subsequently, the rhoptries (orange) and micronemes (blue and red) are newly synthesized within the nascent daughter cells, and the IMCs are fully assembled. The newly formed daughter cells are equipped with a complete set of organelles, including a nucleus, enabling them to initiate a new cell cycle starting from the G1 phase. (Gissot 2022). Image copied from Gissot with license number 1599078-1.

It is noteworthy that during replication, *Toxoplasma gondii* tachyzoites undergo closed mitosis, a process distinct from that observed in mammalian cells. In closed mitosis, the integrity of the nuclear envelope is maintained, and chromosome condensation does not occur (Francia and Striepen 2014). Nuclear division and replication are tightly regulated by the centrosome, a critical organelle composed of three distinct structural domains: the outer core, middle

core, and inner core, each performing specialized functions. The outer core, positioned at the distal end of the nucleus and potentially housing centrioles, plays a role in regulating the budding process. The middle core is essential for coordinating mitosis and cytokinesis, as well as maintaining centromere homeostasis. The inner core, located proximal to the nucleus, participates in the nuclear division directly. The duplication of these centrosomal components occurs sequentially, progressing from the outer core to the inner core (Suvorova et al. 2015; Striepen et al. 2000; Tomasina et al. 2022; Chen and Gubbels 2019; Courjol and Gissot 2018).

The centrocone, a structure positioned at the nuclear periphery (Sheffield and Melton 1968), facilitates the interaction between the mitotic spindle and the cytoplasmic centrosome. The spindle extends through nuclear envelope pores, connecting the centrosome to the centromeres (Striepen et al. 2007). Following the duplication of the inner core, the centrocone also undergoes duplication (Suvorova et al. 2015). During the terminal phase of mitosis, chromosomes are segregated into daughter cells, initially forming a U-shaped nucleus that subsequently divides through fission (Radke et al. 2001).

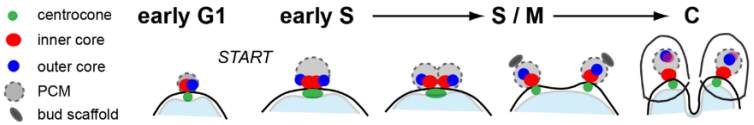

Figure I-10. Morphogenesis of the centrosome during the replication and division of *Toxoplasma gondii.*

The replication and division of the centrocone and centrosome in *Toxoplasma gondii* tachyzoites follow a highly regulated sequence. The outer core of the centrosome duplicates first during the early S phase. In the S/M phase, the duplication of the inner core occurs. Finally, the centrocone undergoes duplication. (Suvorova et al. 2015).

1.2.6.1 SUN-like protein

To ensure proper nuclear positioning and division, the linkage between the nucleus and the cytoskeleton are essential. Presenting among eukaryotic organism, the LINC (linker of nucleoskeleton and cytoskeleton) complex extends across the inner and outer nuclear envelopes, bridging the nucleus and the cytoskeleton. It functions as a foundation in a serious of cellular processes, like the transmission of mechanical forces for nuclear localizing and movement, as well as the regulation of centrosome positioning during DNA replicating and repairing (Sato et al. 2009; Horn 2014; Katsumata et al. 2017; Oza et al. 2009; Wang et al. 2018).

In opisthokonts, SUN (Sad1 and UNC-84) domain proteins and KASH (Klarsicht, ANC-1 and Syne homology) domain proteins together form the LINC complex. The latter is formed by a combination of Sad1, a *S. pombe* protein, and UNC-84, a protein from *C. elegans* (Hagan and Yanagida 1995; Malone et al. 1999). It is a conserved protein domain found in the inner nuclear membrane. This membrane-integrated domain achieves stable intranuclear retention through biochemical anchoring mechanisms involving high-affinity binding interfaces with components of the karyoskeletal network like nuclear lamins (Haque et al. 2006). KASH proteins situated at the outer nuclear envelope, extending into the cytosolic region to engage with cytoskeletal proteins, like actin nucleator formin or proteins that associate with both microtubules and actin (Starr and Han 2002; Patterson et al. 2004; Zhen et al. 2002; Fridolfsson and Starr 2010). Moreover, SUN and KASH domain proteins both contain transmembrane domains (TMD) and interact within nuclear envelope lumen (Padmakumar et al. 2005; Crisp et al. 2006; Tapley and Starr 2013).

While canonical LINC complexes have been documented across diverse eukaryotic organism, the structural and functional homologs mediating cytoskeletal-nuclear coupling remain uncharacterized in apicomplexans. Notably, similar evidence observed in these protozoan pathogens suggest the functional conservation of nuclear-cytoskeletal coupling mechanisms. During the invasion of the tachyzoite, a tight junction appears to constrict both the parasite's body and its nucleus. As a highly dynamic structure, F-actin undergoes continuous remodeling during replication stages and is involved in inner membrane complex (IMC) recycling during endodyogeny, vesicular trafficking, and the development of tachyzoites in the PV (Periz et al. 2017; Whitelaw 2017). During gliding and invasion, the enrichment of F-actin occurs at the basal end and around the nucleus of *Toxoplasma gondii* (Del Rosario et al. 2019); and presents in the cytosol and, most notably, within the nucleus in *Plasmodium falciparum* (Pražák et al. 2024). These findings suggest an interaction between F-actin and the nucleus in apicomplexans. The actin localized near the nucleus may provide structural support during parasite constriction and contribute to efficient invasion (Del Rosario et al. 2019; Yee et al. 2022). This observation may further imply that F-actin, along with a putative apicomplexan nuclear-cytoskeletal coupling system, contributes to nuclear translocation, stabilization, and structural plasticity during the invading process. Furthermore, the pronounced nuclear deformations observed during replication suggest coordinated interactions between the cytoskeleton and nuclear structures to ensure the equitable distribution of nuclei to daughter cells (Del Rosario et al. 2019; McGregor, Hsia, and Lammerding 2016; Suvorova et al. 2015).

Using the ToxoDB database, my colleague Mirjam Wagner identified two proteins with a SUN domain and a presupposed protein with an UNC-50

domain in the genome of *Toxoplasma gondii*, suggesting they are strong candidates as components of an apicomplexan LINC complex (Gajria et al. 2007). KASH domain proteins has not been identified with neither bioinformatics approaches nor educated guesses (Wagner et al. 2023).

The UNC-50 domain protein (TgUNC1) contains several predicted transmembrane domains (Jones et al. 2014) and is situated at the apical part of the nucleus, where the Golgi is also situated (Barylyuk et al. 2020; Wagner et al. 2023). Conditional knockout of unc1 failed to cause obvious growth defects or morphological changes in both Golgi apparatus ultrastructural organization (including cis-trans polarity) of the analyzed cells, suggesting that UNC1 is not an essential gene for *Toxoplasma gondii* (Wagner et al. 2023).

The SUN domain is situated at the central region of TgSLP2 (SUN-like protein 2) (Jones et al. 2014). TgSLP2 exhibits a diffuse, punctate distribution throughout the entire parasite and within the intravacuolar network but is not associated with the nucleus (Wagner et al. 2023).

TgSLP1 (SUN-like protein 1) possesses a canonical SUN structural sequence within its C-terminal region, as well as multiple coiled-coil structures (Jones et al. 2014). This protein exhibits cell cycle-regulated expression dynamics, integrating into the duplicated centrosomal complex. TgSLP1 consistently localizes near the nucleus and exhibits stage-specific expression. It is associated with the mitotic spindle, which facilitates chromosome segregation during parasite's dividing process; however, its localization is independent of mitotic spindle formation (Wagner et al. 2023). Additionally, TgSLP1 is linked to the centrocone, a mitotically active nuclear component implicated in mitotic spindle organization, apicoplast division, and daughter cell development (Gubbels et al. 2006; Lorestani et al. 2010; Wagner et al. 2023). The deletion of

TgSLP1 gene for seven days resulted in no detectable growth in a plaque assay, demonstrating that TgSLP1 is essential for parasite survival (Wagner et al. 2023).

Several components are closely associated with TgSLP1 during different stages of *Toxoplasma gondii* development. For instance, TgCentrin1, a centrin1 homolog that serves as a conserved marker of centriolar structures across species, has been identified at the outer core of centrosomal architecture. In contrast, TgCep250 localizes to the centrosome, where it functions as a structural scaffold bridging the core subdomains and plays a role in ensuring centriolar structure integrity and coordinating mitotic nuclear division (Suvorova et al. 2015; Tomasina et al. 2022; Chen and Gubbels 2019). MORN1, a conserved protein involved in both asexual and sexual development of *Toxoplasma gondii*, is localized at the apical, basal ends and the centrocone of *T. gondii* (Gubbels et al. 2006). Additionally, Nuf2 serves as a kinetochore marker (Farrell and Gubbels 2014), while Chromo1 functions as a centromere marker (Gissot et al. 2012).

1.2.7 Egress

Egress is a procedure occurred when *Toxoplasma gondii* lyses and is released from the host cell following intracellular replication. This stage not only marks the conclusion of one lytic cycle but also serves as a critical prerequisite for initiating the next cycle. The failure of parasites to successfully exit the host cell would significantly impair their survival and proliferation. To complete egress, *Toxoplasma gondii* must breach both the parasitophorous vacuole membrane (PVM) and the host cell PM (Schultz and Carruthers 2018). This process is facilitated by the collaboration of the actomyosin motor system and the micronemal secretion. They could thereby promote parasite egress process (Egarter et al. 2014; Gras et al. 2017; Frénal et al. 2017).

Once intracellular tachyzoites have fully developed within the PV and require dissemination to new host cells, egress may occur spontaneously or be modulated by external stimuli. Various factors, including calcium (Ca^{2+}), pH, potassium (K^{+}), guanylate cyclase (GC), micronemal perforin-like protein 1, and phospholipase lecithin-cholesterol acyltransferase, have been implicated in either inducing or inhibiting egress (McCoy et al. 2012; Bullen et al. 2016; Bisio et al. 2019; Günay-Esiyok et al. 2019; Kafsack et al. 2009; Schultz and Carruthers 2018; Dubois and Soldati-Favre 2019; Carruthers 2019). However, the precise signaling pathways regulating these processes remain largely unresolved.

1.3 Molecular genetic tools for *Toxoplasma gondii*

After years of research, a variety of genetic tools have been established, positioning *Toxoplasma gondii* as a representative organism for apicomplexan biological research. For non-essential genes, knockout can be achieved through the insertion of resistance cassettes. In contrast, for genes that may be essential, conditional manipulation can be performed at multiple levels (Shen, Brown, et al. 2014). At the genetic level, tools such as the dimerizable Cre-mediated recombination (DiCre) system, the CRISPR-associated protein 9 (CRISPR-Cas9) system, and the split Cas9 (sCas9) system enable precise gene editing (Shen, Brown, et al. 2014; Wang et al. 2016; Li et al. 2022).

At the transcriptional level, the U1 gene silencing system, which relies on the U1 small nuclear ribonucleoprotein (U1 snRNP), and the tetracycline-inducible (TET) system are widely utilized for regulating gene expression (Pieperhoff et al. 2015; Meissner et al. 2001; Meissner, Schlüter, and Soldati 2002; Van Poppel et al. 2006). At the protein level, the auxin-inducible degron (AID) system and the destabilization domain (ddFKBP) system allow for conditional protein

degradation, facilitating the establishment of conditional knockout cell lines (Brown, Long, and Sibley 2018; Herm-Götz et al. 2007).

1.3.1 DiCre System

The Cre-lox site-specific recombination system is a widely utilized genetic tool across various species for achieving precise gene excision, inversion, and translocation. This system employs Cre recombinase, an enzyme derived from the P1 bacteriophage, which specifically recognizes a 34-base pair sequence known as the locus of X-over in P1 (loxP) (Sauer 1987; Sauer and Henderson 1988). An advanced iteration of this system, the dimerizable Cre-mediated recombination (DiCre) system, enables conditional control of Cre recombinase activity in *Toxoplasma gondii* with high efficiency (Andenmatten et al. 2013b).

In the context of knockout assays, the dimerizable Cre recombinase is engineered into two non-active fragments, each combined with distinct rapamycin-responsive domains: FKBP12-rapamycin-binding (FRB) domain and FK506-binding protein (FKBP) (Figure I-11) (Kudyba et al. 2021). Upon the addition of rapamycin, these two proteins dimerize, thereby reconstituting the functional DiCre recombinase. The active DiCre then recognizes and binds to loxP sites, catalyzing the deletion of the DNA sequence localized between the 2 loxP sequence (Andenmatten et al. 2013a; Jullien et al. 2003).

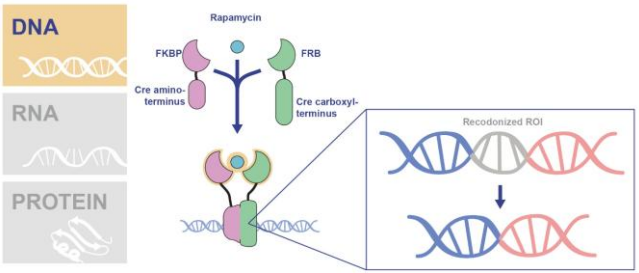

Figure I-11. Conditional knockout with the dimerisable Cre-mediated recombination (DiCre) system.

Parasites are engineered to express two split subunits: the FRB domain is combined with the carboxyl terminus of Cre recombinase and the FKBP interact with the amino terminal region of Cre recombinase. The region of interest (ROI) is flanked by genetically inserted LoxP sites. Rapamycin-mediated chemical induction of FKBP12-FRB heterodimerization triggers the reassembly of Cre recombinase subunits into functional dimers. In DiCre-edited organism, the activation of Cre recombinase by rapamycin results in the deletion of the DNA sequence situated between the LoxP sites, generating a conditional knockout. (Kudyba et al. 2021)

1.3.2 CRISPR/ Cas9

CRISPR (Clustered Regularly Interspaced Short Palindromic Repeats) represents an adaptive immune system originally identified in bacteria. Derived from the type II CRISPR-Cas system of *Streptococcus pyogenes* (Bolotin et al. 2005). A Cas9 nuclease and a guide RNA (gRNA) are involved in the CRISPR-Cas9 system. The gRNA mediates Cas9 endonuclease localization to complementary DNA sequences through sequence-specific hybridization, resulting in a nuclease-induced double-strand break (DSB) (Sander and Joung 2014). In the presence of a DNA donor template, the homology-directed repair (HDR) pathway can facilitate precise insertions, enabling the addition of tags to target proteins. However, *Toxoplasma gondii* predominantly repairs DSBs via the non-homologous end joining (NHEJ) pathway. To circumvent this, the Δku80 parasite line is utilized to suppress NHEJ activity, thereby enhancing HDR efficiency (Vartak et al. 2018). Following HDR-mediated repair, transfected parasites are isolated and sorted into 96-well plates for plaque purification, subsequent culturing, and confirmation through sequencing.

1.4 Super resolution microscopy (SRM)

The optical resolution of traditional light microscopy is constrained by the diffraction barrier (Abbe limit), achieving about 250 nm along both lateral axes. However, the advent of SRM has solved this problem by modulating excitation or activation light in either the temporal or the spatial domain, thereby enhancing resolution to approximately 10 nm. This breakthrough has enabled scientists to visualize subcellular structures with unprecedented detail (Galbraith and Galbraith 2011; Schermelleh et al. 2019).

SRM encompasses several major techniques, comprising single-molecule localization microscopy (SMLM), structured illumination microscopy (SIM), stimulated emission depletion microscopy (STED), expansion microscopy (ExM) and immunogold labeling electron microscopy (Immunogold-EM).

Among these, SMLM techniques, consist of photo-activated localization microscopy (PALM) and stochastic optical reconstruction microscopy (STORM); achieve nanoscale positional determination of single fluorescent molecules via exploiting their stochastic activation and deactivation. These methods enable quantitative subcellular cartography of molecular distributions of samples, providing insights into subcellular organization and dynamics. PALM employs light-inducible fluorophores, like PA-GFP and mEos, which is able to be selectively activated and deactivated. By sequentially activating and precisely localizing subsets of these molecules, PALM constructs a high-resolution image reaching a resolution of approximately 20–30 nm (Betzig et al. 2006). While STORM utilizes fluorophores capable of stochastic converting between emissive and non-fluorescent phases, such as Alexa Fluor 647 and Cy5. By precisely localizing individual fluorophores across multiple imaging cycles, STORM could achieve a higher resolution around 10–20 nm (Rust, Bates, and Zhuang 2006).

SIM improves resolution via performing a striped illumination pattern onto the sample, generating moiré fringes through interference effects. By systematically shifting and rotating the illumination pattern, multiple images are acquired. Leveraging the known properties of the illumination pattern, computational algorithms are applied to demix the superimposed information, thereby reconstructing high-resolution details that surpass the diffraction limit. This approach achieves a resolution of approximately 100 nm. While SIM is particularly suited for dynamic processes in viable specimens offering reduced photodamage and rapid temporal sampling rates. Its resolution remains inferior to that of SMLM (Gustafsson 2000; Schermelleh et al. 2008).

Confocal microscopy is an advanced optical imaging technique that utilizes point-scanning excitation and a confocal aperture to suppress non-planar fluorescence, thereby enhancing image clarity. Typically, a laser serves as the excitation source, generating high-intensity fluorescence or reflectance specifically from the focal plane. This approach significantly improves optical resolution and contrast, while also enabling the reconstruction of three-dimensional (3D) images (Nwaneshiudu et al. 2012).

In this study, the primary SRM techniques employed are STED microscopy (discussed in Section 1.4.1) ExM (detailed in Section 1.4.2) and Immunogold-EM (discussed in Section 1.4.3).

1.4.1 STED

The point-spread function (PSF) represents the inherent limitation of optical systems, describing the diffraction-induced spread of a single point of light as it passes imaging system. It defines the smallest resolvable point source or object, setting the fundamental resolution limit of the system (Galbraith and Galbraith 2011). Stimulated Emission Depletion (STED) microscopy overcomes this

limitation by changing the PSF to decrease its valid diameter. This is achieved by encircling the laser-scanning focal excitation PSF with a ring of longer-wavelength depletion light, which is sufficiently intense to deplete fluorophores in the surrounding region, forcing them into their ground state and preventing fluorescence emission. By improving the intensity of depletion light, the saturated depletion zone expands, further compressing the excitation PSF to a diameter below the diffraction barrier of 200 nm. The resulting sub-diffraction PSF is then imaged across the specimen to produce high-resolution images (Hell and Wichmann 1994; Galbraith and Galbraith 2011).

In cellular imaging, modern commercial STED systems typically achieve lateral resolutions of less than 50 nm (Wegel et al. 2016). An advanced variant, time-gated STED (gSTED), combines temporally modulated excitation pulses with continuous-wave photonic depletion systems and time-correlated acquisition protocol to further enhance resolution and contrast (Vicidomini et al. 2011). Compared to 2D STED, 3D STED systems extend functionality along the z-axis, allowing adjustable tuning between lateral and axial resolution improvements. This capability makes 3D STED particularly suitable for imaging thicker and more densely packed biological structures (Eggeling et al. 2015; Urban et al. 2011).

Standard STED microscopy, often implemented as an add-on to confocal systems, is relatively user-friendly and does not require extensive computational post-processing, although deconvolution is frequently applied to improve signal quality. It supports routine two-color imaging with a variety of fluorophores, though optimal performance is achieved with STED-optimized dyes. Additional imaging channels can be incorporated using conventional confocal modes (Eggeling et al. 2015; Göttfert et al. 2013; Bottanelli et al. 2016).

However, as a targeted imaging technique, STED has inherent limitations. Reducing the fluorescence observation volume decreases signal detection efficiency and necessitates smaller scan steps, which prolongs acquisition times. While small imaging windows enable high-frame-rate imaging, capturing entire cells with sufficient photon counts remains relatively slow (Schermelleh et al. 2019).

1.4.2 Expansion microscopy

The SRM is able to increase the resolution reaching typically 20 to 50 nm (Sahl, Hell, and Jakobs 2017). On the other hand, if the resolution already reach it limitation and cannot be improved further, what we can do is to expand the structure of *Toxoplasma*. ExM is a SRM technique, employing the physical magnification of hydrogel-embedded specimens through controlled polymer network swelling while preserving architecture through polyelectrolyte crosslinking (Fig. I-12 and Fig. I-13) (Chozinski et al. 2016; Dos Santos Pacheco and Soldati-Favre 2021a).

In ExM, the fluorophores on the samples are anchored to a gel matrix, and expand 3-4 times as large as before eventually. Moreover, ExM is compatible and does not rely on specialized instruments (Bertiaux et al. 2021; Halpern et al. 2017; Chozinski et al. 2016). Therefore, the motor can be visualized via combining the expanded samples with SIM and STED in 2D or 3D pattern, so that it is possible to have a further cognition of the structure and localization of the migration motor of *Toxoplasma gondii.*

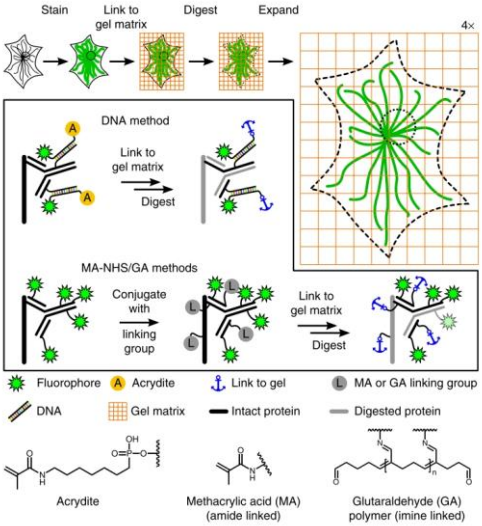

Figure I-12. Schematic diagram of ExM and labeling process.

Two methodologies are illustrated in the box: the DNA-based method and the post-staining linker-group functionalization approach (referred to as the methacrylic acid N-hydroxy succinimidyl ester/glutaraldehyde (MA-NHS/GA) method). In the DNA-based protocol, the sample is labeled using a primary antibody conjugated to both a fluorophore and an acrydite-modified DNA strand. In the MA-NHS/GA protocol, following regular labeling, the sample is further labeled with polymer-linking groups using either MA-NHS or GA. (Chozinski et al. 2016). Image copied from Chozinski et al with license number 1599079-1.

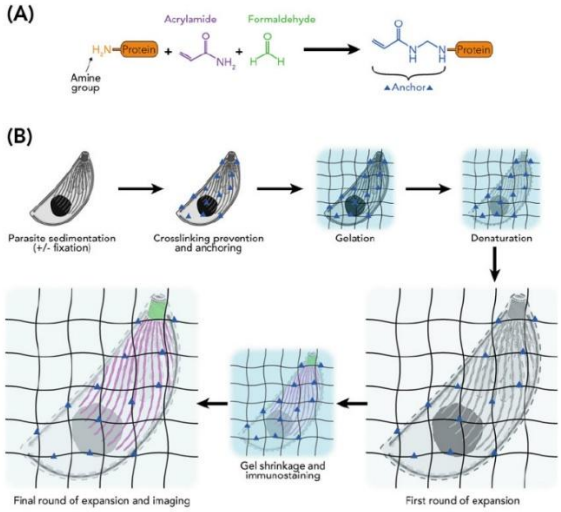

Figure I-13. Scheme of expansion microscopy operations.

(A) The addition of acrylamide (AA) and formaldehyde (FA) buffers creates molecular 'anchors' that bind to free amine groups on proteins within the sample. These anchors subsequently tether the proteins to the gel mesh, ensuring their spatial preservation during expansion. **(B)** The sequential steps of the protocol are as follows: Sample preparation: The sample is prepared with or without prior fixation. Crosslinking prevention and anchor formation: AA/FA buffers are applied to prevent crosslinking and form molecular anchors. Gelation: The sample is embedded in a gel matrix using a monomer buffer, APS as an initiator, and TEMED as an accelerator. Denaturation: The gel is treated with a buffer containing SDS at 95°C for denaturation. First round of expansion: The gel is expanded overnight in deionized water (ddH2O). Gel shrinkage and immunostaining: The gel is treated with PBS and immunostained with antibodies diluted in BSA. Final round of expansion: The gel undergoes a final expansion overnight in ddH2O to achieve the desired resolution for imaging (Dos Santos Pacheco and Soldati-Favre 2021b). Image copied from Dos Santos Pacheco and Soldati-Favre with license number 1599080-1.

Various expansion microscopy (ExM) techniques have been applied in this study, each with distinct methodologies, as illustrated in Figure I-14. In the upper left panel, Protein-retention Expansion Microscopy (proExM) is depicted. This method, referred to as Protocol 1, involves proteinase K-dependent

digestion following pre-immunostaining (Halpern et al. 2017; Chozinski et al. 2016). The upper right panel illustrates an U-ExM protocol that includes a denaturation step at high temperature (95°C) using a strong buffer containing sodium dodecyl sulfate (SDS), referred to as Protocol 2 (also detailed in Figure I-13) (Dos Santos Pacheco and Soldati-Favre 2021a).

Conventional super-resolution microscopy (SRM) often relies on chemical fixation and permeabilization, which can alter the native cellular state and potentially introduce artifacts, leading to biased interpretations (Schnell et al. 2012). Cryofixation, which rapidly immobilizes cells in a vitreous state, is the only method capable of preserving native ultrastructure without introducing artifacts (Neuhaus et al. 1998; Dubochet 2012). Cryo-ExM bridges this vacancy via integrating the benefits of cryopreservation with the high-resolution capabilities of expansion microscopy, offering a robust solution for super-resolution imaging while maintaining cellular integrity. Cryo-ExM (Figure I-14, lower right) employs cryofixation (rapid vitrification) instead of chemical fixation, with subsequent steps identical to U-ExM protocol (Laporte et al. 2022).

The detection of specific protein targets can be challenging according to the observed low protein expression or limited accessibility (Piña et al. 2022). To overcome these limitations, an alternative approach involves fusing the interest protein to TurboID, a biotin ligase that labels proximal lysine residues, followed by detection using fluorescent streptavidin (Branon et al. 2018). Streptavidin-based detection demonstrates significantly higher signal intensity compared to traditional antibody-based methods, substantially enhancing detection sensitivity in both ExM and correlative light and electron microscopy (CLEM) without compromising resolution (Kim et al. 2016). Notably, proteins localized within phase-separated regions, which are often resistant to antibody labeling,

can be effectively detected using streptavidin. Additionally, streptavidin imaging enables the resolution of fluctuating, time- and location-dependent molecular groups and, under some conditions, provides insights into the history of dynamic protein interactions (Odenwald et al. 2023). The lower left panel illustrates the TurboID ExM process, which combines Protocol 2 with streptavidin labeling instead of antibodies for TurboID-expressing strains.

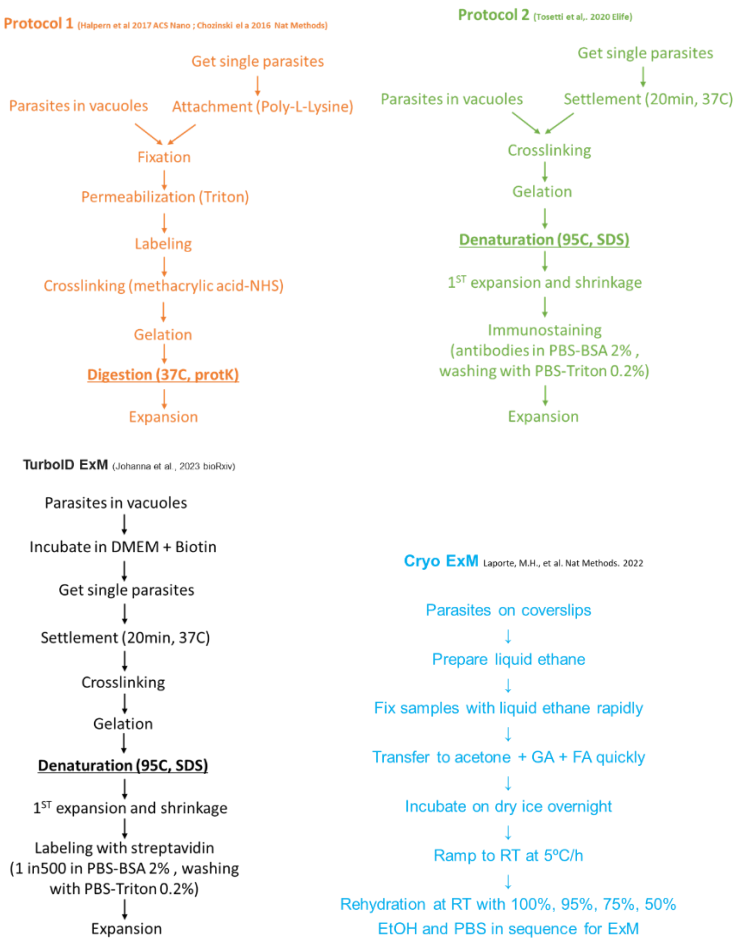

Figure I-14. Main steps of four expansion microscopy methods.

Upper left: Schematic representation of the primary steps in proteinase K (protK)-based Expansion Microscopy (ExM). This method involves proteinase K digestion following pre-immunostaining to retain proteins within the expanded gel matrix. **Upper right**: Schematic depiction of the key steps in high-temperature-based ExM. This protocol includes a denaturation step at 95°C using a buffer comprising SDS to facilitate protein unfolding and gel expansion. **Lower left**: Schematic illustration of the TurboID ExM process. This approach combines high-temperature-based ExM with streptavidin labeling,

utilizing TurboID-mediated biotinylation for enhanced detection of target proteins. **Lower right**: Schematic overview of the cryofixation step in Cryo-ExM. This method employs rapid vitrification to preserve native cellular ultrastructure, followed by steps identical to high-temperature-based ExM for gelation, denaturation, and expansion.

Improvements in ExM methods have resulted in the development of increasingly refined and iterative methods. A 20-fold expansion has been achieved through sequential fourfold expansion processes (Chang et al. 2017; M'Saad and Bewersdorf 2020). It is worth noting that, these methods present several limitations, including complex and prolonged processing durations, limit expansion ratios and risk of structural integrity alterations. An alternative method involves the use of modified gel chemistries, which enable a 10-fold expansion but necessitate special machine for oxygen extraction during gel polymerization (Truckenbrodt et al. 2018). Additionally, a 'one-step 4× and 12× 3D-ExM' method has been developed, allowing for either fourfold or twelvefold expansion while ensuring both three-dimensional isotropic expansion and the structural preservation of biological specimens (Norman et al. 2024).

1.4.3 Immunogold labeling electron microscopy (Immunogold-EM)

Immunogold-EM is a high-resolution immunolabeling technique designed to detect and localize specific proteins, antigens, or cellular structures at the ultrastructural level. This method employs gold nanoparticles as markers, along with the high resolution of EM with the specificity of immunolabeling to achieve nanometer-scale precision in molecular localization within cellular and tissue samples (Lučić, Förster, and Baumeister 2005).

For immunostaining of cryosections, electron-dense protein-A (PA)/gold particles (PAG) serve as highly effective markers. These particles are of high-

contrast visualization compared to host cytosol and provide clear, measurable signals in both transmission electron microscopy (TEM) and scanning electron microscopy (SEM) (Slot and Geuze 2007). Gold particles are chemically inert, minimizing nonspecific interactions with the sample, and can be conjugated to antibodies, protein A, or streptavidin, enabling specific binding to target molecules. This versatility allows for double- or even triple-labeling experiments (Roth, Bendayan, and Orci 1978; Geuze et al. 1981; Griffiths and Lucocq 2014). Gold markers are available in various sizes, typically ranging from 3 to 15 nm, which is ideal for immuno-electron microscopy applications (Geuze et al. 1981; Slot and Geuze 1981).

Sample preparation involves fixation with glutaraldehyde and paraformaldehyde to preserve ultrastructural integrity. Cryosections are then prepared, and primary antibodies specific to the target antigen are applied. Secondary antibodies conjugated to PAGs are used to label the target molecules. For imaging, samples are stained with electron-dense contrast agents such as uranyl acetate or lead citrate. In TEM or SEM images, gold particles appear as distinct, dark electron-dense spots, enabling precise localization of the target molecules (Slot and Geuze 2007; Saibil 2022).

2 Aim of study

As an obligate intracellular pathogen, *T. gondii* depends on gliding, invading, replication and egress to survive and proliferate. With the availability of genetic tools, *Toxoplasma gondii* functions as a representative model for studying other apicomplexans. Investigating the localization of molecular motors involved in migration and invasion can provide insights into the mechanisms underlying parasite motility.

However, due to the limited optical resolution of microscopes, the mechanism of motility remains not well understood. Even with super-resolution microscopy, achieving optimal resolution to accurately localize and characterize the motor structure remains a challenge.

Therefore, the key lies in employing appropriate technologies and methodological approaches to achieve a further understanding. Utilizing ExM to physically expand the sample by 3-4 times, combined with the high resolution of SRM, may enable the visualization of the motor.

Conversely, based on Mirjam Wagner's findings, TgSLP1 is necessary for in nuclear division during the replication of *Toxoplasma gondii*. As a candidate of the LINC complex, TgSLP1 may responsible for nuclear processes in coordination with F-actin, including positioning, protection, and deformation during invasion.

Therefore, the aim of this project is to visualize key motor factors responsible for the migration and invasion of *T. gondii*. Additionally, this study will explore the potential existence of different motility models. Furthermore, the role and function of TgSLP1 will be investigated during the various phases of cell division with SRM.

AIM OF STUDY

1. Optimize and implement various Expansion Microscopy (ExM) protocols for *Toxoplasma gondii*, along with STED for high-resolution imaging of candidate proteins at the nanoscale.
2. Tag specific proteins located at the inner and outer cores of the centrosome, and components of the kinetochore and centromeres. Apply the SRM to investigate the dynamic behavior of the Sun-like protein 1 (TgSLP1) during parasite division process.
3. Investigate the localization of the glideosome complex, including actin, Myosin A (MyoA), glideosome-associated protein 45 (GAP45), glideosome-associated connector (GAC), formin 1 (FRM1), and Myosin H (MyoH), to confirm its proposed location between PM and IMC in line with the linear motor model.

3 Materials and Methods

3.1 Materials

3.1.1 Equipment

Table III-1. Equipment.

Manufacturer	Description
Rhost	620 Manual Cryo-Plunger
Zeiss	Axio Vert.A1 fluorescence microscope
Leica	DMi8 wide-field microscope
Abberior	3D STED microscope
Eppendorf	Mastercycler EP Gradient (PCR thermocycler)
	Centrifuge 5910 Ri
	thermomixer C
	thermomixer
	pipettes
Hettich	Centrifuge
Thermoscientific	Centrifuge
Roth	Centrifuge
Lonza	4D-Nucleofactor™ electroporation units
BD bioscience	ACSAria™ III Cell Sorter
BioRad	Mini Trans-Blot Electrophoretic Transfer Cell
	PowerPac Basic Power Supply
	Mini-Sub Cell GT Cell Horizontal electrophoresis system
Hartenstein	pipettes
	Vacuum pump
Starlab	ErgoOne® single & multi-channel pipettes
	Vortexer
NIPPON Genetics	FastGene Blue/Green LED Transilluminator
Thermo Fisher Scientific	NanoDrop Spectrophotometer
	CO2-Incubator
	Safety cabinets
	Owl EasyCast minigel electrophoresis system
LI-COR Biosciences	Odyssey CLx-1849
Scientific industries	Vortex-Genie 2
Memmert	Incubator
New brunswick scientific	Incubator shaker
Heidolph	shaker
Sarstedt	shaker
Flow Laboratory	shaker
KERN	Scale
Sartorius	Analytical balances
Wagner&Munz	PH meter
PHOENIX Instrument	Water Bath
Haier biomedical	-80 °C freezer

Bosch	Fridge & -20 ℃ freezer
Siemens	Fridge & -20 ℃ freezer
Sharp	Microwave

3.1.2 Software

Table III-2. Computer software.

Software	**Description**
ToxoDB	National Institute of Allergy and Infectious Diseases (NIAID)
NEB tools™: Tm Calculator	New England Biolabs (NEB)
Basic Local Alignment search tool (BLAST), Primer-BLAST	National Institute for Biotechnology Information (NCBI)
ApE Plasmid Editor	University of Utah (by M. Wayne Davis, v.2.0.53c)
Clustal Omega	Clustal Omega
Las X software (v.3.4.2.183668)	Leica Application Suite X (Las X)
Imspector 16.3.14274	Abberior microscope
Fiji (ImageJ) v1.53c	National Institutes of Health (NIH)
InkscapeTM: Open Source Scalable Vector Graphics Editor	Inkscape Project
Microsoft Excel Worksheet 2016	Microsoft

3.1.3 Consumables, biological and chemical reagents

Table III-3. Consumables and chemical and biological reagents.

Manufacturer	**Description**
Faust Lab Science	TPP cell culture flask 150 cm^2 with filter
	TPP cell culture test plates (6-well, 12-well, 24-well and 96 well)
	TPP centrifuge tubes (15 ml and 50ml)
	TPP cell culture dishes (6-cm and 10-cm)
	TPP cryo tubes
	TPP cell scrapers
	Syringe filter
	Gloves
Ibidi	µ-Dish 35 mm high
Roth	DMSO (Dimethyl sulfoxide)
	TAE Buffer 50x, NaCl,
	Sodium acetate
	Sodium chloride (NaCl)
	Sodium hydroxide
	SDS (Sodium dodecyl sulphate)
	Acetic acid (100%)
	Acetone ⩾99.7%

	Ethanol
	Methanol Rotisolv ⩾ 99.98%
	Glycine
	Glycerine
	Magnet, tweezer, cell scratcher and spreaders, parafilm
	Filter nylon 0,2 µm
	Microscope slides
Eppendorf	Tips (1000 µl, 200 µl, 10 µl)
	Eppendrof (2.0 ml and 1.5ml)
Greiner Bio-One	Aspiration pipette
Sarstedt	Serological Pipettes
Thorlabs	Lens Tissues
	Low autofluorescence immersion oil
Hartenstein	Cover slips (12 mm)
	Agar Bacteriology grade
	Tryptone BioChemica
	Yeast extract BioChemica
	Incuwater-clean
Avantor	PCR tubes
	Petridish
	HEPES
Assistent	Counting chamber
Biochrom	Ultra pure water
	Trypsin/EDTA
BioRad	TEMED (Tetramethylenediamine)
	APS (Ammonium persulfate)
	40% Acrylamide
	N,N'-methylenebisacrylamide (Bis, 2% w/v)
Zeiss	Immersion Oil 518F 30°C Zeiss
Merck/Sigma	Rapamycin
	DNA Ladder 250bp
	Tris base, Tris-HCl
	Triton TX-100, Tween-20
	L-glutamine
	DMEM (Dulbecco's modified Eagle's medium, high glucose)
	PBS 1x
	DL-Dithiothreitol (DTT)
	EDTA (Ethylenediaminetetraacetic acid)
	Sodium acetate
	BSA (Bovine serum albumin)
	Poly-L-lysine solution
	Gentamycin solution 50 mg/mL
	Ampicillin sodium crystallin
	Biotin
	Sodium deoxycholate
	Trypsin-EDTA solution
	Sucrose, glucose
	MgSO4
	EGTA
	MES

	Methacrylic Acid-NHS (MA-NHS)
	Sodium Acrylate
	MgCl2
	36.5-38% Fomaldehyde
	Sodium Acrylate
Thermo	Hoechst 20 mM
	Proteinase K (600 U/mL in glycerol)
	ProLong™ gold antifade mountant
	10× PBS Buffer (pH 7.4)
	Carl Zeiss™ immersion oil
	K_2SO4
	HBSS
	10× TAE Buffer (pH 8.3)
BioSell	FBS (Fetal bovine serum)
Science services	20% PFA (Paraformaldehyde)
SMS-Medipool	Braun Omnifix syringes 1 mL
	Braun Injekt Syringe 5 mL
	Sterican needle 26G
Biotium	GelRed Nucleic Acid Gel Stain
Linde	CO2, Dry ice
Biozym	Biozym LE GeneticPure Agarose
New England Biolabs	T4 DNA ligase
	T4 DNA Ligase Reaction buffer
	Q5 High-Fidelity DNA Polymerase
	dNTP (deoxynucleotide) Mix
	SOC Outgrowth Medium
	DNA ladder 1kb (plus),
	Gel Loading Dye, purple (6x), no SDS
MP Biomedicals	Guanidine HCl

3.1.4 Kits

Table III-4. Kits.

Company	**kit**
Blirt	ExtractMe DNA Clean-Up&Gel-Out Kit, ,
	ExtractMe genomic DNA Kit
	ExtractMe plasmid Mini Kit
Lonza	P3 Primary cell 4D nucleofector X Kit L

3.1.5 Buffers, solutions and medium

Table III-5. Buffer for molecular cloning.

Buffer	**Components**
Annealing buffer	10 mM Tris, pH 7.5 - 8.0

	50 mM NaCl 1mM EDTA diluted in ddH_2O

Table III-6. Buffer for cells culture and freezing.

Buffer	**Components**
Ampicillin (1000X)	100 mg/ml Ampicillin power in ddH_2O
LB-Medium	10 g/l tryptone 5 g/l yeast extract 10 g/l NaCl dissolved in ddH_2O
LB-Agar	1.5 % (w/v) agar in LB-Medium
50% glycerol	50 % glycerol (v/v) in 50 % ultrapure water (v/v)
DMEM (complete)	4 mM L-glutamine 10 % FCS (v/v) 20 µg/ml gentamicin in 500 ml DMEM
2x Freezing media	25% FBS (v/v) 10% DMSO (v/v) in DMEM

Table III-7. Buffer for phenotypic assays and fixations.

Buffer	**Components**
Endo buffer	44.7 mM K_2SO4 10 mM MgSO4 100 mM sucrose 5 mM glucose 20 mM Tris 0.35% w/v BSA adjust pH to 8.2
Gliding Buffer	1 mM EGTA 100 mM HEPES in HBSS buffer
Rapamycin (1000X)	50 µM in DMSO
4% PFA	20% PFA in PBS
Cytoskeleton buffer: CB1	MES 10 mM pH 6.1 KCl 138 mM $MgCl_2$ 3 mM EGTA 2 mM 5% PFA
Cytoskeleton buffer: CB2	MES 10 mM pH 6.1 KCl 163.53 mM $MgCl_2$ 3.555 mM EGTA 2.37 mM sucrose 292 mM
CB mix buffer	CB1 and CB2 mix in 4:1 ratio

Table III-8. Buffer for ExM.

Buffer	Components
10% TEMED (v/v)	100 µl Tetramethylethylenediamine in 900 µl water.
10% APS (w/w)	0.1 g Ammonium persulfate in water
38% (w/w) SA	19 g of Sodium Acrylate powder in 31 ml water
Monomer solution (MS)	500 µl 38% SA 250 µl 40% AA 50 µL 10% BIS 100 µL 10× PBS mix on ice keep at -20 °C for at least one night before use
Denaturation buffer	200 mM SDS 200 mM NaCl 50 mM Tris-Base Adjust the pH to 9
Antibody diluent solution	BSA 2% in PBS
Washing solution	0.2% Triton TX-100 in PBS
MA-NHS buffer	1 M Methacrylic Acid-NHS powder in anhydrous DMSO store at -20 °C
Monomer buffer (different from MS)	0.8625 g Sodium Acrylate 5 mL 40% Acrylamide 0.375 mL 2% Bis 1.169 g NaCl 1 mL 10× PBS Add water to final volume of 10 mL Store at 4 °C
Digestion Buffer	3 mL 10× TAE Buffer 2.3 g Guanidine HCl 0.15 mL Triton X-100 Add water to final volume of 30 mL Store at 4 °C

3.1.6 Antibodies and dyes

Table III-9. Primary antibodies for IFA and ExM.

Antibodies	Species	Dilution IFA	Dilution ExM	Reference
Beta Tubulin Toxo	Rabbit	1:1000	1:500	
Centrin	Mouse	1:200	1:100	Sigma 04-1624
Centrin	Rabbit	1:1000	1:500	Abcam ab11257
Camelid sdAb α-GFP-ATTO 488	Camelid	1:500	1:250	NanoTag Biotechnologies: N0304-At488-L

GAP45	Rabbit	1:1000	1:500	Soldati, D.
GAC	Rabbit	1:1000	1:500	Prof. Dominique Soldati-Favre, University of Geneve
GFP	Mouse	1:1000	1:500	Roche 11814460001
GFP	Rabbit	1:1000	1:500	Abcam #ab290
HA	Rat	1:1000	1:500	Roche 11867423001
HA	Rabbit	1:1000	1:500	Sigma H6908
Halo polyclonal	Rabbit	1:1000	1:500	Promega #G928A
IMC1	Mouse	1:1000	1:500	Ward, G.
Ron2	Rabbit	1:1000	1:500	Boothroya
SAG1	Mouse	1:1000	1:500	Sebastian Lourido
SNAP tag	Rabbir	1:1000	1:200	Biozol
Tubulin acetylated	Mouse	1:500	1:250	sigma, cat# T6793
Tubulin acetylated (Lys40)	Rabbit	1:1000	1:500	Merck ABT241

Table III-10. Secondary antibodies for IFA and ExM.

Antibodies	**Species**	**Dilution IFA**	**Dilution ExM**	**Reference**
AlexaFluor 488 goat-anti-mouse	Goat	1:5000	1:1000	Invitrogen A-11001
AlexaFluor 488 goat anti-rabbit	Goat	1:3000	1:1000	Invitrogen A-11008
AlexaFluor 488 goat-anti-rat	Goat	1:5000	1:1000	Invitrogen A-11006
AlexaFluor 546 goat-anti-mouse	Goat	1:3000	1:1000	Invitrogen A-11030
AlexaFluor 594 goat-anti-mouse	Goat	1:3000	1:1000	Invitrogen A-11005
AlexaFluor 594 goat-anti-rabbit	Goat	1:3000	1:1000	Invitrogen A-11012
AlexaFluor 594 goat-anti-rat	Goat	1:3000	1:1000	Invitrogen A-11007
AlexaFluor 647 chicken anti-rat	Chicken	1:3000	1:1000	Invitrogen A-21472
AlexaFluor 647 goat anti-mouse	Goat	1:3000	1:1000	Invitrogen A-21235

AlexaFluor 647 goat anti-rabbit	Goat	1:3000	1:1000	Invitrogen A-21245

Table III-11. Dyes for IFA and ExM.

Dye	Dilution in IFA	Dilution in ExM	Origin / cat. Number
Janelia Fluor HaloTag ligand 549	200 nM	400 nM	Promega GA111A
Janelia Fluor HaloTag ligand 646	20 nM	40 nM	Promega GA112A
Streptavidin AlexaFluor 488 conjugate	1:1000	1:500	Invitrogen S11223
Streptavidin AlexaFluor 594 conjugate	1:1000	1:500	Invitrogen S11227

3.1.7 Cells lines

Table III-12. Mammalian cells.

Cell	Source
Human foreskin fibroblasts (HFF, SCRC-1041)	LGC/ ATCC ® SCRC-1041™

Table III-13. Bacteria cells.

Cell	Source
DH5α Competent Escherichia coli (High Efficiency)	New England Biolabs (NEB; C2987I)

Table III-14. Generated or used *Toxoplasma gondii* strains.

Strains	Source/reference
DiCreΔku80	(Andenmatten et al. 2013a)
RH-Δku80-DiCre-LoxP-TgSLP1-sYFP2-LoxP	(Wagner et al. 2023)
RH-Δku80-DiCre-LoxP-TgSLP1-sYFP2-LoxP-CEP250_L1-3xHA	This study
RH-Δku80-DiCre-LoxP-TgSLP1-sYFP2-LoxP-Nuf2-3xHA	This study
RH-Δku80-DiCre-LoxP-TgSLP1-sYFP2-LoxP-CEP250_L1-3xHA	This study
RH-Δku80-CbEmerald	(Periz et al. 2017)
RH-Δku80-CbEmerald-MyoA-SNAP	Meissner Lab
RH-Δku80-CbEmerald-FRM1-Halo	Meissner Lab
RH-Δku80-IMC1-Halo-MyoA-SNAP	Meissner Lab
RH-Δku80-DiCre-LoxP-FRM1-Halo-loxP	Meissner Lab
RH-Δku80-DiCre-FRM1-TurboID	Meissner Lab

RH-Δku80-DiCre-FRM1-3xHA	Meissner Lab
RH-Δku80-DiCre-FRM1-Halo-GAC-SYFP2	Meissner Lab
RH-Δku80-DiCre-MyoH-Halo	Meissner Lab

3.1.8 Oligonucleotides

Table III-15. Sequences of generated sgRNAs.

Name	Sequence	PAM
TgSLP1_sgRNA-Cterm-tag	TTTCTGGGCATGCCTAGTTG	AGG
TgSLP1_sgRNA-Upstr-LoxP	GTTTCTGGCTGCTCTGAGCA	CGG
CEP250_L1_sgRNA-Cterm-tag	TGGCGATCCAGTCTCAACAG	TGG
Nuf2_sgRNA-Cterm-tag	CCGAGTAGAGCACCGATCT	TGG
Chromo1_sgRNA-Cterm-tag	CGACAGTGGACGAACCGGTC	AGG

Table III-16. Oligonucleotides.

Name	Sequence	Purpose
TgSLP1_sgRNA-Cterm-tag-fw	AAGTTGTTTCTGGGCATGCCTAGTTGG	integration into Cas9YFP-sgRNA vector
TgSLP1_sgRNA-Cterm-tag-rv	AAAACCAACTAGGCATGCCCAGAAACA	integration into Cas9YFP-sgRNA vector
TgSLP1_Cterm-tag-donor-fw	GCCTGAGAGTCCACGGCGAGAAGGCGGTGCTGAAGTCCACCACCCTCAACGCTAAAATTGGAAGTGGAGG	PCR amplification of the repair template
TgSLP1_Cterm-tag-donor-rv	AGCATGTGCGACTGCTTTGCTTTCTTTGCCTACGTTTCTGGGCATGCCTAATAACTTCGTATAATGTATGCTATACG	PCR amplification of the repair template
TgSLP1_sgRNA-Upstr-LoxP-fw	AAGTTGTTTCTGGCTGCTCTGAGCAG	integration into Cas9YFP-sgRNA vector
TgSLP1_sgRNA-Upstr-LoxP-rv	AAAACTGCTCAGAGCAGCCAGAAACA	integration into Cas9YFP-sgRNA vector
TgSLP1_Upstr-LoxP-donor	GCCGCTGCTTCTCCTTCGCCGTGCTCAGAGCAGCATAACTTCGTATAGCATACATTATACGAAGTTATCAGAAACATCCTGCGATGGACTCCTTCGAGCG	repair template
TgSLP1_5UTR-fw	CAGCGGGCTTCTGTATTTGC	genotyping
TgSLP1_internal-fw	CTGAAGGAGAAGCCGGTACG	genotyping
TgSLP1_3UTR-rv	GCAGTTGGGCATTCCATTTCG	genotyping
TgSLP1_Upstr-LoxP-contr-rv	GATGTTTCTGATAACTTCGTATAATGTATGC	genotyping

CEP250_L1_sgRNA-Cterm-tag-fw	AAGTTGTGGCGATCCAGTCTCAACAGG	integration into Cas9YFP-sgRNA vector
CEP250_L1_sgRNA-Cterm-tag-rv	AAAACCTGTTGAGACTGGATCGCCACA	integration into Cas9YFP-sgRNA vector
CEP250_L1_sgRNA-Cterm-tag-donor-fw	CTTCGACAAGGATCAGCACAGGAAGGGGAAAGTCGTCGCTTTCGGGGCGAGCTAAAATTGGAAGTGGAGG	PCR amplification of the repair template
CEP250_L1_sgRNA-Cterm-tag-donor-rv	TGCTCGTCCATAAACATCGCTACTGCAGAGGCTTGGCGATCCAGTCTCAAATAACTTCGTATAATGTATGCTATACG	PCR amplification of the repair template
CEP250_L1_5UTR-fw	CACCTGTCCGCTTTCAATTC	genotyping
CEP250_L1_internal-rv	CAACACTCTACGAACCTGTC	genotyping
Nuf2_sgRNA-Cterm-tag-fw	AAGTTGCCGAGTAGAGCACCGATCTG	integration into Cas9YFP-sgRNA vector
Nuf2_sgRNA-Cterm-tag-rv	AAAACAGATCGGTGCTCTACTCGGCA	integration into Cas9YFP-sgRNA vector
Nuf2_sgRNA-Cterm-tag-donor-fw	CAAGGGAGCCCAGAGAAGACGGCGACTTTCCAATGTATAGTCACGCCGAGGCTAAAATTGGAAGTGGAGG	PCR amplification of the repair template
Nuf2_sgRNA-Cterm-tag-donor-rv	GCCAAAGTTCTCCGAGTGTCCGTACACCGGAAACTTTCTCCATGCCAAGAATAACTTCGTATAATGTATGCTATACG	PCR amplification of the repair template
Nuf2_5UTR-fw	AGCGAGAACGAGAATCCGAC	genotyping
Nuf2_internal-rv	CGAGTGTCCGTACACCGGAA	genotyping
Chromo1_sgRNA-Cterm-tag-fw	AAGTTGCGACAGTGGACGAACCGGTCG	integration into Cas9YFP-sgRNA vector
Chromo1_sgRNA-Cterm-tag-rv	AAAACGACCGGTTCGTCCACTGTCGCA	integration into Cas9YFP-sgRNA vector
Chromo1_sgRNA-Cterm-tag-donor-fw	CCGTCTGCGGGAGGTTCCAACGCTCTCCAGTGTTCTCTTGTGTCGCTGGCGCTAAAATTGGAAGTGGAGG	PCR amplification of the repair template
Chromo1_sgRNA-Cterm-tag-donor-rv	CCAGTCTCGTGGAAGCGGTGCAACGCCTCTGGGATTCCGTTCGGCCTGACATAACTTCGTATAATGTATGCTATACG	PCR amplification of the repair template
Chromo1_5UTR-fw	CGTTCGTTTCAGATGAGTCC	genotyping
Chromo1_internal-rv	GGTATAGAGACAGCGCGTTG	genotyping

3.2 Methods

3.2.1 Molecular biology

3.2.1.1 Restriction digest

To integrate the sgRNAs into the Cas9_YFP vector, endonucleases were used for restriction digestion.

Table III-17. Restriction digest reaction.

Component	Volume/ weight
Cas9_YFP plasmid	5 µg
10x rCutSmart buffer	5 µL
BsaI-HFv2	5 µL
ddH_2O	up to 50 µL

Incubate the mixture at 37 °C for 2 hours. The backbones were then checked by agarose gel electrophoresis and purified by DNA purification kit.

3.2.1.2 Agarose gel electrophoresis

Agarose gel electrophoresis was conducted to separate and analyze DNA fragments. Agarose gels were prepared through dissolution of the powder in TAE buffer followed by heating until fully dissolved, and incorporating 1–2 µL of GelRed (depending on gel size) for subsequent visualization. DNA samples were mixed with 6× purple loading dye and diluted with water to achieve a final 1× concentration before loading. Electrophoresis was performed at 80–120 V for 20–40 minutes, depending on DNA fragment size and applied voltage. DNA ladders (250 bp or 1 kb plus) served as molecular weight markers for fragment size determination. After electrophoresis, DNA bands were visualized using a UV transilluminator.

3.2.1.3 Annealing of Oligonucleotides

Single-guide RNAs (sgRNAs) were obtained from Thermo Fisher Scientific. After appropriate dilution, 2 µL of forward and reverse primers (10 pmol/µL each) were combined in a PCR tube with 16 µL of annealing buffer. The reaction mixture was incubated at 90-95 °C for 5 minutes, followed by cooling to room temperature to facilitate subsequent ligation.

3.2.1.4 Ligation

To integrate the sgRNA sequences into the Cas9YFP plasmid backbone, 5 µL of annealed primers from the previous step were combined with 25–50 ng of the Cas9YFP vector, 1 µL of T4 DNA ligase, 1 µL of 10× T4 buffer, and ultrapure water to a final volume of 10 µL. The ligation reaction was carried out for 2 hours at room temperature or overnight at 16 °C.

3.2.1.5 Bacteria transformation

To obtain the Cas9YFP-sgRNA plasmid, the ligation reaction product was transformed into chemically competent *Escherichia coli* DH5α cells. A 50 µL aliquot of bacteria stored at -80 °C was thawed on ice and incubated with 5–10 µL of the ligation product for 30 minutes. The mixture underwent a heat shock at 42 °C for 30 seconds, followed by a 3-minute incubation on ice. Subsequently, 400 µL of LB medium was added, and the sample was incubated at 37 °C for 1 hour with shaking. The transformed bacteria were then plated onto LB agar containing 100 µg/mL ampicillin and incubated overnight at 37 °C.

Single bacterial colonies from the LB agar plate were picked and transferred into liquid LB medium supplemented with 100 µg/mL ampicillin. The cultures were then incubated overnight at 37 °C with shaking in preparation for plasmid extraction or cryopreservation stocks with 50% glycerol.

3.2.1.6 Plasmid extraction

The bacteria were first pelleted, and plasmid DNA was subsequently isolated using the ExtractMe Plasmid Mini Kit, according to the company's protocol. The plasmid DNA was finally eluted for subsequent steps.

3.2.1.7 Concentration measurement and sequencing of DNA

Plasmid DNA concentrations were determined using a Nanodrop spectrophotometer, according to the company's instructions. Based on the concentration calculations, the appropriate amounts of purified PCR products, plasmids, and primers were sent to Eurofins Genomics for sequencing.

3.2.1.8 Genomic DNA extraction

After pelleting, the genomic DNA of *Toxoplasma gondii* was extracted with the ExtractMe Genomic DNA Kit, following the manufacturer's instructions.

3.2.1.9 Polymerase chain reaction

In this study, polymerase chain reactions (PCR) were utilized to generate repair templates for transfection and to confirm whether the genetically modified *Toxoplasma gondii* strains, following FACS sorting, maintained correct DNA integration. For genotyping, parasites were first pelleted, resuspended in 18 µL of elution buffer, and 2 µL of proteinase K from the ExtractMe Genomic DNA Kit. The mixture was incubated at 50°C for 1 hour and subsequently boiled at 95°C for 10 minutes. The resulting product was then used as a template for PCR. The PCR reactions were mediated by Q5 High-Fidelity DNA Polymerase (Table III-18), with the thermocycling conditions outlined in Table III-19. The DNA renaturation temperature was determined based on the respective gene

sequences of the primers (TmCalculator; NEB), while the extension time was adjusted according to the size of the amplified DNA fragment.

Table III-18. PCR reaction using Q5 High-Fidelity DNA Polymerase (25-µL).

Component	Volume (µL)
5X Q5 reaction buffer	5
10 mM dNTPs	0.5
10 µM forward primer	1.25
10 µM reverse primer	1.25
Q5 high-fidelity DNA polymerase	0.25
Template DNA	1
Ultrapure water	15.75

Table III-19. Thermocycling conditions of PCR reactions with Q5 polymerase.

Process		Temperature (°C)	Time (s)
Initial denaturation		98	30
35 x	denaturation	98	10
	renaturation	50-72	30
	extension	72	60-240
Final extension		72	120-300
hold		4	∞

3.2.1.10 Ethanol precipitation of DNA

For *Toxoplasma gondii* transfection, plasmid DNA and the repair template must first undergo ethanol precipitation. 10 µg of plasmid DNA and repair template were added to 0.1 volumes of 3M sodium acetate and 2.5–3 volumes of 100% pre-cold ethanol, followed by thorough vortexing to ensure homogeneous mixing. These components were then incubated at -80°C for 1 hour or -20°C overnight to enhance precipitation, particularly when DNA levels were low. Alternatively, immediate centrifugation at full speed for 1 hour at 0°C was performed.

After incubation, the sample was spun at full speed at 0°C for 30 minutes. The precipitated pellet was washed twice with 0.5 mL of 70% pre-cold ethanol, with centrifugation at 0°C for 15 minutes per wash. The supernatant was then sucked away, and the precipitated DNA was either dried upside down in a tissue culture hood or stored in the final ethanol wash at -20°C for later use in transfection.

3.2.1.11 DNA purification

The DNA was purified using An ExtractMe DNA Clean-Up&Gel-Out Kit following the company's instructions.

3.2.2 Cell biology

3.2.2.1 Culturing of host cells

HFFs were cultured and maintained in DMEM supplemented with 50 mL FBS, 15 mL L-glutamine, and 250 µL gentamicin at 37 °C in a 5% CO_2 atmosphere.

For experimental use or continued culture, HFFs were subcultured at a 1:4 ratio weekly. The medium was sucked away, and the confluent HFFs were washed with pre-warmed PBS, which was then discarded. Trypsin-EDTA was used to eliminate the attachment between the cells and culture flask, followed by incubation at 37 °C with 5% CO_2 for 10 minutes to ensure complete cell detachment. To neutralize the trypsinization process, pre-warmed complete DMEM was added, achieving the desired 1:4 dilution. The diluted HFF suspension was then transferred into fresh culture dishes, plates, or flasks for further maintenance.

3.2.2.2 Culturing of *T. gondii*

Freshly released tachyzoites were cultured in dishes, plates, or flasks containing a confluent monolayer of HFFs in complete DMEM at 37 °C in a 5% CO_2 atmosphere.

3.2.2.3 Cryopreservation and recovery of *Toxoplasma gondii*

Cryopreservation of tachyzoites in late-stage vacuoles was performed using pre-prepared cryotubes containing 800 µL of 2× freezing medium. The complete DMEM medium was removed, and 800 µL of DMEM buffer was added to the cells. The cells were then scraped, transferred to the prepared cryotubes, and subsequently frozen and stored at -80°C.

For recovery, the frozen parasites were thawed and transferred onto a confluent monolayer of HFFs. The cultures were incubated at 37 °C with 5% CO_2, and the complete DMEM medium was changed after several hours.

3.2.2.4 Transfection of *Toxoplasma gondii*

To generate parasite lines, tachyzoites in late-stage vacuoles were transfected using the P3 Primary Cells 4D-Nucleofector X Kit L. The infected human foreskin fibroblasts were detached from the culture dish using a tip, and *T. gondii* were released by passing the suspension three times through a 26G needle.

A volume of 500 µL to 1 mL of healthy parasites, depending on the vacuole density, was collected in a 2 mL tube and spun at 1,500 rpm for 5 minutes for precipitation. The precipitated plasmid DNA and repair template (as described in Section 3.2.1.10) were resuspended in 100 µL of buffer P3 and subsequently used to resuspend the parasite pellet. The resulting product was thoroughly

mixed, transferred to a cuvette, and subjected to electroporation using the FI-158 program on the Amaxa 4D-Nucleofector system.

Following electroporation, the cuvette was rinsed with complete DMEM medium, and the parasites were transferred to a culture dish or plate for incubation to establish stable transfection. While for transient transfection, 20 µL of electroporated parasites were added to coverslips in 24-well plates containing HFF cells. After approximately 24 hours, the parasites were fixed for imaging.

3.2.2.5 Isolation of *Toxoplasma gondii* clones with FACS sorting

After 24–48 hours of growth, parasites expressing nuclear Cas9YFP were visualized using a fluorescence microscope. Fluorescence-activated cell sorting (FACS) was then employed to isolate these parasites. HFFs containing parasite vacuoles were detached by scraping, subjected to syringe lysis using 26G needles, and filtered through 3-µm filters to obtain extracellular parasites. These parasites were subsequently sorted using a FACSAria III Cell Sorter, with 5–10 YFP-positive parasites sorted into individual wells of a 96-well plate containing HFFs. After five days of incubation, single plaques were screened and selected for PCR analysis and microscopy examination.

3.2.3 Phenotypic assays

3.2.3.1 Immunofluorescence assay (IFA)

For imaging intracellular parasites, tachyzoites within vacuoles were fixed along with HFFs on coverslips in 24-well plates or light dishes. To image extracellular parasites, the parasites were first released and filtered to remove host cell debris before being transferred onto poly-L-lysine-coated coverslips or light

dishes. Fixation was performed using 4% paraformaldehyde (PFA), 100% methanol, or CB mix buffer at room temperature for 20 minutes.

To permeabilize the fixed samples, they were incubated in PBS containing 0.2% Triton X-100 for 20 minutes. Following permeabilization, a blocking step was performed by incubating the samples in PBS with 2% BSA for 40 minutes at room temperature.

Subsequently, the primary antibody, diluted in PBS with 2% BSA, was applied for a one-hour incubation at room temperature. For fluorescently labeled parasites, incubation was conducted in the dark. After primary antibody incubation, the samples were washed 3 times with PBS under gentle shaking.

Next, the diluted secondary antibody or fluorescent dyes were applied for incubation in the dark for 45 minutes at room temperature. Following this, the samples were washed three times with PBS under gentle shaking. If necessary, nuclear staining was performed using DAPI or Hoechst, followed by an additional washing step before mounting the coverslips for imaging.

3.2.3.2 Gliding assay

The freshly released parasites were pelleted and resuspended in pre-warmed gliding buffer. The parasites were then transferred onto coverslips in a 24-well plate and incubated at 37°C. After 20 minutes, the parasites were fixed for further analysis (Del Rosario et al. 2019).

3.2.3.3 Invasion assay

Freshly released parasites (3 mL) were pelleted and resuspended in 400 µL of Endo buffer, then incubated at 37°C for 10 minutes. The parasites were subsequently allowed to settle onto coverslips containing a confluent layer of

HFFs for 3 minutes at room temperature, followed by a 20-minute incubation at 37°C. The liquid was gently removed and replaced with pre-warmed culture medium. The samples were incubated for an additional 5 minutes to allow for parasite invasion. Afterward, the samples were fixed with CB mix buffer for 10 minutes, followed by treatment with 50 mM NH_4Cl, a PFA quenching solution, for 10 minutes. The samples were then washed three times with PBS and stored at 4°C for future analysis.

3.2.4 Microscopy

All microscopy images were acquired using either a Leica DMi8 widefield microscope or an Abberior 3D STED microscope. Confocal and STED imaging were conducted exclusively on the Abberior 3D STED microscope. Image acquisition was performed using Leica LasX software and Imspector. Image processing and analysis were conducted using Fiji (ImageJ) (Schindelin et al. 2012) and art work and diagrams in Inkscape software.

3.2.4.1 Ultrastructure Expansion Microscopy (U-ExM)

To prepare samples for imaging, intracellular or extracellular *Toxoplasma gondii* are either fixed or left unfixed on 12-mm coverslips within a 24-well plate. Each coverslip containing samples is treated with 500 µL of a formaldehyde/acrylamide (FA/AA) mixture, prepared by combining 38 µL formaldehyde, 50 µL acrylamide, and 912 µL phosphate-buffered saline (PBS). The plate is then sealed with parafilm to avoid evaporation, and incubated at 37°C for five hours.

Twenty minutes prior to gelation, aliquots of TEMED, APS, and monomer solution (MS) are thawed on ice. Ten minutes before gelation, a 10-cm dish containing wet paper and parafilm is placed at -20°C and subsequently

transferred to ice. Coverslips are removed from the FA/AA mixture and placed upright on a tissue to eliminate excess liquid. A polymerization solution is prepared by mixing 5 µL of 10% TEMED with 90 µL MS, followed by the addition of 5 µL of 10% APS, ensuring thorough mixing. A 40-µL droplet of this mixture is then placed onto parafilm for each coverslip, with the coverslip positioned parasite-side down. The samples are maintained on ice for 5 minutes and incubated at 37°C for one hour.

Following polymerization, the gel is transferred to a 6-well plate containing 2 mL of denaturation buffer and shaken for 15 minutes to facilitate separation. It is then transferred to a 1.5-mL microcentrifuge tube for incubation at 80–95°C for 1.5 hours. After incubation, the buffer is removed, and the gel is soaked in water within a 50-mL Falcon tube for overnight expansion.

Once expansion is complete, water is removed, and PBS is added to induce gel shrinkage. The gel is trimmed to fit the wells of a 24-well plate and incubated with a primary antibody at twice the concentration used for immunofluorescence assays, in 500 µL PBS-BSA (2%). The plate is sealed with parafilm and incubated at 37°C with agitation for three hours. The antibody mixture is then aspirated, and the gel is washed three times with 1 mL PBS-Triton (0.2%) for ten minutes each at 37°C with agitation. Next, a secondary antibody diluted in PBS-BSA (2%) is added, and the gel is incubated at 37°C with agitation for two hours in the dark, followed by three additional washes. Finally, the buffer is removed, and the gel is expanded overnight in water within a 15-mL Falcon tube.

For imaging, excess water is removed from the gel, which is then transferred to a light dish, and the location of parasites is determined using a microscope.

Once the parasites are identified, the gel is mounted onto a poly-L-lysine-coated light dish for further imaging (Dos Santos Pacheco and Soldati-Favre 2021a).

3.2.4.2 Protein-retention Expansion Microscopy (proExM)

To permeabilize the fixed sample, incubate the samples in PBS-Triton (0.2%) for 20 minutes. Following permeabilization, perform a blocking step by incubating the samples in PBS-BSA (2%) for 40 minutes at room temperature. Subsequently, add the primary antibody at twice the concentration used for standard immunofluorescence assays (IFA) in PBS-BSA (2%) or apply a fluorescent dye, and incubate for one hour at room temperature. If working with fluorescent parasites, maintain incubation in the dark. After primary antibody incubation, wash the samples three times with PBS under gentle shaking.

Next, add the secondary antibody at a 1:1000 dilution in PBS-BSA (2%) and incubate in the dark for 45 minutes at room temperature. Following incubation, wash the samples three times with PBS under gentle shaking. If necessary, stain the nuclei using DAPI or Hoechst and repeat the washing step before proceeding with imaging.

Prior to gelation, the sample undergoes a preparation process involving the modification of amine groups with MA-NHS. A 1 M MA-NHS stock solution in DMSO is diluted to a final concentration of 50 mM in PBS (50 µL in 1 mL) immediately before use to prevent rapid hydrolysis in water. The solution is vortexed immediately after dilution to ensure proper mixing. The sample is then incubated with the MA-NHS buffer at room temperature for 30 minutes. Following incubation, the buffer is completely removed, and the sample is washed three times with PBS to eliminate any residual reagent.

For gelation, the sample is first treated with a monomer buffer for five minutes. A monomer solution is then prepared by mixing 100 µL of monomer solution with 2 µL of 10% TEMED and 2 µL of 10% APS. This mixture is vortexed briefly to ensure homogeneity. Subsequently, 70 µL of the prepared solution is placed onto a parafilm surface, and the sample slide is inverted onto the mixture. The polymerization process is carried out at room temperature for 20 minutes, allowing the gel to form on the sample.

Prepare the digestion buffer by adding 10 µL of Proteinase K to 1 mL of digestion buffer, achieving a final concentration of approximately 6 U/mL. The sample is then incubated in a humidified incubator at 37°C for a duration ranging from three hours to overnight to facilitate digestion. Following digestion, the digestion buffer is removed, and water is added to initiate sample expansion. After 30 to 60 minutes, the water is replaced, and this process is repeated two to three times or until the specimen is fully expanded. More frequent water exchanges or the use of thinner hydrogel samples can accelerate the expansion process.

For imaging, following the protocol used in U-ExM, excess water is removed from the gel before transferring it to a light dish. The position of the parasites is then identified using a microscope. Once localized, the gel is mounted onto a poly-L-lysine-coated light dish to facilitate further imaging (Halpern et al. 2017).

3.2.4.3 TurboID ExM

For extracellular parasite biotin labeling, late vacuole-stage *Toxoplasma gondii* within human foreskin fibroblasts (HFF) are used. The culture medium is removed, and intracellular parasites are incubated in 4 mL of DMEM along with 150 µM biotin at 37°C for 30 minutes. Longer incubation periods (1 hour or 4.5 hours) do not yield significant differences.

Following incubation, parasites are collected by mechanical disruption through scraping, syringe passage, and filtration. The parasites are then precipitated by centrifugation at 600 × g for 5 minutes, after which the supernatant is removed, and the pellet is resuspended in 500 µL PBS.

A maximum of 200 µL of the parasite suspension is applied to a 12-mm round coverslip in a 24-well plate and allowed to settle for 15 minutes. Extra buffer is carefully removed using tissue from the side, and the sample is treated with an acrylamide/formaldehyde (AA/FA) buffer at 37°C for 5 hours. For gelation, 90 µL of monomer buffer is mixed with 3 µL of 10% APS and 3 µL of 10% TEMED. A 40-µL droplet of this solution is placed per coverslip, and polymerization is conducted on ice for 5 minutes, followed by incubation at 37°C for 1 hour.

The sample is then shaken in denaturation buffer for 10 minutes and subsequently incubated at 95°C for 90 minutes. The first round of expansion is carried out by immersing the gel in deionized water (ddH_2O) overnight. This is followed by immersion in PBS to induce gel shrinkage. The gel is then incubated with streptavidin (1:500 dilution) at 37°C for 3 hours under gentle agitation. After incubation, the sample is washed 3 times with PBS-Triton (0.2%), each wash lasting 10 minutes. A second expansion step is performed by incubating the gel in ddH_2O overnight. Finally, the sample is mounted and imaged (Odenwald et al. 2023).

3.2.4.4 Expansion microscopy with cryofixation (Cryo-ExM)

For cryo-fixation, 6-mm coverslips are coated with poly-L-lysine (1:5–1:10 dilution) and incubated at room temperature for 20 minutes. In an Eppendorf tube with perforations, a fixation solution consisting of acetone (-20°C) with 0.025% glutaraldehyde (GA) and 0.5% formaldehyde (FA) is prepared. The poly-L-lysine solution is then removed, and samples are added to the coverslips,

incubating at 37°C for approximately 20 minutes. The cryo-fixation setup is pre-cooled with liquid nitrogen, and ethane gas is converted into liquid ethane liquefied within a container cooled by liquid nitrogen. Excess liquid is removed from the sample, and fixation is performed using tweezers equipped with a homemade locking mechanism. The sample is then quickly immersed in liquid ethane before being transferred sequentially to liquid nitrogen and the acetone fixation solution, ensuring that the temperature remains low throughout the process. Samples are incubated on dry ice overnight, followed by a controlled temperature ramp-up to room temperature at a rate of 5°C per hour on a shaker.

Rehydration is performed at room temperature through sequential incubations: 100% ethanol for 5 minutes, 95% ethanol twice for 5 minutes each, 75% ethanol for 3 minutes, and 50% ethanol for 3 minutes. Samples are subsequently stored in PBS until further use, taking care to prevent pellet dissolution, which may occur during the 75% or 50% ethanol washes.

Coverslips are then incubated overnight at 37°C in a freshly prepared solution of 1% acrylamide (AA) and 0.7% FA in PBS (25 µL AA, 19 µL FA, and 956 µL PBS per 1 mL solution) for crosslinking. 10% TEMED, 10% APS and MS are thawed on ice for approximately 30 minutes before gelation. A metal block covered with wrinkle-free parafilm is prepared as a gelation surface. To an 18-µL aliquot of monomer solution (sufficient for two 6-mm coverslips; 35 µL for a 12-mm coverslip), 1 µL of TEMED is added and mixed, followed by 1 µL of APS with brief vortexing. A 9-µL droplet of monomer solution is placed onto the parafilm, and coverslips are positioned cell-side down on the droplet. Gelation proceeds on ice for 5 minutes, followed by sealing and incubation at 37°C for 45 minutes to 1 hour.

Following, coverslips with gels are transferred into pre-warmed (95°C) denaturation buffer within a 1.5-mL tube (for 6-mm coverslips) and incubated at 95°C for 1.5 hours. Gels are washed twice with PBS in a 6-well plate under agitation. The PBS is then replaced with deionized water (ddH_2O) and incubated for 10 minutes, followed by a second ddH_2O incubation for 30 minutes to complete the first round of expansion.

Gels are shrunk by washing twice with PBS for approximately 15 minutes per wash and then transferred to a 1.5-mL Eppendorf tube and incubated with primary antibody (at twice the standard immunofluorescence concentration) in PBS containing 3% BSA and 0.1% Tween-20. Incubation is conducted for 3 hours at 37°C or overnight at 4°C under agitation. The samples are then washed three times with PBS-Tween (0.1%) (10 minutes each at room temperature with agitation). Secondary antibody incubation follows, performed at 37°C for 2.5 hours with agitation, followed by three additional washes with PBS-Tween (0.1%). Gels are then expanded in ddH_2O for imaging, stored in PBS, or labeled with NHS, Hoechst, or DAPI as required (Prof. Gautam Dey's laboratory).

3.2.5 Data analysis

For double-labeled Expansion Microscopy (ExM) section images, Fiji (ImageJ) was utilized to analyze fluorescence intensity and spatial distance, providing insights into the positional relationship between the two structures. Measurements were conducted at fifteen distinct locations per parasite, including five points at the apical region, five at the midsection, and five at the basal region.

For the analysis of immunogold labeling, beads localized between the PM and the IMC, those associated with the IMC, and those within the cytosol were counted separately. Beads localized in regions lacking structural integrity of

Toxoplasma gondii were categorized as undefined. The distribution of beads was then quantified accordingly.

Quantification data were plotted and visualized using Microsoft Excel. Statistical significance was assessed using a two-tailed Student's t-test, with p-values reported as follows: *** $p < 0.001$, * $p < 0.05$, and n.s. (not significant). All experiments were performed in biological triplicates, with mean values derived from three independent assays. Error bars represent the standard deviation.

4 Results

Given that SRM overcomes the diffraction barrier inherent in traditional light microscopy, the combination of STED and ExM has been employed to visualize subcellular structures and dynamic processes at the nanometer scale in *Toxoplasma gondii*.

These SRM approaches have been further utilized to investigate the localization and function of the SUN-like protein TgSLP1, as well as to analyze the spatial organization of the gliding motor complex in *Toxoplasma gondii*.

Results regarding TgSLP1 have been published in **Wagner, Mirjam, Yuan Song, Elena Jiménez-Ruiz, Sonja Härtle, and Markus Meissner. 2023. 'The SUN-like protein TgSLP1 is essential for nuclear division in the apicomplexan parasite *Toxoplasma gondii*', Journal of cell science, 136.**

The results related to motility are currently being prepared for publication.

4.1 Establishment of expansion microscopies

To investigate the ultrastructure of proteins in *Toxoplasma gondii*, various ExM protocols were applied and optimized to achieve a three to fourfold physical expansion while preserving internal structural integrity. This was followed by imaging using 3D-STED microscopy. In this study, various fixation methods, primary and secondary antibodies, and reaction conditions were systematically evaluated to determine the most effective approach for high-resolution imaging.

4.1.1 Ultrastructure Expansion Microscopy (U-ExM)

The U-ExM protocol that was established in 2021 (Dos Santos Pacheco and Soldati-Favre 2021a) was modified and applied, as described in section 3.2.4.1.

To minimize protein damage, the denaturation temperature was set to 80 °C instead of the standard 95 °C. Additionally, a 0.2% PBS-Triton solution was used as the washing buffer, as 0.1% PBS-Tween was found to be ineffective for immunostaining under the conditions of this study.

Following the U-ExM procedure, the gel expanded to approximately three times its original volume (Fig. IV-1, left column). Compared to standard immunofluorescence assay (IFA) data obtained using a Leica DMi8 widefield microscope, the resolution was significantly enhanced when utilizing U-ExM in conjunction with the Abberior 3D-STED microscope (Fig. IV-1, right column). To evaluate the resolution and fluorescence intensity after U-ExM during parasite invasion, the invasion assay and U-ExM were conducted as described in Sections 3.2.3.3 and 3.2.4.1. A ring-shaped zone of tight attachment between the *T. gondii* and host cell membranes, the tight junction, was labeled using an anti-Ron2 antibody (Beck et al. 2014), while microtubules were stained with an antibody against acetylated tubulin. The acetylated tubulin staining remained stable and clearly visible following high-temperature denaturation, making it a reliable control in subsequent U-ExM experiments.

However, despite testing various time points and incubation temperatures, staining with dyes (such as Janelia Fluor HaloTag ligand) in the U-ExM protocol was unsuccessful, regardless of whether pre- or post-labeling methods were employed.

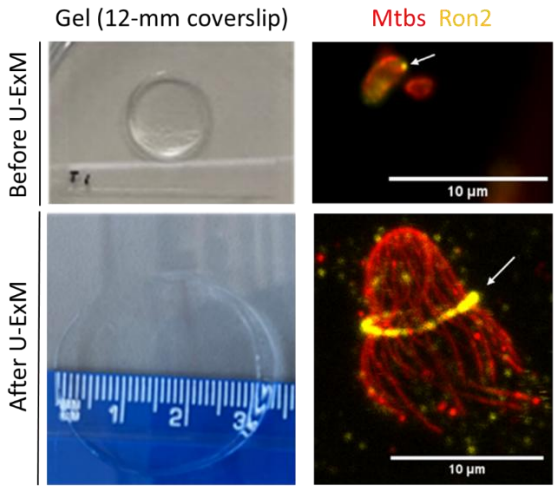

Figure IV-1. Comparison of ultrastructure expansion microscopy (U-ExM) before and after application.

Left column: Following U-ExM, the gel expanded to approximately three times its original size. **Right column:** After U-ExM and imaging with STED microscopy, both the volume and resolution of the parasite increased. Microtubules (Mtbs) were labeled with acetylated tubulin (red), while the tight junction ring was labeled using an anti-Ron2 antibody (yellow), as indicated by white arrows. Before U-ExM: Leica DMi8 widefield microscope, 100× objective. After U-ExM: 2D STED microscopy, 60× objective. Scale bar: 10 µm

4.1.2 Protein-retention Expansion Microscopy

The Protein-retention Expansion Microscopy (proExM) protocol used in this study is based on the literature published in 2017 (Halpern et al. 2017) for *Giardia*, a flagellated protozoan, was applied in this study to *Toxoplasma gondii*. The detailed protocol is described in section 3.2.4.2. Unlike U-ExM, labeling in ProExM was performed prior to digestion with 6 U/mL Proteinase K and subsequent expansion. A digestion time of either 3 hours or overnight yielded no observable differences. Due to the prolonged reaction time, an

incubation temperature of 37 °C was sufficient. In contrast to U-ExM, dye staining produced clear results; however, fluorescence signals from antibody staining were inferior compared to staining with dyes (Figure IV-14d). To optimize antibody staining, both pre- and post-labeling approaches were tested, along with increased antibody incubation times and reduced Proteinase K digestion times. Despite these efforts, antibody staining remained unsuccessful. Additionally, the expansion achieved with ProExM was not as good as U-ExM.

4.1.3 TurboID ExM

Formin 1 (FRM1) is a protein essential for generation of F-actin and is associated to the ring-like structure anchored to the conoids of both maternal and daughter cells. It is a protein expressed at low levels in *Toxoplasma gondii*, making its visualization particularly challenging, especially after the reduction in antigen density caused by physical expansion. However, for FRM1-Halo strain, a high cytosolic signal was detected with the Halo-antibody in U-ExM.

To determine the native distribution of these proteins, we aimed to identify a labeling method or marker that could provide a stronger signal than traditional antibody-based detection in ExM. Given that streptavidin is able to label multiple lysine residues on both the bait protein and nearby proteins; it has been demonstrated to offer significant advantages for detecting low-abundance proteins in ExM (Odenwald et al. 2023).

Thus, streptavidin labeling combined with U-ExM (short as TurboID ExM in this article) was applied to the *Toxoplasma gondii* strain 'FRM1-TiD' and the ΔKu80 DiCre *Toxoplasma gondii* strain as a negative control, following the protocol in Section 3.2.4.3. To optimize the labeling conditions, different biotin incubation

periods (0.5 h, 1 h, and 4.5 h) were tested; however, no obvious differences were detected in the results.

The images presented in Figure IV-2 were obtained using TurboID ExM combined with STED imaging using the Abberior 3D-STED microscope. In the expanded view, black arrows indicate the FRM1 signal in extracellular (mother) parasites, highlighting a distinct double-ring structure at the conoid. However, as the FRM1 signal becomes detectable in daughter cells (red arrows), the clarity of the double-ring structure in mother cells appears to diminish. Notably, the FRM1 signal is stronger in daughter cells than in mother cells. Additionally, FRM1 was observed to be distributed and accumulated in specific cytosolic structures within both mother and daughter cells.

As a negative control, the ΔKu80 DiCre strain, which lacks the target protein for TurboID, underwent the same experimental procedures as the FRM1-TiD strain. However, despite the absence of the target protein, a signal was still detected throughout the parasite, with accumulation at the conoid and within the cytosol (Figure IV-3). This high background signal in TurboID ExM complicates the distinction between the true FRM1 signal and nonspecific labeling, thereby limiting the method's applicability in *Toxoplasma gondii* research.

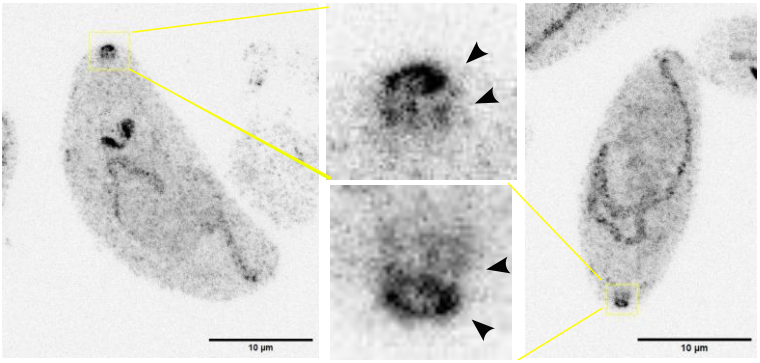

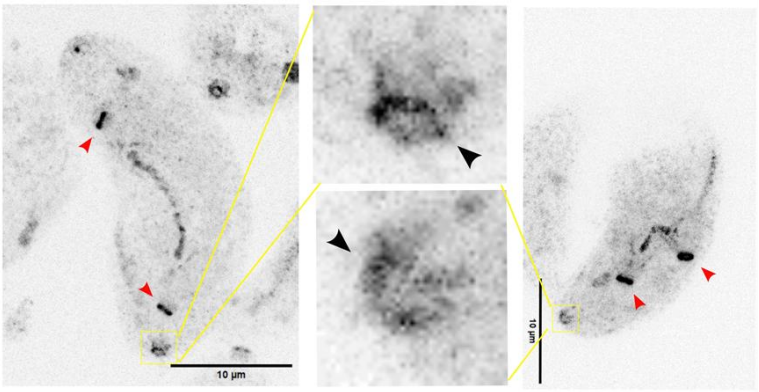

Figure IV-2. Distribution of FRM1 using TurboID ExM.

Confocal sections of TurboID ExM captured with a 100× objective (Abberior 3D-STED microscope). The FRM1-TiD strain was incubated with biotin for 1 hour and subsequently labeled with Alexa-488-conjugated streptavidin. Mitochondrial signal was also labeled by streptavidin in the cytosol with unfixed form. Black arrows: FRM1 signal at the mother cells; red arrows: FRM1 signal at the daughter cells. Scale bar: 10 µm.

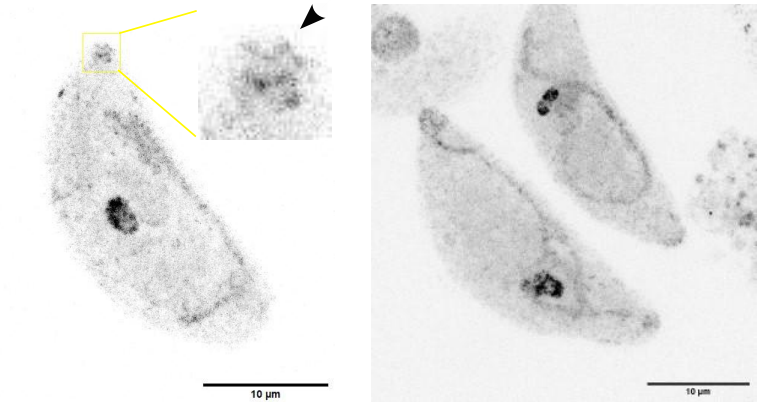

Figure IV-3. TurboID ExM causes background in negative control.

Confocal sections of TurboID ExM captured with a 100× objective (Abberior 3D-STED microscope). The ΔKu80 DiCre strain was incubated with biotin for 1 hour and

subsequently labeled with Alexa-488-conjugated streptavidin. Black arrows: FRM1 signal at the mother cells. Scale bar: 10 µm.

4.1.4 Expansion microscopy with cryofixation

Compared to chemical fixation, cryofixation is considered the gold standard for preserving native cellular architecture (Laporte et al. 2022). To gain a more accurate representation of the native ultrastructure associated with gliding motility and to enhance visualization, expansion microscopy with cryofixation (Cryo-ExM) was explored and applied to *Toxoplasma gondii*. The Cryo-ExM protocol employed in this study was developed in Prof. Gautam Dey's laboratory at the European Molecular Biology Laboratory (EMBL) in Heidelberg and is detailed in Section 3.2.4.4.

N-hydroxy succinimide ester (NHS-ester) is a chemical reagent that was utilized to label the primary amines of proteins in *Toxoplasma gondii* (Figure IV-4). NHS labeling in Cryo-ExM led to extensive coverage of the expanded parasite's surface and enabled the visualization of vesicular structures.

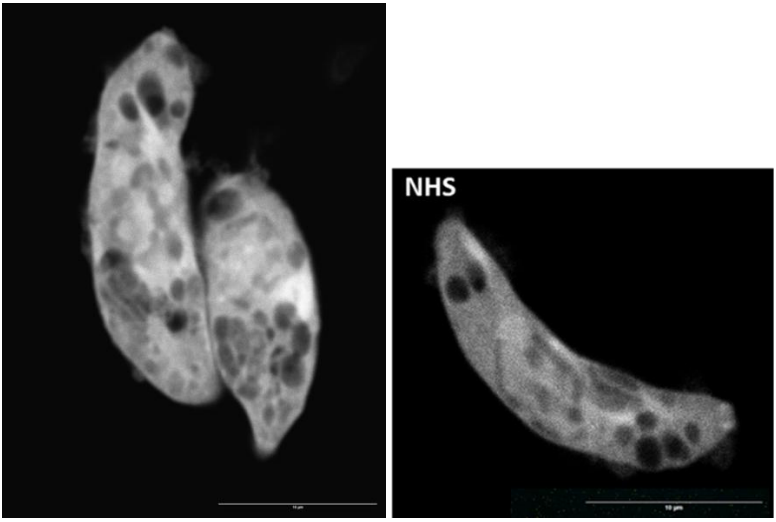

Figure IV-4. NHS-ester labelling of tachyzoites using Cryo-ExM.

A maximum projection image of primary amines in *Toxoplasma gondii* was obtained using Cryo-ExM, revealing proteins on the surface and vesicular structures. The experiment was conducted by Yuan Song and Dr. Javier Periz in Prof. Gautam Dey's laboratory at EMBL. Images were captured by Dr. Javier Periz using an Abberior 3D-STED microscope (100× objective, confocal) with NHS-ester Alexa-647 labeling. Scale bar: 10 µm.

In summary, Section 4.1 presents the testing and optimization of various ExM techniques and labeling methods. In the subsequent sections, these methodologies were applied to investigate two biological questions: the distribution of SLP1 during nucleus dividing process and the mechanisms of gliding motility in *T. gondii*.

4.2 The nuclear division in *Toxoplasma gondii* relies on TgSLP1

As a linker between the nucleoskeleton and cytoskeleton, the LINC complex is crucial for linking nuclear and cytoplasmic functions by bridging the nuclear membranes and anchoring the cytoskeleton to the nucleus (Haque et al. 2006).

In opisthokonts, the LINC complex consist of SUN domain proteins and KASH domain proteins (Tapley and Starr 2013).

4.2.1 Previously completed work by Mirjam Wagner

As the foundation of this study, my colleague Mirjam Wagner identified TgSLP1 (SUN-like protein 1) and TgSLP2 (SUN-like protein 2), both containing a SUN domain, along with a hypothetical protein possessing an UNC-50 domain in the *Toxoplasma gondii* genome as strong potential members of an apicomplexan LINC complex. Her findings suggest that TgSLP1 is a critical protein essential for mitosis and potentially associated with the centrocone (Wagner et al. 2023) (described in Section 1.2.6.1).

However, the images obtained using the Leica DMi8 widefield microscope lack the necessary resolution to make definitive conclusions regarding its precise localization and function (Figure IV-5).

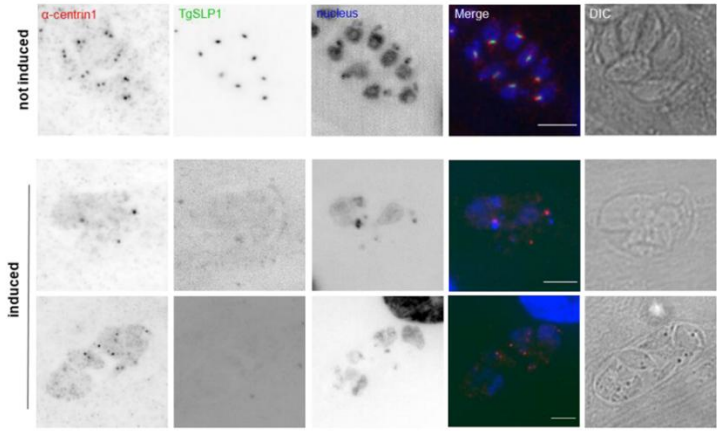

Figure IV-5. IFA results of the *T. gondii* with or without TgSLP1 captured by Mirjam Wagner.

IFA images captured by Mirjam Wagner using Leica. Scale bars: 5 µm (Wagner et al. 2023).

Thus, super resolution microscopy was applied to analyze the localization and relationships between TgSLP1 and other components of centrocone in the following sections.

4.2.2 Localization of TgSLP1 during the division

To characterize TgSLP1, this study used a 'RH-Δku80-DiCre-LoxP-TgSLP1-sYFP2-LoxP' *Toxoplasma gondii* strain generated by Mirjam Wagner (Wagner et al. 2023; Wagner 2023). The TgSLP1 was labeled with a fluorescent protein sYFP2, and a LoxP site, enabling locus excision upon rapamycin induction.

Given that TgSLP1 appears to divide following the division of the outer core, as indicated by its colocalization with the outer core marker centrin1 (Wagner et al. 2023); investigating its relationship with specific cellular components in different phases of tachyzoite development is crucial for understanding its localization and function. To assess the subcellular localization of TgSLP1 in relation to the inner core centrosome, kinetochore, and centromeres, the proteins Cep250_L1 (Suvorova et al. 2015), Nuf2 (Farrell and Gubbels 2014) and Chromo1 (Gissot et al. 2012) were endogenously labeled with a 3×HA tag at the C-terminal end using CRISPR/Cas9 (Stortz et al. 2019), as detailed in section 3.2. Despite multiple transfection attempts, we failed to establish a *Toxoplasma gondii* strain with endogenously 3×HA-tagged MORN1. Transient transfection of parasites expressing fluorescently tagged MORN1 resulted in overexpression phenotypes, complicating the distinction between the effects of TgSLP1 knockout and the phenotypic consequences of MORN1 overexpression.

For 'TgSLP1-sYFP2-Cep250_L1-3xHA', 'TgSLP1-sYFP2-Nuf2-3xHA' and 'TgSLP1-sYFP2-Chromo1-3xHA' *Toxoplasma gondii* strains, correct addtion of the tags was proved by PCR (part pf data shown in Figure IV-6 as an example).

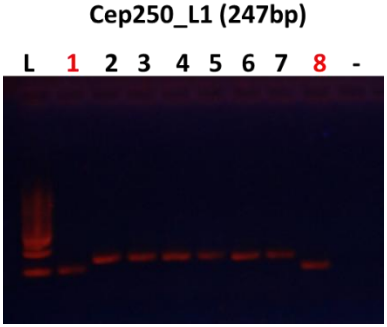

Figure IV-6. PCR result of 'TgSLP1-sYFP2-Cep250_L1-3xHA' *Toxoplasma gondii* strains.

No.1 and no.8 were positive strains. **L**: DNA Ladder 250bp (Sigma). -: negative control.

U-ExM was employed to investigate the localization of TgSLP1, microtubules (Mtbs), and Cep250_L1 using tri-labeling, yielding high-resolution images with a substantial expansion factor (Figure IV-7). The localization of Cep250_L1 was observed in proximity to the mitotic spindle (Figure IV-7, merged channel). However, the TgSLP1 signal was either undetectable or nonspecific. Some TgSLP1 signals appeared as background fluorescence overlapping with the red channel (Figure IV-7b).

This result also highlights the limitations of U-ExM, as discussed in Section 4.1.1.

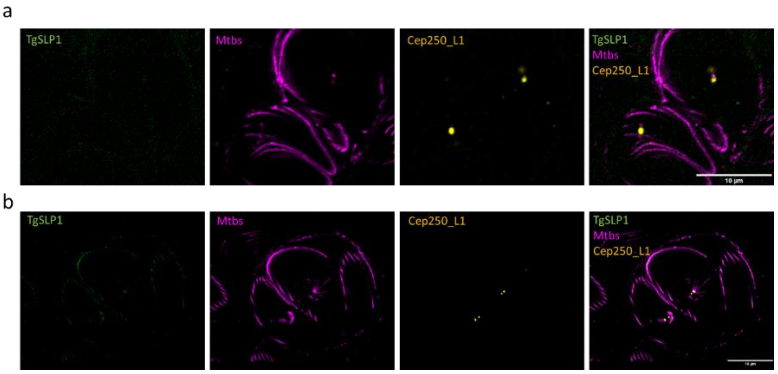

Figure IV-7. Tri labeling of TgSLP1, Mtbs and Cep250_L1 using U-ExM.

Representative images illustrate the distribution of SUN-like protein 1 (TgSLP1), microtubules (Mtbs), and Cep250_L1 in *Toxoplasma gondii*. TgSLP1 was tagged with sYFP (green), Mtbs were labeled with an acetylated tubulin antibody (magenta), and Cep250_L1 was labeled with an HA antibody (yellow). **(a)** The TgSLP1 signal was not detected. **(b)** The specific signal of TgSLP1 was not observed, while Cep250_L1 appeared to be closely associated with the mitotic spindle. Maximum projection images were acquired using confocal microscopy with a 100× objective. Scale bar: 10 µm.

Consequently, localization analysis was conducted exclusively using STED super-resolution microscopy to elucidate the spatial relationships between TgSLP1 and key cellular structures, including the centrosome, kinetochore, and centromeres, across stages of the cell cycle (Figure IV-8). The resolution of STED is sufficient for the localization analysis.

At the beginning of S-phase, a single centrosome and a single TgSLP1 signal were detected. In late S-phase, Cep250_L1 underwent division, whereas TgSLP1 remained undivided. During the transition from late S-phase to the early M-phase, TgSLP1 divided and exhibited a close connection with the centrosome (Fig. IV-8a, left column). Although TgSLP1 remained connected to centrosome, its division occurred a little later than that of the inner core of the centrosome.

As shown in the middle column of Fig. IV-8a, in early S-phase, Nuf2 colocalized with TgSLP1 as a single signal, similar to Cep250_L1. However, in late S-phase stage, both proteins duplicated and divided simultaneously. In M-phase, Nuf2 and TgSLP1 remained colocalized during the budding process.

TgSLP1 was also associated with Chromo1, a centromere marker. Unlike Cep250_L1, Nuf2, and TgSLP1, Chromo1 remained undivided until M-phase (Figure IV-8a, right column), making it the last component in this study to undergo division.

Earlier researches characterized structural dynamics of the apicomplexan centrosome throughout mitotic progression, demonstrating that the outer core separates first, followed by the inner core, and subsequently the centromeres (Suvorova et al. 2015; Tomasina et al. 2022). Collectively, these data indicate that the duplication and division of TgSLP1 occur simultaneously with the kinetochore (Nuf2) and are associated with the centrosome, including both the outer core (Centrin1) and inner core (Cep250_L1). This process may contribute to the division of centromeres, as marked by Chromo1, as illustrated in Figure IV-8b.

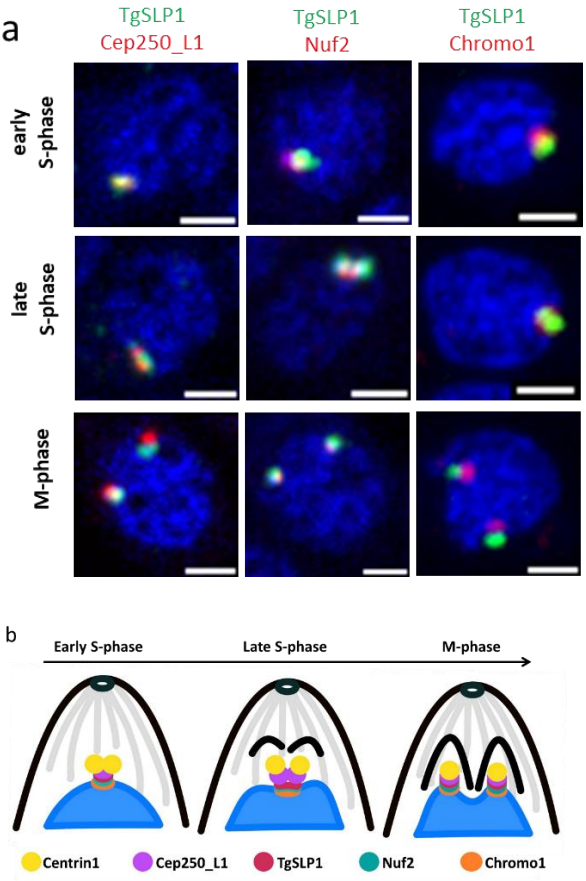

Figure IV-8. TgSLP1 is found at the kinetochore and appears to connect the centromeres to the nuclear menbrane during cell division.

(a) 3D-STED SRM of parasite nuclei that are in different cell cycle stages expressing TgSLP1-sYFP2 and Cep250_L1-3×HA (inner core centrosome), Nuf2-3×HA (kinetochore) or Chromo1-3×HA (centromeres). TgSLP1 was labeled with GFP antibody; Cep250_L1, Nuf2 and Chromo1HA were labeled with HA antibody; nuclei were stained with Hoechst 33342. Scale bars: 1 µm. **(b)** Schematic diagram of the *Toxoplasma gondii* centrosome (outer core: centrin1, yellow; inner core: Cep250_L1, purple), kinetochore (Nuf2, red) and centromeres (Chromo1, orange) in regard to TgSLP1 (green) in different stages of the cell cycle.

4.2.3 Knockout of TgSLP1 results in compromised centromere integrity

Previous Studies in other eukaryotes have shown that the LINC complex, particularly SUN proteins, is necessary for kinetochore assembling (Yadav and Sanyal 2018). To investigate the function and role of TgSLP1 in division cycle of *Toxoplasma gondii*, the knockout assay was performed under induction for 48h. A non-induced control was included for the same time points.

To gain a further understanding of centrosome morphology, we also applied STED to visualize the *T. gondii* engineered to express epitope-tagged Cep250_L1, Nuf2, and Chromo1, cultured under rapamycin-treated and untreated conditions. Phenotypic data of *Toxoplasma gondii* vacuoles was obtained with IFA (Figure IV-9a).

For untreated tachyzoites, all the components mentioned above are closely associated (Figure IV-9a). The results of Centrin1 and Cep250_L1 analysis revealed that the outer and inner cores of the centrosome remained connected in some instances, suggesting that their interaction may not be affected by the loss of TgSLP1. However, the intensity of Centrin1 appeared abnormal, with noise signal detected (Figure IV-9a, left column, KO). In the absence of TgSLP1, incorrect localization and division of the kinetochore and centromeres (Nuf2 and Chromo1) were observed, resulting in their clustering and random distribution within the nucleus (Figure IV-9a, middle and right columns, KO). These findings indicate that TgSLP1 may play a role in linking the centrosome to the kinetochore and centromeres (Figure IV-9b).

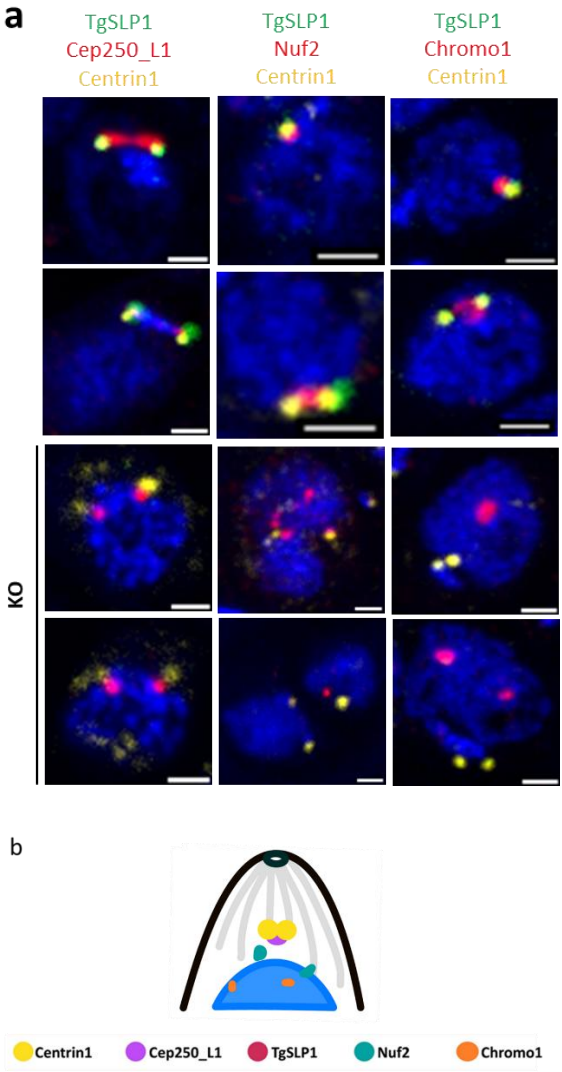

Figure IV-9. The conditional knockout of TgSLP1 results in unsuccessful nuclear division.

(a) 3D-STED super-resolution microscopy of parasite nuclei expressing Cep250_L1-3×HA, Nuf2-3×HA or Chromo1-3×HA in TgSLP1 and TgSLP1-cKO parasites. TgSLP1 was labeled

with GFP antibody; Cep250_L1, Nuf2 and Chromo1HA were labeled with HA antibody; centrin1 was visualized with centrin1 antibody and the nuclei were stained with Hoechst 33342. Scale bars: 1 µm. **(b)** Schematic representation of centrosome (outer core: centrin1, yellow; inner core: Cep250_L1, purple), kinetochore (Nuf2, red) and centromeres (Chromo1, orange) in TgSLP1-cKO parasites.

The *Toxoplasma gondii* vacuoles displaying normal and abnormal Centrin1 signals were quantified under conditions with and without rapamycin induction. Quantification analysis was conducted using Microsoft Excel (Figure IV-10). In non-induced parasites, more than 92% of vacuoles exhibited normal Centrin1 signal intensity and localization. In contrast, following 48 hours of rapamycin induction, fewer than 5% of vacuoles retained normal Centrin1 localization.

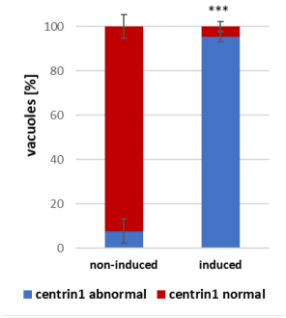

Figure IV-10. Measurement of vacuoles with both normal and abnormal centrin1 signals.

A total of 100 PV were counted under both under rapamycin-treated and untreated conditions. The experiment was performed in three biological replicates. Error bars represent the standard deviation (s.d.). ***P < 0.001.

4.3 Super resolution to analyze the machinery for gliding and invasion in *Toxoplasma gondii*

As described in Section 1.2.5, *Toxoplasma gondii* relies on gliding motility for survival. The prevailing linear model describes a tiny space between the PM and IMC. This space is maintained by GAPs and contains essential motor components, including MyoA, F-actin, GAPs, and GAC proteins. During motility, proteins expressed from apical complex organelles engage with the actin-guided motor complex then undergoes translocation, generating a propulsive force that drives the parasite in the inverse orientation (Frenal et al. 2017; Venugopal and Marion 2018; Dos Santos Pacheco et al. 2022; Graindorge et al. 2016; Tardieux and Baum 2016).

However, certain data obtained from different time points and various techniques do not fully align with this model, suggesting that the linear model may not be the sole or entirely accurate mechanism of motor complex in *T. gondii* (Egarter et al. 2014; Periz et al. 2017; Yasuda et al. 1988; Periz et al. 2019).

Due to the challenges associated with imaging apicomplexan actin and the resolution limitations of standard light microscopy techniques, which are insufficient to resolve the 30-nm axial space, the linear motor components have not been directly visualized (Halpern et al. 2017)

4.3.1 F-actin is distributed throughout the cytosol of *Toxoplasma gondii*

Actin, as the most critical structural component of gliding motility, is believed to orchestrate the coordination of all other motor elements to facilitate cellular migration. A *Toxoplasma gondii* strain in which the actin chromobody (Cb) is

fused to Emerald GFP was used to analyze the localization of F-actin (Shaner, Patterson, and Davidson 2007). This construct was specifically designed to bind to parasite F-actin without altering the overall quantity of F-actin (Periz et al. 2017). Building upon this cell line, additional structures were subsequently tagged using CRISPR/Cas9 technology to enable colocalization analysis. In the present study, the 'CbEmerald-MyoA-SNAP' strain was dual-labeled to investigate the spatial distribution of F-actin and Myosin A, thereby facilitating the precise localization of motor complexes (Periz et al. 2019).

The U-ExM data revealed that MyoA is distributed across the entire parasite surface, except at the posterior end. F-actin was observed beneath MyoA within the cytosol of tachyzoites during migration and invasion. Actin filaments accumulated at the posterior pole of the tachyzoite, forming a distinct ring structure (Figure IV-11a, indicated by arrows). Additionally, actin filaments were released from the basal end of the tachyzoite to the external environment (Figure IV-11b, indicated by arrows). During parasite replication, F-actin forms a circular formation at the conoid of a daughter cell and appears to be distributed along the basal surface of the daughter cell (Figure IV-11c, indicated by arrows).

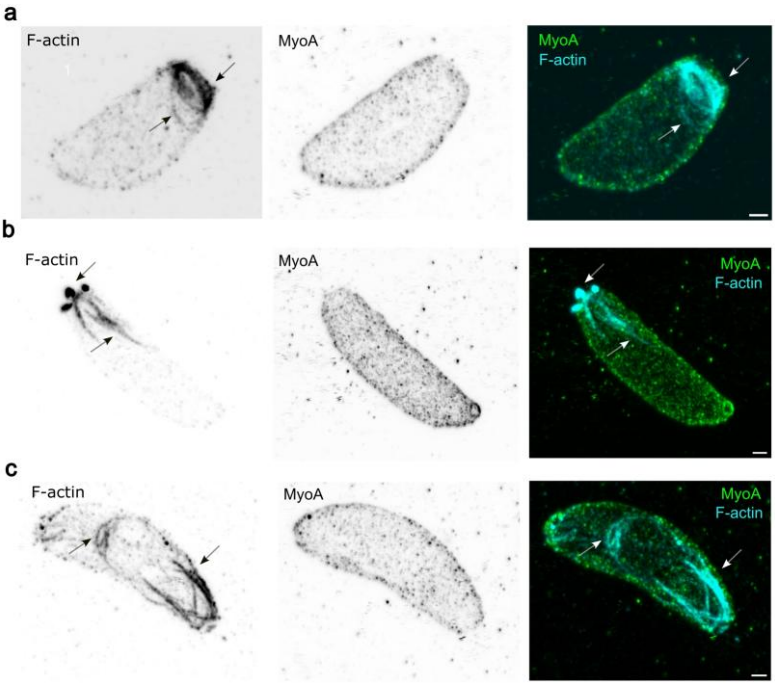

Figure IV-11. Dual Labeling of F-Actin and MyoA in *Toxoplasma gondii* Using U-ExM.

Representative maximum projection images obtained via U-ExM illustrate the distribution of MyoA-SNAP (labeled with SNAP antibody, shown in green) and F-actin (labeled with CbEmerald GFP, shown in cyan) in tachyzoites during migration and invasion. **(a)** F-actin (indicated by arrows) form an annular structure at the posterior part of the tachyzoite. **(b)** F-actin (indicated by arrows) extend outward from the basal aperture of the tachyzoite. **(c)** F-actin (indicated by arrows) form a ring at the conoid and the surface of a daughter cell. Images were acquired using STED microscopy with a 60× objective. Scale bar: 2 µm.

To analyze the relationship between F-actin and MyoA, a quantification was conducted as described in Section 3.2.5. Fluorescence intensity and spatial distribution measurements were obtained from fifteen distinct locations per parasite—five at the apical region, five at the midsection, and five at the basal

region—to provide a comprehensive representation of their localization. Figure IV-12 presents one representative example of these measurements, indicating that actin exhibits relatively low fluorescence intensity and is positioned beneath MyoA.

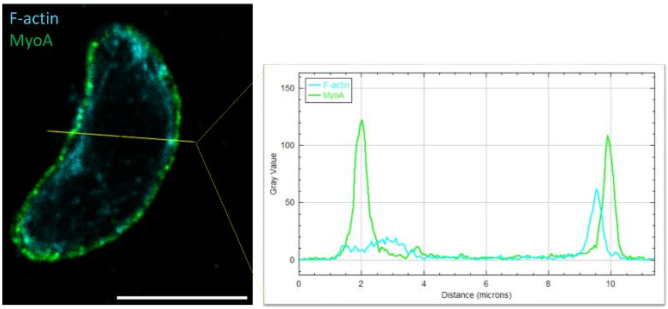

Figure IV-12. Analysis of positional relationship between F-actin and Myosin A.

For 'CbEmerald-MyoA-SNAP' U-ExM section, Fiji (ImageJ) was utilized to analyze fluorescence intensity and spatial distance at a certain location (yellow line). Green: MyoA; cyan: actin-CbEmerald GFP. Scale bar: 10 µm.

For each parasite, fifteen measurements were taken at distinct locations, including five points at the apical region, five at the midsection, and five at the basal region. The quantitative data were analyzed using mathematical calculations and subsequently plotted using Microsoft Excel (Figure IV-13).

$$\frac{Distance_{actin}}{Distance_{MyoA}} = \frac{distance_{Actin\ Fluorescence\ signal\ last\ appears} - distance_{Actin\ Fluorescence\ signal\ first\ appears}}{distance_{MyoA\ Fluorescence\ signal\ last\ appears} - distance_{MyoA\ Fluorescence\ signal\ first\ appears}}$$

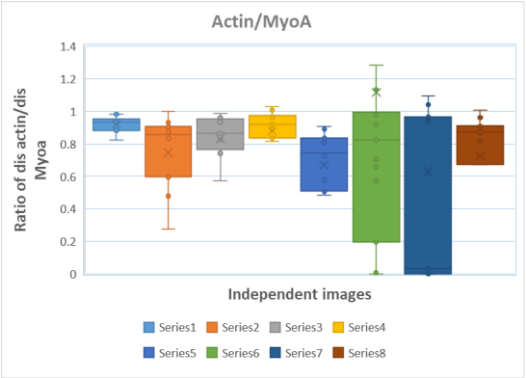

Figure IV-13. Quantification of the spatial correlation between F-Actin and MyoA.

The spatial relationship between F-Actin and MyoA was quantified by calculating the ratio of $distance_{Actin}$ to $distance_{MyoA}$. This analysis was conducted using data obtained from eight parasites (measurements 12, 13, 17, 18, 19, 5, 21, and 8) and plotted using Microsoft Excel. The experiments were performed in independent biological triplicates to ensure reproducibility and statistical robustness. dis = distance. Series: fluorescence intensity and spatial distribution measurements at fifteen distinct locations for one parasite.

Quantification of the relative positioning between F-Actin and MyoA (Figure IV-13) demonstrates that the majority of the ratios of $distance_{Actin}$ to $distance_{MyoA}$ are less than one. This observation indicates that nearly all fluorescence signals corresponding to Actin in these replicates were localized on the cytosolic side relative to the fluorescence signals of MyoA. The occasional ratios exceeding one may correspond to released Actin, as depicted in Figure IV-11b.

Despite extensive efforts, we have been unable to conclusively determine whether F-actin localizes at the PM-IMC space or not of *Toxoplasma gondii*.

4.3.2 Myosin A is situated on the exterior of inner membrane complex 1 and the subpellicular microtubules.

To investigate the colocalization of MyoA and subpellicular microtubules (Mtbs), U-ExM was performed on gliding and invading parasites (Figure IV-14a and IV-14b, respectively). MyoA was labeled using a SNAP (green) antibody, while Mtbs were labeled with an acetylated tubulin antibody (magenta). Figure IV-14a depicts a protruding tachyzoite, in which tubulin polymers fibers are clearly visualized. In contrast, Figure IV-14b captures an invading, non-protruding parasite with a distinct TJ. MyoA appears to be distributed in a non-uniform manner, accumulating near the apical polar ring in the protruding parasite (Figure IV-14a, expanded view). Additionally, a fluorescence accumulation of MyoA is observed at the tight junction region (Figure IV-14b, expanded view).

According to the linear model, MyoA is localized between the PM and IMC in *Toxoplasma gondii*. To investigate its precise localization, an antibody against the surface protein SAG1 was used to label the PM. However, in U-ExM, SAG1 exhibited non-specific labeling (data not shown), necessitating the use of ProExM without permeabilization (Figure IV-14c). In invading parasites, MyoA-YFP was not labeled, while SAG1-Halo was stained using Janelia Fluor HaloTag ligand 646. As expected, the region of the tachyzoites that inside the host cell remained unstained due to the absence of Triton 100 treatment. MyoA-YFP was detected covering the parasite surface, though some areas appeared deformed. This deformation may be attributed to ProExM processing, despite its relatively mild effects compared to U-ExM.

Due to limitations in antibody compatibility, a triple-labeling experiment for MyoA, IMC1, and microtubules (Mtbs) was conducted using ProExM. Janelia

Fluor HaloTag dye was used to label IMC1-Halo, while SNAP and acetylated tubulin antibodies derived from rabbit and mouse were employed to label MyoA and Mtbs, respectively to avoid the antibody influence from same or close species (Figure IV-14d).

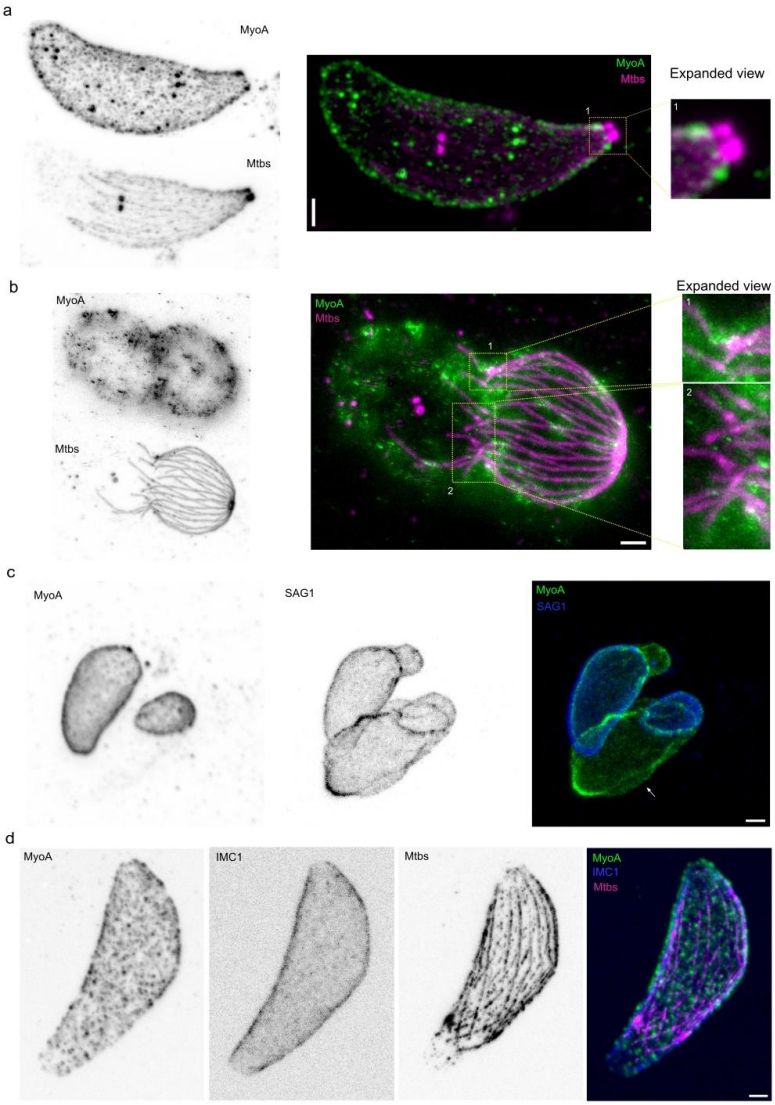

Figure IV-14. Locolization analysis of MyoA using U-ExM and proExM

Representative maximum projection images from U-ExM and proExM experiments illustrate the distribution of MyoA-SNAP (labeled with SNAP antibody, shown in green)

and acetylated tubulin antibody (magenta). **(a)** A parasite labeled with MyoA-SNAP and acetylated tubulin antibodies is displayed in single and merged channels. The images reveal the accumulation of MyoA-SNAP below the conoid, with no detectable distribution at the conoid itself. **(b)** An invading parasite labeled with MyoA-SNAP and acetylated tubulin antibodies is shown in single and merged channels. The images demonstrate the accumulation of MyoA-SNAP at the tight junction and its distribution above the subpellicular microtubules (Mtbs). **(c)** The distribution of MyoA-YFP and SAG1-halo (blue) during invasion is depicted under proExM conditions, showing that the invaded surface of tachyzoites remained unstained with halo antibody without permeablization. SAG1 was labeled with halo antibody; MyoA was labeled with GFP antibody. **(d)** A tri-labeled single parasite is presented, showing MyoA-SNAP (with SNAP antibody), IMC1-halo dye (blue), and acetylated tubulin antibody in single and merged channels. Images were acquired using STED microscopy ((a) and (b), MyoA), or confocal microscopy, with a 60× objective. Scale bar: 2 μm.

However, the antibody signals obtained with ProExM were weaker compared to those observed in U-ExM, and the expansion factor was also lower. The reduced expansion multiple was insufficient for accurately analyzing the colocalization of MyoA with either the PM or the IMC.

To further analyze the colocalization of MyoA and IMC1 while avoiding issues arising from antibodies derived from similar or identical species, an anti-IMC1 antibody was used for direct labeling. Utilizing U-ExM combined with STED microscopy, the resolution achieved was sufficient to distinguish these two structures (Figure IV-15), demonstrating that Myosin A is localized above IMC1.

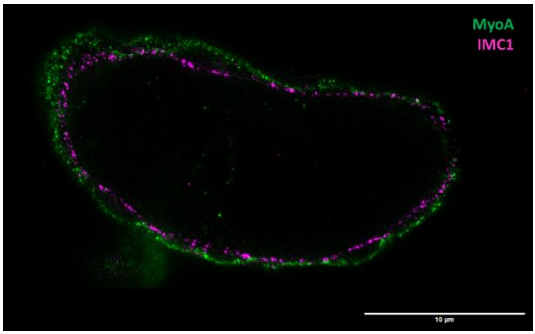

Figure IV-15. Localization analysis of MyoA and IMC1 using U-ExM.

A representative sectional image from U-ExM experiments illustrates the distribution of MyoA-SNAP (labeled with SNAP antibody, shown in green) and IMC1 antibody (magenta). Image obtained using STED microscopy with 100× obj. Scale bar: 10 µm.

To analyze the positional relationship of MyoA and IMC1, the analysis was conducted using mathematical calculations, and the results were subsequently plotted using Microsoft Excel (Figure IV-16). The methodology was consistent with the quantification approach used for Actin and MyoA, as detailed in Sections 3.2.5 and 4.3.1. The analysis revealed that the majority of the ratios of $distance_{IMC1}$ to $distance_{MyoA}$ were less than one, further confirming that IMC1 localizes beneath MyoA. The occasional ratios exceeding one may arise from background interference caused by poly-L-lysine or may represent a genuine signal of MyoA, suggesting the presence of an additional population of MyoA within the cytosol.

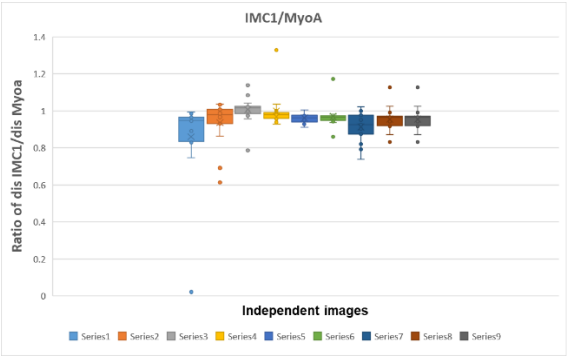

Figure IV-16. Quantification of the spatial relationship between IMC1 and MyoA.

The spatial relationship between IMC1 and MyoA was quantified by calculating the ratio of $distance_{IMC1}$ to $distance_{MyoA}$. This analysis was conducted using data obtained from nine parasites (measurements 1 to 9) and plotted using Microsoft Excel. The assays were repeated for three times independently to ensure reproducibility and statistical robustness. dis = distance. Series: fluorescence intensity and spatial distribution measurements at fifteen distinct locations for one parasite.

It is important to note that the morphology of IMC1 and MyoA appears slightly different from what is observed under immunofluorescence assay (IFA) and live imaging. This discrepancy may be attributed to the series of treatments involved in expansion microscopy (ExM), such as denaturation or expansion processes. Nevertheless, the primary objective of determining the positional relationship between the two proteins has been successfully achieved, and the results of the colocalization analysis remain reliable.

Based on the finding that MyoA localizes above IMC1 and the Mtbs, further colocalization analysis of IMC1 and Mtbs was conducted on both gliding and invading parasites using U-ExM (Figure IV-17). The results revealed that Mtbs localize beneath IMC1 (Figure IV-17a, expanded view 1, indicated by the yellow arrow). In gliding parasites, IMC1 was observed to distribute along the parasite's surface, with the exception of the posterior hole (Figure IV-17, expanded views 2). Figure IV-17b demonstrates that Mtbs localize below IMC1 at the tight junction (indicated by the yellow arrow). The orthogonal views further corroborate the colocalization results, and the structure of tubulin polymers fibers is clearly depicted in both protruded (Figure IV-17a, expanded views 3) and non-protruded parasites (Figure IV-17b, expanded view).

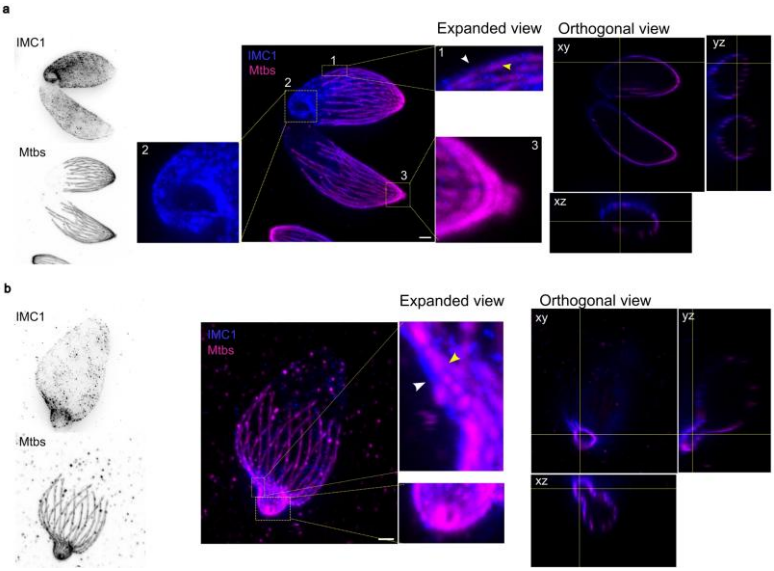

Figure IV-17. Localization analysis of IMC1 and Mtbs using U-ExM.

Representative images illustrate the distribution of inner membrane complex 1 (IMC1) and microtubules (Mtbs) in tachyzoites during migration and invasion. **(a)** Extracellular parasites labeled with IMC1-halo antibody (blue) and acetylated tubulin antibody (magenta) is displayed in single and merged channels. **(b)** An invaded parasite labeled with IMC1-halo antibody (blue) and acetylated tubulin antibody (magenta) is shown in single and merged channels. Image obtained using STED microscopy with 60× obj. Scale bar: 2 µm.

4.3.3 EM imaging indicates the existence of two populations of MyoA

The localization quantification revealed that the majority of MyoA localizes above IMC1, while a subset localizes below, suggesting the potential existence of an additional population of MyoA on the cytosolic side (Figure IV-16). To investigate this possibility, the MyoA-SNAP cell line was fixed using 4%

paraformaldehyde and 0.1% glutaraldehyde and subsequently sent to Prof. Katherina Psathaki's laboratory for immunogold-labeling electron microscopy (EM) analysis. In this study, the maximum distance between the epitope and the gold particle should not exceed 20 nm when using a standard primary antibody. This distance is influenced by the size of the primary antibody used. For labeling, 10-nm electron-dense protein-A (PA)/gold particles (PAG) against rabbit was employed for binding to the Fc-subunit of the primary antibody in a 1:1 ratio labeling specifically transmission electron microscopy (TEM). Immunogold-labeling EM is a highly effective technique for achieving precise mapping of antigens at the subcellular scale. (Slot and Geuze 2007; Tokuyasu 1973; Tokuyasu 1980).

Figure IV-18 is presented as an example, suggesting MyoA distributed in the cytosol, associated with IMC (yellow arrows), or between PM and IMC (magenta arrows).

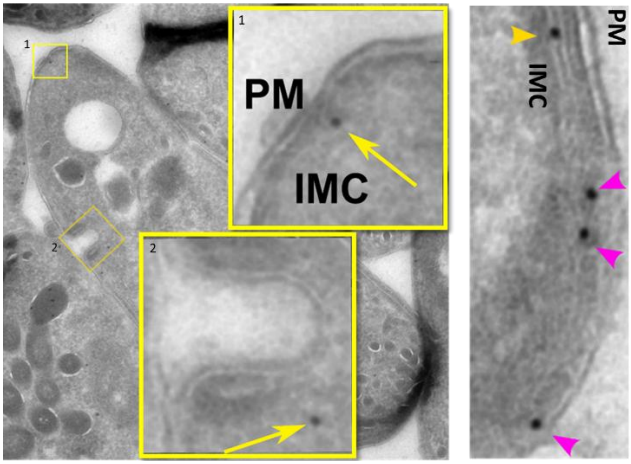

Figure IV-18. Distribution analysis of MyoA using immunogold-labeling EM.

The yellow arrows indicate MyoA associated with IMC1 or localized within the cytosol, while the magenta arrows highlight populations of MyoA localized between the PM and IMC in the immunogold-labeling EM data. Images developed by Prof. Katherina Psathaki's laboratory.

For the immunogold-labeling EM data, labeled MyoA beads were counted and categorized into four groups: (A) located between PM IMC, (B) associated with the IMC, (C) undefined due to a lack of structural integrity in *Toxoplasma gondii*, and (D) present within the cytosol (Table IV-1). Based on these classifications, quantitative analysis was conducted using Microsoft Excel (Figure IV-19).

Table IV-1. Classification of labeled MyoA beads.

replications	beads FOV	A. PM-IMC	B. IMC associated	C. not define	D. cytosolic
1	25	1	4	2	18
2	154	15	14	32	93
3	275	29	31	27	188

*Immunogold-labeling EM for MyoA were performed in biological triplicates.

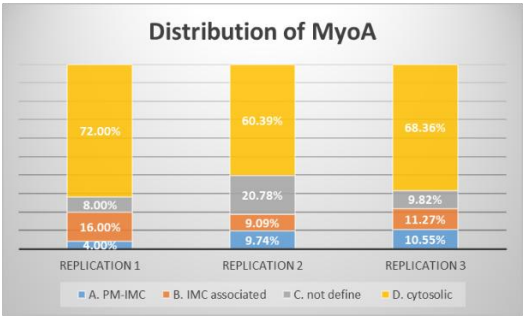

Figure IV-19. Quantification of MyoA distribution using immunogold-labeling EM.

Quantification data were analyzed and visualized using Microsoft Excel. **(A)** MyoA beads located between PM and IMC (blue). **(B)** MyoA beads associated with the IMC (orange). **(C)** MyoA beads undefined (grey). **(D)** MyoA beads present within the cytosol of parasites. R: replication.

IgG-gold complexes generate a higher number of gold particles but exhibit lower precision. This is due to the frequent combination with two or more gold particles to the primary antibody, which increases the distance between the gold marker and the target epitope. Immunogold-labeling EM revealed a limited number of labeled MyoA particles, with even fewer observed between the PM and the IMC. This may be attributed to the low binding efficiency of protein A-gold (PAG). However, populations of MyoA associated with IMC1 or located beneath the IMC were detected.

4.3.4 EM reveals the distribution of MyoA in association with GAP45

Another key component of the motor complex is GAP45, which functions to connect and maintain the space between PM and IMC while also associating with MyoA. To determine its localization, U-ExM was performed.

The shooting angle of Figure IV-20a clearly depicts the tubulin polymer fibers at the conoid, as well as the 22 subpellicular microtubules extending from the conoid. However, a significant gap is observed between GAP45 and the microtubules (section z7; indicated by the yellow and white arrows, respectively), a feature that was not visualized in the immunofluorescence assay (IFA). This observation suggests that GAP45 may have lost its connection to the IMC, likely due to the denaturation process involved in U-ExM, which includes high-temperature (80°C) treatment and sodium dodecyl sulfate (SDS) exposure.

In the absence of a connection to the IMC, GAP45 adopts an expanded morphology at the tight junction, possibly due to the mechanical forces exerted during invasion (Figure IV-20b, yellow arrows). However, certain regions retain their connections; for instance, the expanded view reveals an association

between GAP45 and the microtubules, suggesting that GAP45 is localized above the microtubules. These findings are align with the linear model.

The apparent artifacts observed in GAP45 localization highlight the importance of conducting IFA controls in parallel with ExM to ensure accurate interpretation of structural relationships.

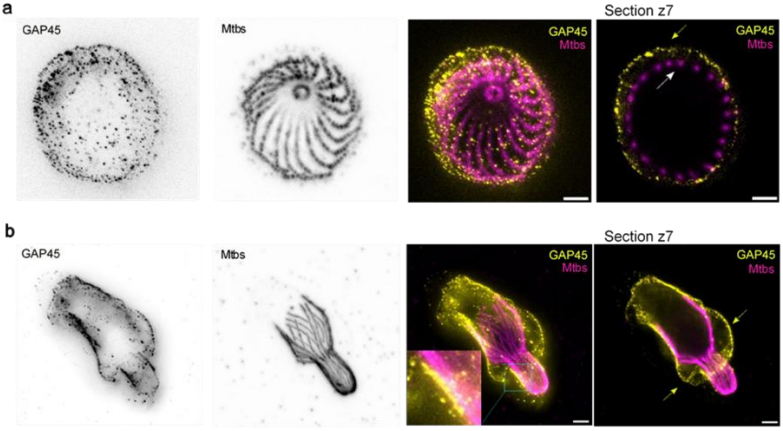

Figure IV-20. Localization analysis of GAP45 and Mtbs using U-ExM.

Representative images showing distribution of glidesome associated protein 45 (GAP45) and microtubles (Mtbs) in tachyzoites during gliding and invasion. **(a)** U-ExM Max projection and section z7 of gliding parasite with GAP45 antibody (yellow; indicated by the yellow arrow) and acetylated tubulin antibody (magenta; indicated by the white arrow) in single channel and merge channels, respectively. **(b)** U-ExM Max projection of invading parasite with GAP45 antibody (yellow; indicated by yellow arrows) and acetylated tubulin antibody (magenta) in single channel and merge channels, respectively. Image obtained using STED microscopy with 60× obj. Scale bar: 2 µm.

4.3.5 GAC is an active protein found in both the conoid and the cytosol.

Although GAC (Glideosome-Associated Connector) has not been described as localized in close proximity to most motor components, it function as a critical factor in the motility of *Toxoplasma gondii*. GAC facilitates motility by interacting with and connecting microneme protein-2 (MIC2) to the actomyosin system. Additionally, GAC binds to actin, stabilizing and translocating actin filaments, thereby contributing to the parasite's gliding movement. It has been previously identified to situated at the conoid, and its proper positioning is dependent on AKMT (apical lysine methyltransferase) (Lamarque et al. 2014; Jacot et al. 2016; Tosetti et al. 2019).

However, fluorescence recovery after photobleaching (FRAP) assay data generated in our laboratory (not shown here) revealed that the fluorescence signal of GAC exhibited rapid recovery following photobleaching, suggesting that GAC is a highly dynamic protein.

Consequently, expansion microscopy was applied to the *Toxoplasma gondii* strain 'GAC-YFP'. Despite multiple attempts, GAC signals remained undetectable using U-ExM. Therefore, proExM was utilized to analyze the distribution of GAC. Single-channel imaging revealed that GAC was localized not only at the conoid but also accumulated at the basal part of the tachyzoite (Figure IV-21, top left panel; white arrow) and within the cytosol. Notably, no GAC accumulation was observed at the tight junction of invading parasites (Figure IV-21, top right panel).

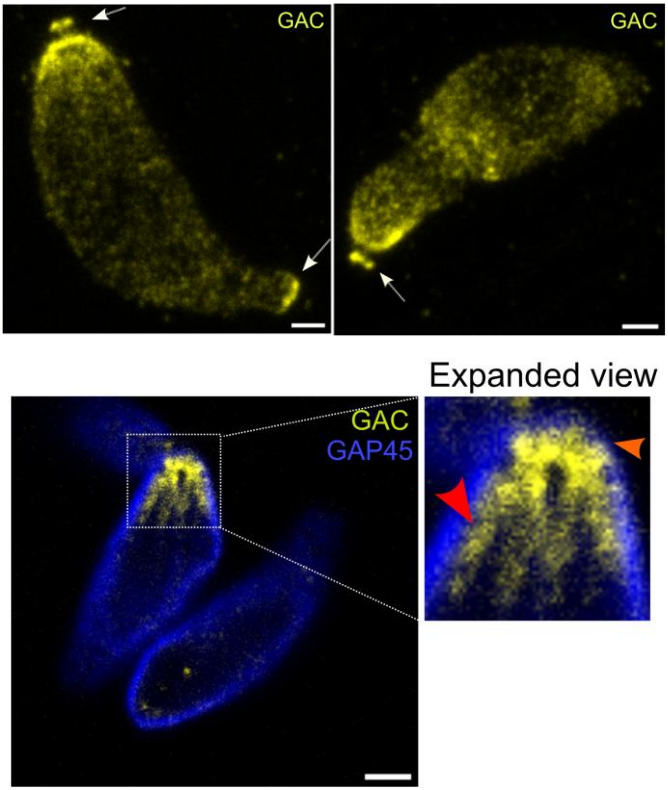

Figure IV-21. Localization Analysis of GAC Using ProExM.

Top Panel: Representative images illustrating the distribution of GAC during gliding and invasion. No antibodies or dyes were used for visualization of strain GAC-YFP. **Bottom Panel**: Representative image depicting the colocalization of GAC and GAP45 in tachyzoites. GAP45 was labeled with an antibody (blue), while GAC was visualized without the use of antibodies or dyes (yellow). Section was acquired using confocal microscopy with a 100× objective. Scale bar: 2 µm.

For further localization analysis, proExM was employed to examine the colocalization of GAC and GAP45 (Figure IV-21, bottom panel). GAP45 was labeled using a specific antibody, whereas no antibody or dye was used to stain

GAC-YFP. The expanded view indicates that GAC is localized beneath GAP45 (orange arrow) and exhibits a filament-like structure (red arrow) at the conoid within the cytosol of the parasite.

The filament-like structure observed at the conoid suggested a potential association between GAC and the subpellicular microtubules (Mtbs) extending from the conoid. To investigate this possibility, acetylated tubulin antibody was used for colocalization analysis of Mtbs and GAC in proExM (Figure IV-23). In this analysis, GAC again exhibited a filament-like structure. Despite the weak signal of Mtbs, some associations between GAC (white arrows) and Mtbs (blue arrows) were observed in the expanded views. However, as an antibody-based marker, the signal of acetylated tubulin was difficult to detect in proExM, despite its stability in U-ExM.

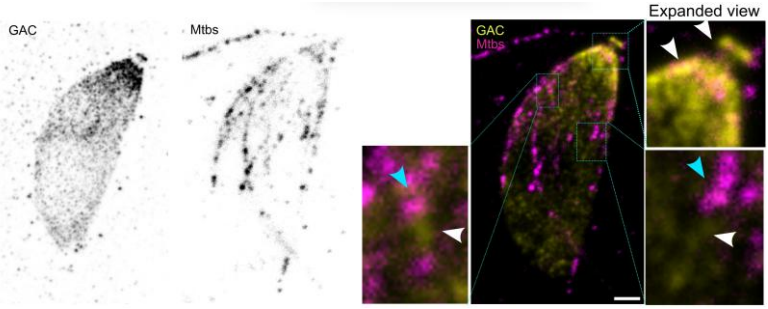

Figure IV-22. Localization analysis of GAC and Mtbs using proExM.

Representative image illustrating the colocalization of GAC and microtubules (Mtbs) in tachyzoites. Microtubules were labeled with an acetylated tubulin antibody (magenta), while GAC was visualized without the use of antibodies or dyes (yellow). GAC exhibited a filament-like structure at the apical part and associated to Mtbs at some sites. Images were acquired using confocal microscopy with a 100× objective. Scale bar: 2 µm.

To optimize the labeling of Mtbs and GAC-YFP, both β-tubulin and acetylated tubulin antibodies were used simultaneously to enhance the fluorescence

intensity of Mtbs. Additionally, a nanobody against GFP that recognize YFP in the GAC-YFP strain was employed to improve signal detection. The results of the double-labeling experiment (Figure IV-23, top panel) and labeling with only the GAC-YFP nanobody (Figure IV-23, bottom panel) are presented. With the enhanced fluorescence signal, finer structural details became visible. Notably, GAC appeared to form a double-ring structure at the conoid, which may correspond to the PCRs and the APR. Additionally, a signal was detected between the two rings (Figure IV-23, bottom panel), which may be associated with the intra-conoidal microtubules. Furthermore, GAC was distributed throughout the cytosolic region of the tachyzoites and exhibited accumulation at the posterior pole and specific regions within the parasite, as indicated by the white and black arrows.

However, due to limitations in antibody signal strength and the expansion factor, the precise association between Mtbs and GAC remains uncertain and requires further investigation.

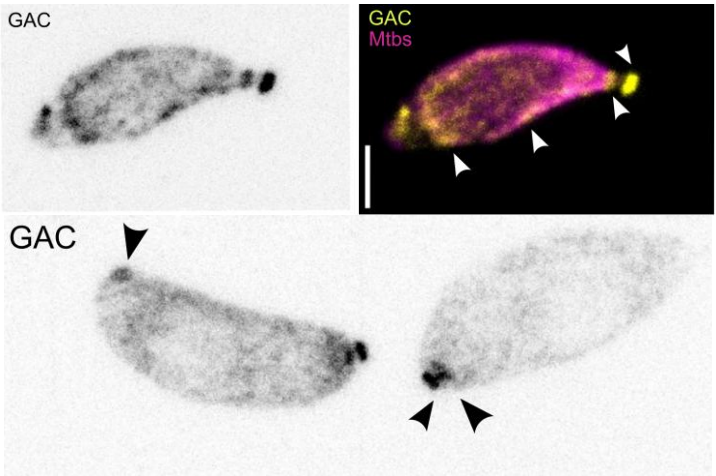

Figure IV-23. Localization analysis of GAC using proExM.

Top panel: Representative images illustrating the colocalization of GAC and microtubules (Mtbs) in a gliding parasite, displayed in single and merged channels. A nanobody was utilized to label GAC-YFP, while beta-tubulin and acetylated tubulin antibodies were employed to label Mtbs. **Bottom panel**: Representative image depicting the localization of GAC in tachyzoites. A nanobody was used to label GAC-YFP. Images were captured with a confocal microscope with a 100x objective. Scale bar: 2 µm.

4.3.6 FRM1 and MyoH are potential dynamic components of the conoid

Formin 1 (FRM1) has been reported to produce F-actin, playing a role in initiating and maintaining motility during gliding and invasion. It is also tightly anchored to the conoid of both maternal and daughter cells (Stortz et al. 2019; Pruyne et al. 2002).

To investigate the localization of FRM1, immunofluorescence assay (IFA) was performed using tri-labeling of FRM1-Halo antibody, acetylated tubulin antibody, and CbEmerald in gliding parasites. The results indicate that FRM1 localizes at the conoid and is also distributed within the cytosol of the parasite (Figure IV-24). Furthermore, FRM1 was found to accumulate in specific cytosolic regions where microtubules (Mtbs) are localized (Figure IV-24; magenta and yellow arrows) and where actin accumulates (Figure IV-24; black arrows).

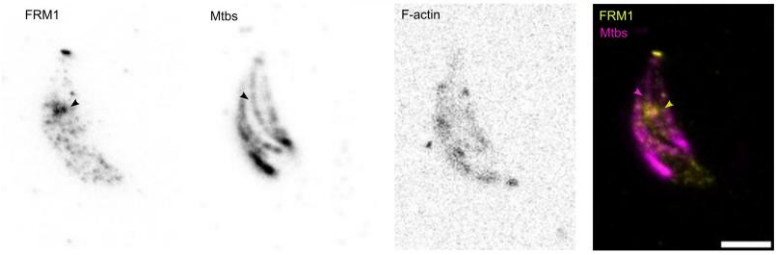

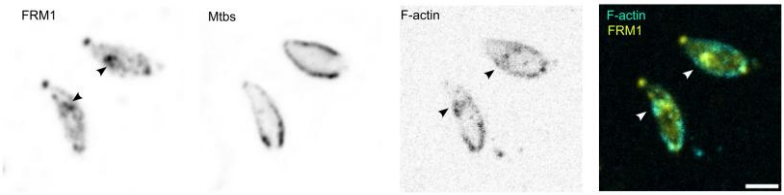

Figure IV-24. Localization analysis of FRM1 using IFA.

Representative images illustrating the colocalization of FRM1 (yellow), Mtbs (magenta) and Actin (cyan) in a gliding parasite, displayed in single and merged channels. Halo and acetylated tubulin antibodies were used for labeling. Images were captured with a STED microscopy using a 100x objective. Scale bar: 2 µm.

To obtain a more detailed visualization, U-ExM was applied to the FRM1-Halo strain. As a stable control in this method, conoidal fibers (Figure IV-25, expanded view 1, magenta arrow) and subpellicular microtubules were clearly observed. The results indicate that FRM1 forms a ring structure at the preconoidal ring localization (Figure IV-25, expanded view 1, yellow arrow). Additionally, FRM1 is distributed throughout the cytosol and appears to be connected to microtubules on the exterior (Figure IV-25, expanded view 2, yellow arrows). The cytosolic signal of the Halo antibody was not detected in either the control strain lacking the Halo tag or the FRM1 KO strain in both IFA and U-ExM. (data not shown).

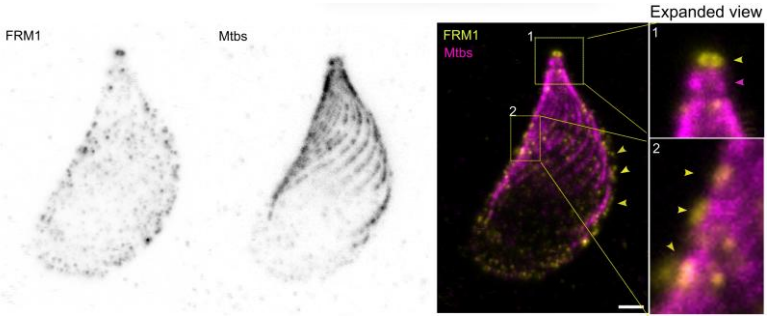

Figure IV-25. Localization analysis of FRM1 and Mtbs using U-ExM.

U-ExM Max projection showing distribution of FRM1 with Halo antibody (yellow; indicated by yellow arrows) and Mtbs with acetylated tubulin antibody (magenta; indicated by the magenta arrow) in tachyzoites in single channel and merge channels, respectively. 2D STED x60 obj. Scale bar: 2 µm.

However, the cytosolic distribution of FRM1 observed in both IFA and U-ExM had not been previously detected in IFA experiments using the FRM1-Halo strain labeled with Janelia Fluor HaloTag ligand. To further validate these findings, the FRM1-HA strain was labeled with HA antibody and analyzed using U-ExM. The results confirmed that FRM1 is localized at the preconoidal ring region of the maternal cell and at the conoid of daughter cells (Figure IV-26, left panel). Additionally, FRM1 signals were detected in the cytosol and along the microtubules (Figure IV-26, right panel, white arrows); however, the signal was significantly less compared to that observed in samples labeled with the Halo antibody.

Since the Halo antibody specifically detects Halo-tagged proteins with high expression levels, such as IMC1-Halo and MyoH-Halo, it remains unclear whether the cytosolic signal observed with the Halo antibody represents true FRM1 localization or is merely background noise. Alternatively, the sporadic

FRM1 signals that detected in the cytosol using the HA antibody and Janelia Fluor Halo Tag ligand may according to low protein expression. Therefore, the question of whether FRM1 is distributed in the cytosol or associated with microtubules remains unresolved and requires further investigation.

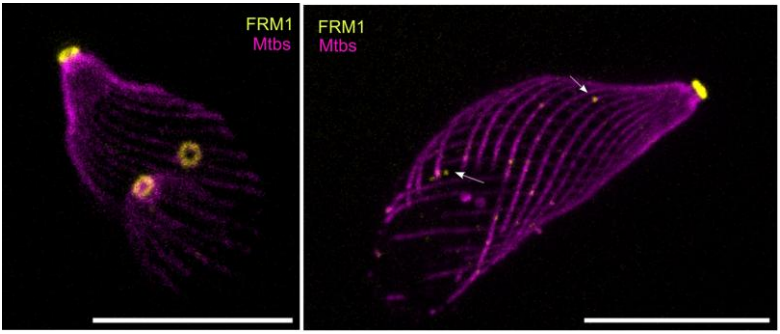

Figure IV-26. Localization analysis of FRM1 and Mtbs using U-ExM.

U-ExM Max projection showing distribution of FRM1 with HA antibody (yellow; indicated by white arrows) and Mtbs with acetylated tubulin antibody in tachyzoites in merge channels, respectively. 2D STED x100 obj. Scale bar: 10 µm.

Similar to FRM1, MyoH was described localized at the conoid and plays an important role in *T. gondii* motility. For instance, Myosin H (MyoH) translocates polymerized F-actin from preconoidal rings to the apical polar ring, facilitating conoid protrusion. It also collaborates with MyoA to drive F-actin translocation along the pellicle, enabling actin accumulation at the basal pole and generating the propulsive force necessary for gliding motility. Additionally, MyoH assists in extending the moving junction (MJ) and functions as a translocator for GAC, contributing to the coordination of the actomyosin system (Dos Santos Pacheco et al. 2022; Jacot et al. 2016; Meissner, Schlüter, and Soldati 2002).

Although the specificity of Halo antibodies in FRM1-Halo samples remains to be evaluated, no similar cytosolic signals were observed in the MyoH-Halo strain. The U-ExM section (Figure IV-27, top panel) and maximum projection (Figure IV-27, bottom panel) demonstrated that MyoH colocalized precisely with the conoidal fibers formed by microtubules (white arrows). However, a few MyoH-Halo signals were identified in the tachyzoite's cytosol (white arrows). Although the signal may result from poly-L-lysine background staining, it is suggested that MyoH may exhibit dynamic properties, as the signal is localized exclusively in the cytosol.

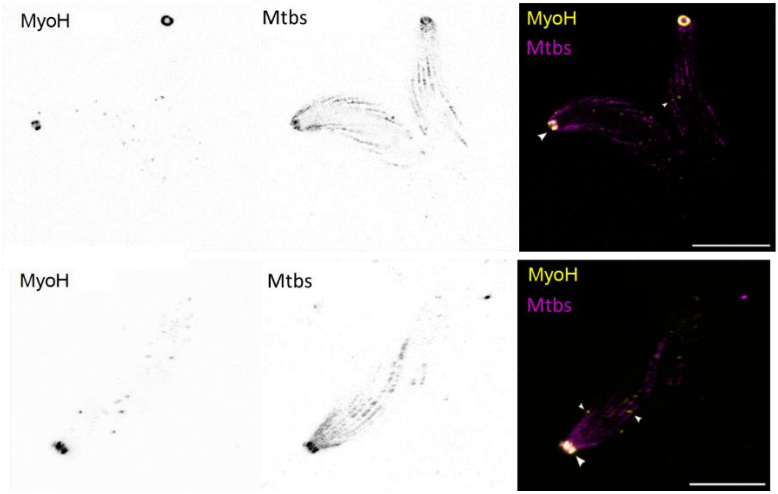

Figure IV-27. Localization analysis of MyoH and Mtbs using U-ExM.

U-ExM section (top panel) and Max projection (bottom panel) showing distribution of MyoH with Halo antibody (yellow; indicated by white arrows) and Mtbs with acetylated tubulin antibody in tachyzoites in single channel and merge channels, respectively. 2D STED x100 obj. Scale bar: 10 µm.

5 Discussion

Many biochemical techniques disrupt the native organization of biological structures; however, microscopy enables the study of biological systems while preserving their spatial organization.

The target of this study is to establish SRM to visualize the native ultrastructure of *Toxoplasma gondii* and investigate key biological processes, such as replication and gliding motility in apicomplexans.

5.1 Application of SRM

The optical resolution of traditional light microscopy is limited by the diffraction barrier, around 250 nm, which constrains the analysis of TgSLP1 and other related structures during nuclear division in *Toxoplasma gondii*. STED overcomes this limitation by modifying the PSF, which defines the smallest resolvable point source or object. In this study, colocalization and functional analysis of TgSLP1 were performed using three-dimensional STED (3D-STED) super-resolution microscopy, enabling a detailed examination of cellular structures and their dynamics.

As the motor components are reported to be localized at the 30-nm PM-IMC space, a significantly higher resolution is needed for the analysis of gliding motility. To address this challenge, we first applied expansion microscopy (ExM) to achieve a 3–4-fold physical expansion of the specimen, along with imaging using STED. In this study, various ExM methods, labeling techniques, and fixation protocols were applied or optimized to achieve higher resolution and improved signal preservation. Additionally, the applicable conditions, as well as the advantages and limitations of each method, were systematically evaluated.

ExM is an effective technique for enlarging microscopic structures; however, achieving a three- to fourfold expansion is sometimes challenging, particularly in samples with a high cell density. Additionally, as the expansion factor increases, antigen density decreases, which can lead to the apparent discontinuity of otherwise uniform structures. To mitigate this issue, a doubled antibody concentration was used in ExM, highlighting the necessity of balancing expansion efficiency with signal preservation rather than solely maximizing the expansion factor.

The resolution, benefits, and limitations of SRM tools are summarized in Table V-1. SMLM offers the highest resolution; however, it is limited by slow acquisition times. STED microscopy enables rapid imaging but necessitates specialized laser systems. SIM is well-suited for live imaging but offers only moderate improvements in resolution. ExM differs from these techniques by physically enlarging the sample rather than relying on optical resolution enhancement (Betzig et al. 2006; Rust, Bates, and Zhuang 2006; Gustafsson 2000; Hell and Wichmann 1994; Schermelleh et al. 2019).

Table V-1. Comparison of Super-Resolution Microscopy Techniques.

Technique		**Resolution (nm)**	**Disadvantages**	**Advantages**
SMLM	PALM	~20-30	Slow acquisition, mainly for fixed samples	molecular localization, high resolution
	STORM	~10-20		Single-molecule tracking, high resolution
SIM		~100-120	Limited resolution improvement,	Live-cell imaging, low phototoxicity

		reconstruction artifacts	
STED	~30-50	Uses depletion laser to sharpen resolution	Fast imaging, live-cell compatible
ExM	~60-70 nm (better with iterations)	Sample prep complexity, possible molecular distortion (discussed in following sections)	Works with standard microscopes, large-area imaging

In this study, ExM is combined with STED microscopy to achieve improved resolution.

5.1.1 U-ExM

As the primary method employed, U-ExM offers significant advantages, including a high expansion factor and the preservation of strong antibody signals. However, the high-temperature denaturation step required for U-ExM presents certain limitations and challenges. For instance, staining with dyes such as the Janelia Fluor Halo Tag ligand was attempted under various conditions but remained unsuccessful. Additionally, despite the denaturation temperature being set at a relatively low 80°C, experiments analyzing GAP45 produced artificial results and non-specific labeling of SAG1, highlighting the critical need for immunofluorescence assay (IFA) controls.

To better preserve the native structure, the denaturation temperature was reduced to 80°C in this study. According to previous research (Dos Santos Pacheco and Soldati-Favre 2021a), PBS-Tween 0.1% was used for washing; however, in our case, no detectable fluorescent signal was observed with this

buffer. This may be attributed to the relatively low denaturation temperature (80°C). Consequently, PBS-Triton 0.2% was used as an alternative.

Since imaging requires mounting the gel on poly-L-lysine-coated light dish, IFA controls are also essential for distinguishing true protein signals from background artifacts.

In conclusion, U-ExM is a robust technique suitable for stable, antibody-labeled proteins; however, at least one IFA control should be included in initial experiments to validate the results.

5.1.2 ProExM

Protein-retention Expansion Microscopy (ProExM) is an ExM protocol that is more compatible with dyes than antibodies. Since dye molecules are significantly smaller than antibodies, this method is particularly advantageous for visualizing fine structures. In the analysis of GAC, ProExM exhibited milder digestion compared to U-ExM. Additionally, for proteins tagged with fluorescent markers such as YFP or GFP, ProExM without antibody labeling produced superior results compared to U-ExM using antibodies.

Although 37°C is not the optimal temperature for Proteinase K digestion, the prolonged reaction time ensured sufficient enzymatic activity at this temperature. Both three-hour and overnight digestion periods were tested, with no observable differences in outcome.

In summary, ProExM is well-suited for dye staining and the visualization of YFP- or GFP-tagged proteins. However, its limitations include weaker fluorescent signals for antibody labeling and a lower expansion factor compared to U-ExM.

5.1.3 TurboID ExM

In fixed samples, the total amount of a given protein remains constant. However, when a sample undergoes physical expansion by a factor of 3–4, antigen density is inevitably reduced. This effect is particularly pronounced in low-abundance proteins, where dilution renders detection challenging. To address this limitation, TurboID ExM was developed to analyze proteins of low expression level.

By fusing the target protein with TurboID, a biotin ligase that labels lysine residues in close proximity, and subsequently detecting biotinylation with fluorescently labeled streptavidin, this method enhances signal strength. Streptavidin labeling has been shown to produce a stronger signal than antibody-based detection due to its ability to label multiple lysine residues on both the bait protein and nearby proteins, whereas antibodies bind to only a few (polyclonal) or a single (monoclonal) epitope of the target protein (Odenwald et al. 2023).

As anticipated, TurboID ExM enabled clear visualization of FRM1 in *Toxoplasma gondii* in this study. However, the extensive lysine biotinylates not only the target polypeptides but also proximal interactors, resulting in a high background signal. This non-specific labeling complicates the identification of the true signal of the target protein, thereby limiting the broader applicability of TurboID ExM in future studies.

5.1.4 Cryo-ExM

Common chemical fixation methods typically involve the use of aldehyde-based chemical crosslinkers, such as paraformaldehyde (PFA), acrylamide (AA), and formaldehyde (FA), or cold methanol for protein precipitation. These chemical

fixation techniques have been employed in protocols for U-ExM, proExM, TurboID ExM, and Immunofluorescence Assay (IFA). However, these chemical reactions, along with subsequent permeabilization steps, may potentially alter the native cellular state. For instance, in the IFA of TgSLP1, samples were initially fixed with 4% PFA, but the signals for Cep250_L1, Nuf2, Chromo1, TgSLP1, and Centrin1 were difficult to visualize. In contrast, when the samples were fixed using cold methanol, the signals were significantly improved. This observation aligns with previous reports indicating that cold methanol treatment enhances antibody accessibility to target proteins (Neuhaus et al. 1998).

Cryofixation is the only fixation method capable of preserving the native ultrastructure by rapidly immobilizing specimen in a vitreous state. This fixation method has been widely utilized in EM as well as been integrated into Expansion Microscopy (ExM) since 2022, combining the benefits of native structure preservation with the high-resolution capabilities of expansion microscopy (Laporte et al. 2022).

The Cryo-ExM experiment conducted on *Toxoplasma gondii* was performed in the laboratory of Prof. Gautam Dey at EMBL. The NHS-ester labeling provided insights into the global proteome of *Toxoplasma gondii*. The cryofixation system is currently being established in our laboratory and is expected to be extensively applied in future research.

5.1.5 Other expansion microscopy

Over time, numerous variants of Expansion Microscopy (ExM) have been developed, each offering unique advantages and challenges.

10x ExM achieves a tenfold physical expansion of biological specimens. However, it requires optimization of hydrogel properties to ensure isotropic expansion and mitigate potential distortions or uneven expansion in complex tissue structures (Guo et al. 2025). Additionally, the increased volume resulting from 10× expansion may result in a significant reduction in signal-to-background ratio (Wen et al. 2023). An alternative approach involves modified gel chemistries that enable tenfold expansion but necessitate specialized apparatus for oxygen removal during gel polymerization (Truckenbrodt et al. 2018).

Iterative expansion microscopy (iExM) employs multiple rounds of expansion to achieve extreme expansion (>20-fold), pushing resolution to molecular scales. However, this method increases sample fragility, the risk of distortion, and the complexity of preparation due to repeated expansion cycles (Chang et al. 2017; M'Saad and Bewersdorf 2020).

Ex-SMLM integrates ExM with SMLM, such as STORM or PALM, to achieve ultra-high resolution (~5 nm) by combining physical expansion with molecular localization. Limitations include the computational demands of single-molecule tracking, the requirement for highly stable labeling and expansion (Kuo et al. 2024; Zwettler et al. 2020).

In this study, ExM was combined with STED, termed Ex-STED, enabling super-resolution imaging of expanded samples (Woglar et al. 2022). Additionally, Ex-STED is constrained by the requirement for STED-compatible secondary antibodies or dyes. Furthermore, the expanded samples are more susceptible to photobleaching due to prolonged STED laser depletion during imaging (Oracz et al. 2017; Göttfert et al. 2017).

Additionally, a ‘one-step 4× and 12× 3D-ExM’ method has been developed, which reportedly allows for either fourfold or twelvefold expansion while ensuring three-dimensional isotropic expansion and preserving the structural integrity of biological specimens (Norman et al. 2024).

5.2 TgSLP1 localization analysis with SRM

Previously, no analogous complex had been revealed in apicomplexans. However, given that the nucleus is positioned at the posterior pole of *T. gondii*, we hypothesized that apicomplexans possess a analogous mechanism that assembles the nucleus with the cytoskeleton.

During her dissertation, my colleague Mirjam Wagner identified SLP1 as a potential candidate of the LINC complex (see section 1.2.6.1). While the role of SLP1 during endodyogeny has been established using diverse phenotypic assays and live-cell imaging (Wagner et al. 2023), the exact location of this protein in relation to other components of the centrocone could not be established without super-resolution microscopy.

Attempts to analyze TgSLP1 using ExM and STED microscopy were unsuccessful, as the TgSLP1 signal was either undetectable or exhibited nonspecific labeling following ExM. Consequently, we applied STED microscopy alone, which provided sufficient resolution to clearly visualize the localization of TgSLP1 and its relationship with other components during nucleus division.

5.2.1 Localization of TgSLP1 during the nuclear division

The TgSLP1-sYFP2 clonal line with LoxP sites utilized in this study was previously generated by Mirjam Wagner (Wagner et al. 2023). Since TgSLP1 is not distinctly detectable until the S-phase, imaging was primarily conducted during early S-phase, late S-phase, and M-phase (mitosis) in *Toxoplasma gondii*.

To precisely determine the localization of TgSLP1, the proteins Cep250_L1, Nuf2, and Chromo1 were tagged to mark the inner core centrosome, kinetochore, and centromeres (Suvorova et al. 2015; Farrell and Gubbels 2014; Gissot et al. 2012), respectively, enabling the assessment of colocalization. The data suggest that these structures duplicate and divide in a sequential manner: the inner core of the centrosome, TgSLP1, the kinetochore, and the centromeres. Consistently, their spatial distribution along the nuclear axis follows the same order, from the distal to the proximal end: the inner core of the centrosome, TgSLP1, the kinetochore, and the centromeres (Figure IV-8).

In this study, colocalization between the outer core of the centrosome (Centrin1) and TgSLP1 was not examined throughout the entire S-phase and M-phase. However, based on previous studies on parasite centrosome morphological dynamics, the outer core of the centrosome is known to divide prior to the inner core (Suvorova et al. 2015; Tomasina et al. 2022).

MORN1 is a protein localized at the centrocone. However, despite multiple attempts, we failed to generate a stable, double-labeled cell line co-expressing TgSLP1 and MORN1. Transient transfection of parasites expressing fluorescently tagged MORN1 resulted in overexpression phenotypes, making it challenging to differentiate between the effects of TgSLP1 knockout (KO) and MORN1 overexpression. Consequently, this approach was not suitable for further analysis.

5.2.2 Function of TgSLP1 during the nuclear division

Colocalization analysis suggests that TgSLP1 functions as a linker between the inner core of the centrosome and the kinetochore. To explore the role of TgSLP1 in nuclear division, a knockout assay was conducted. The dynamics of the DiCre system in *T. gondii* have been extensively studied (Andenmatten et

al. 2013a); however, knockout efficiency often does not reach 100%. Immunofluorescence assays revealed residual TgSLP1 expression after 24 hours of treatment (Wagner et al. 2023), prompting us to conduct most assays after 48 hours of rapamycin treatment to ensure more complete depletion of the protein.

To obtain a more comprehensive understanding of centrosome defects, triple labeling of 'Centrin1-TgSLP1-Cep250_L1,' 'Centrin1-TgSLP1-Nuf2,' and 'Centrin1-TgSLP1-Chromo1' was performed and analyzed in both induced and non-induced parasites. In control group, these structures were closely associated as predicted.

In parasites lacking TgSLP1, the outer and inner cores of the centrosome remained intact. Although the signal of Centrin1 seems abnormal, their interaction was not seriously disrupted by the absence of TgSLP1. This suggests that, in the absence of TgSLP1, apicoplast duplication and division can still occur, but is uncoupled from karyogenesis. Although not directly tested, it appears that the centrosome remains in proximity to the apicoplast.

Notably, the kinetochore and centromeres exhibited aberrant localization relative to the centrosome in induced parasites, indicating disruption of the centrosome-kinetochore linkage. This implies that TgSLP1 localizes particularly to kinetochore-associated spindle during mitosis, and is likely responsible for kinetochore clustering and division. This result aligns with the requirement of SUN proteins for kinetochore assemblage (Yadav and Sanyal 2018). Furthermore, TgSLP1 is critical for centromere association with the centrocone, and subsequently for the division of the centromeres.

Since proteins interacting with SUN domain proteins are always conserved in species or phylum, non-canonical LINC complexes have been identified in

various species, where they function to connect the centrosome to the nucleus. In *C. elegans*, the centrosome is tethered to the nucleus via the SUN-KASH pair SUN-1 and ZYG-12 (Malone et al. 2003; Zhou et al. 2009). In mice, SUN1 and SUN2 form complexes with syne-2 (nesprin-2) to facilitate nuclear-centrosome assemblage during neurogenesis and neuronal movement (Zhang et al. 2009). Additionally, research in budding yeast identified an atypical centrosome-associated LINC complex composed of the SUN protein Mps3 and the KASH-like protein Mps2 during mitosis (Chen et al. 2019).

Toxoplasma gondii deficient in TgSLP1 exhibit severe defects in centrosome assemblage and nuclear division, which is aligns with established SUN-domain protein roles in nuclear-centrosomal coupling observed in *C. elegans* and *S. cerevisiae*. However, *sun-1* knockout *C. elegans* individuals exhibit complete centrosome-nuclear separation (Malone et al. 2003). The pronounced nuclear division defects observed upon TgSLP1 deletion are consistent with its proposed role as a component of the LINC complex and revealed a functional relationship between the nucleus and the mitotic spindle. Nevertheless, KASH-like protein that serve as interactors for TgSLP1 has yet to be identified.

5.2.3 Relationship between TgSLP1 and actin

F-actin is a highly dynamic structure undergoes continuous remodeling during replication stages and plays a crucial role in organizing tachyzoites in the PV (Periz et al. 2017). During the parasite's invading procedure, F-actin was found to accumulate at the basal pole, around the nuclear periphery, and at the tight junction, which constricts both the parasite's body and its nucleus (Whitelaw 2017; Periz et al. 2017; Del Rosario et al. 2019). This observation suggests an interaction between F-actin and the nucleus.

Additionally, as observed in several species, cytoskeletal proteins, such as actin, related to KASH domain proteins, which subsequently engage with SUN domain proteins linked to the inner nuclear envelope (Zhen et al. 2002; Starr and Han 2002; Patterson et al. 2004; Padmakumar et al. 2005; Fridolfsson and Starr 2010). Mirjam Wagner also found that the actin polymerization center appears to be in close proximity to TgSLP1. However, in subsequent tests, actin-modulating drugs were observed to have no influence on TgSLP1 localization across the whole intracellular phases (Wagner 2023). This suggests that the stabilization or depolymerization of actin does not directly affect SUN domain proteins in *Toxoplasma gondii*.

5.3 Linear model and hypothetical alternative models

5.3.1 Linear model

The linear model describes the motor complex localized between PM and IMC comprising MyoA, F-actin, GAPs, and GAC proteins (Frenal et al. 2017). FRM1, GAC, MyoA, and MyoH play critical roles in initiation, stabilization, translocation of F-actin; as well as in conoid protrusion and the movement of the tight junction (details see Section 1.2.5) (Frenal et al. 2017; Venugopal and Marion 2018; Dos Santos Pacheco et al. 2022; Graindorge et al. 2016; Tardieux and Baum 2016; Pruyne et al. 2002). In coordination with other organelle proteins, the actin-based motor system is active (Venugopal and Marion 2018). This coordinated activity generates the central propulsive force essential for gliding motility in the parasite.

Although the linear gliding motility model is currently the most widely accepted, a reassessment is warranted based on a review of the literature, the development of conditional knockout (KO) approaches, and advancements in microscopy techniques. Immunogold staining data from electron microscopy

have revealed relationship between actin and Mtbs (Yasuda et al. 1988). Additionally, data from our laboratory indicate that parasite invasion and migration can still occur even when MyoA, MyoC, or actin is knocked out (Egarter et al. 2014). Further evidence indicates that cytosolic filamentous actin (F-actin) is associated not only with microtubules but also with the parasite periphery (Periz et al. 2019). Moreover, MyoA exhibits a dynamic localization pattern, cycling between the apical and basal extremities of *T. gondii*, with localized accumulation and internalization at specific sites. The observed localization of F-actin and the dynamic distribution of MyoA suggest that the motor complex serves as a maintainer of parasite plasticity.

The linear motor components have not been visualized in live or fixed samples in the space underneath the parasite plasma membrane due to two challenges, the difficulty to image apicomplexan actin, and the limitation of resolution of standard light microscopy methods that cannot resolve the 30 nm PM-IMC space (Halpern et al. 2017).

5.3.2 The distribution of F-actin may be conserved among apicomplexan parasites

F-actin serves as a critical factor in the migration and invasion processes of *Toxoplasma gondii*. U-ExM and confocal microscopy were employed to analyze parasites in which F-actin was specifically labeled using Chromobodies-Emerald. This approach serves as a robust tool for visualizing the dynamics of parasitic F-actin. Compared to other actin probes, Chromobodies (Cb) offer several advantages, including reduced cellular toxicity, minimal interference with F-actin dynamics, no alteration in the total quantity of F-actin, and a high signal clarity. These features make Cb an effective and reliable tool for studying actin-related processes in *Toxoplasma. gondii* (Panza et al. 2015; Periz et al. 2017).

In contrast to the linear model, F-actin was observed to localize beneath MyoA during migration and invasion processes, forming a distinct circular formation at the cytosolic posterior site of some tachyzoites. Additionally, F-actin was found to be released into the extracellular environment from the posterior pole or distributed along the conoid and basal surface of daughter cells. Consistently, F-actin has also been observed in the cytosol and extending through the basal pore of *Plasmodium falciparum*, suggesting that it may traverse this opening to facilitate recycling (Pražák et al. 2024). The localization of F-actin near the preconoidal rings has also been identified in *Cryptosporidium parvum* and *Toxoplasma gondii* in recent studies, suggesting that this feature may be restricted to apicomplexan parasites (Martinez et al. 2023; Pražák et al. 2024). However, in apicomplexan parasites, F-actin is likely to exist as short filaments in vivo and remains relatively unstable (Pospich et al. 2017; Sahoo et al. 2006; Wetzel et al. 2003; Angrisano et al. 2012). Given the denaturation/digestion and reduced abundance in expansion microscopy (ExM), the accurate positioning of F-actin between the PM and the IMC of *Toxoplasma gondii* remains unresolved. Consequently, further investigation is necessary to elucidate this aspect of actin localization and its functional implications.

5.3.3 Myosin A may also be localized in the cytosol

To investigate the localization of Myosin A (MyoA), two super-resolution microscopy techniques were employed in this study. Ultra-Expansion Microscopy (U-ExM) data revealed that MyoA is positioned on the outer side of IMC1 and exhibits a non-uniform distribution, while IMC1 is localized on the outer surface of the subpellicular microtubules (Mtbs). This observation aligns with the linear model; however, the potential presence of a cytosolic MyoA population cannot be excluded.

In contrast, quantification of immunogold-labeling EM data identified MyoA populations associated with IMC1 or situated at the cytosolic side of the IMC. These findings suggest that rather than being a static, anchored structure, MyoA may exhibit dynamic behavior, necessitating IMC permeability during morphological changes associated with parasite migration and invasion.

5.3.4 GAC may associated with actin or microtubules

GAC was previously describeld localized at the apical pole and relies on AKMT, an apical lysine methyltransferase for positioning. However, fluorescence recovery after photobleaching (FRAP) assay data from our laboratory (not shown here) demonstrated that the fluorescence of GAC rapidly recovered after bleaching. This rapid recovery indicates that fluorescent molecules were efficiently transferred to the bleached region, suggesting that GAC is a highly dynamic protein with significant mobility within the cellular context. It is also suggested that during gliding motility and invasion, GAC is proposed to serve as a dynamic linkage of F-actin and the adhesion complex, potentially acting in a spring-like manner (Vahokoski et al. 2014; Kumpula et al. 2019). Additionally, GAC must align parallel to F-actin and the PM to fit the 30-nm space between PM-IMC (Hung et al. 2022).

In this study, GAC was observed to localize predominantly at the preconoidal ring and the apical polar ring, with additional distribution throughout the cytosolic region of the parasite. In some instances, GAC exhibited enrichment at the posterior pole and specific regions within the parasite. This corresponds to the observation that GAC is connected to F-actin. However, in invading parasites, no accumulation of GAC was detected at the tight junction, where F-actin occasionally accumulates.

Furthermore, similar to Mtbs, GAC displayed a filament-like structure and was observed to localize between the two rings at the conoid. Given its highly dynamic nature, GAC may interact with multiple cellular components without stable anchoring. Therefore, further experiments are are needed to clarify the precise structural correlation between GAC and Mtbs.

5.3.5 Formin 1 and Myosin H may not function solely as anchored proteins at the conoid

The FRM1 co-localization experiment presented significant challenges, as the data obtained varied depending on the antibodies or dyes used for labeling. A distinct FRM1 signal was observed when labeled with the Halo antibody, both in IFA and U-ExM. In contrast, minimal signal was detected when FRM1 was labeled with the Halo dye or HA antibody. The labeling efficiency of the Halo antibody, Janelia Fluor HaloTag ligand, and HA antibody is variable and does not reach 100%. However, the Halo antibody is a rabbit polyclonal antibody that can bind multiple secondary antibodies, and it is expected to specifically target Halo-tagged proteins with high expression levels, such as IMC1-Halo and MyoH-Halo.

In contrast, the sporadic FRM1 signals detected in the cytosol using the HA antibody and Janelia Fluor HaloTag ligand may be attributed to the low-expressed protein. Therefore, it remains unclear whether the cytosolic signal observed with the Halo antibody represents genuine FRM1 localization or background noise. As a result, the precise localization of FRM1—whether distributed within the cytosol or associated with microtubules—remains unresolved and warrants further investigation.

U-ExM analysis of MyoH-Halo demonstrated that MyoH colocalized precisely with the conoidal fibers formed by microtubules. Despite being labeled with

the same Halo antibody, only a few MyoH-Halo signals were detected in the cytosol of the parasites, in contrast to the cytosolic signals observed for FRM1. This discrepancy may be attributed to the higher expression level of MyoH compared to FRM1. Additionally, the observed distribution of MyoH suggests that it may function as a dynamic component of the conoid.

5.3.6 GAP45 is a linker between IMC1 and PM

The results obtained from U-ExM and immunogold-labeling EM reveal that GAP45 is associated with the IMC, localizes at PM-IMC space, colocalizes with MyoA, and is positioned above the microtubules. According to the U-ExM data, GAP45 is also a protein that is prone to degradation, which may result in a loss of connection with subpellicular microtubules. These findings align with the predictions of the linear model and confirm that GAP45 serves as a structural connector linking the PM and IMC in *Toxoplasma gondii*.

5.3.7 Hypothetical alternative models

Returning to the central question—where are the key motor components located in *Toxoplasma gondii*? In summary, super-resolution microscopy (SRM) revealed the distribution of F-actin, MyoA, GAC, and MyoH within the cytosol of the parasite. MyoA and GAP45 were detected at PM-IMC space. Additionally, GAC, FRM1, and MyoH were localized at the conoid, yet they also participate in gliding motility. Lastly, the potential localization of F-actin within the PM-IMC space and the possibility of FRM1 functioning as a dynamic protein cannot be excluded. The comparison of motor component localization described in the linear model and the motor localization observed in this study is summarized in Table V-2.

Table V-2. Comparison of motor component localization.

Component	**Linear model**	**In this study**
F-actin	Between PM-IMC	Localized and accumulated in cytosol
MyoA	Anchored between PM-IMC	Localized between PM-IMC and in cytosol
GAP45	Connector of PM-IMC	Connector of PM-IMC
GAC	At the apical pole	Dynamic protein, localized at PCRs and APR
FRM1	At the coniod	Localized at PCRs, may localized at cytosol, may be dynamic
MyoH	At the coniod	Localized at coniod, may localized at cytosol, may be dynamic

Based on these findings, we propose an alternative model: the hybrid motor model. In this model, we propose that the IMC is permeable, allowing actin to flow through the IMC via the open alveolar sutures. Additionally, MyoA may also pass through the permeable IMC alongside actin, facilitating its recycling (Figure V-1). Alternatively, migration could be driven exclusively by microtubule-based mechanisms, as FRM1 and MyoH appear to be associated with microtubules. Further investigation is required to elucidate the precise mechanisms underlying these processes.

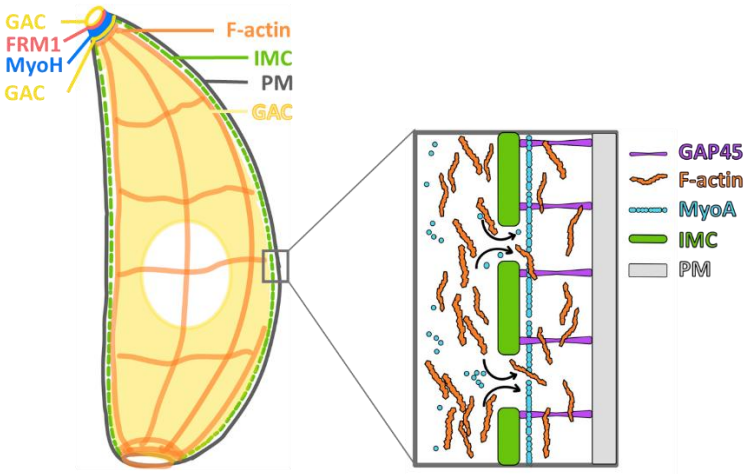

Figure V-1. Schematic Representation of Hybrid Linear Models.

GAC is localized at PCRs, APR and in the cytosol. FRM1 and MyoH are localized at the PCRs and conoid, respectively. The IMC is permeable, allowing actin to flow outside through the gap. When the alveolar structure opens, cytosolic actin flows out and later returns along with MyoA. Orange: F-actin; cyan: MyoA; purple: GAP45; yellow: GAC; red: FRM1; blue: MyoH and white: IMC; green: IMC; grey: PM.

5.4 Outlook

In this study, SRM was utilized to further analyze the localization and function of SUN-like protein 1. However, the LINC complex of *Toxoplasma gondii* comprises not only SUN domain proteins but also KASH domain proteins. Therefore, the potential KASH-like protein candidates proposed by Mirjam Wagner warrant further investigation.

Based on super-resolution microscopy (SRM) data on the gliding motility of *Toxoplasma gondii*, we proposed Hybrid Linear Models. However, further

studies are necessary to validate or refine these models. Advanced techniques such as expansion microscopy, cryofixation, and electron microscopy may be integrated, along with components that specifically bind to low-expressed proteins with high fluorescence intensity. These approaches could enable the resolution of nanoscale structures, allowing for the investigation of whether actin and GAC are localized in PM-IMC space, whether GAC associates with microtubules, and whether Formin 1 and Myosin H exhibit dynamic behavior.

6 Summary

Super-resolution microscopy (SRM) techniques each possess distinct advantages, limitations, and specific conditions for application. The selection of an appropriate method should be guided by the properties of the interest protein and the availability of suitable antibodies or fluorescent dyes for labeling.

SUN and KASH domain proteins are fundamental components of LINC complexes, which have been well-studied in many eukaryotic systems. However, their presence and functional significance in apicomplexan parasites remain poorly understood, despite indirect evidence suggesting their existence. In collaboration with Mirjam Wagner, this study investigates the subcellular localization and functional role of TgSLP1, a SUN-like protein, in *T. gondii* using SRM. Our results indicate that TgSLP1 is critical for maintaining centrocone assemblage and ensuring precise nuclear division during endodyogetic process. We hypothesize that TgSLP1 is a member of apicomplexan-unique LINC complex, which mediates the connection between the bipartite centrosome and centromeres. However, the identification of potential KASH-like interactors was left as an open question for future research.

As an obligate intracellular protozoan, *Toxoplasma gondii* relies on an actin-based gliding mechanism for its dissemination and host cell invasion. These processes are facilitated by a conserved motility apparatus known as the glideosome, which comprises essential molecular components, including filamentous actin (F-actin), myosins, glideosome-associated proteins (GAPs), and glideosome-associated connector (GAC) motor complexes. These components collectively mediate force generation and transmission, enabling parasite movement and host cell penetration. The linear model has been the

predominant framework for explaining *Toxoplasma gondii* motility. However, recent advancements in conditional knockout (KO) strategies, microscopy technologies, and a comprehensive review of existing literature suggest the need for a reevaluation of this model to better align with emerging experimental evidence.

SRM studies have revealed the situation of F-actin, MyoA, GAC, and MyoH within the cytosol of *Toxoplasma gondii*. MyoA and GAP45 were found localized at PM-IMC space, while GAC, FRM1, and MyoH were localized at the conoid and implicated in gliding motility. Additionally, the potential presence of F-actin within the PM-IMC space and the dynamic behavior of FRM1 require further investigation. Based on these observations, we propose alternative hybrid linear models for parasite motility. One model suggests that the IMC is permeable, allowing actin and MyoA to traverse its open alveolar structure, facilitating actin recycling. Alternatively, motility may be driven solely by microtubule-based mechanisms, given the association of FRM1 and MyoH with microtubules. Further researches are required to elucidate the potential mechanisms and validate our hypotheses.

7 ZUSAMMENFASSUNG

Die Verfahren der Super-Resolution-Mikroskopie (SRM) weisen jeweils unterschiedliche Vorteile, Einschränkungen und spezifische Anwendungsbedingungen auf. Die Auswahl einer geeigneten Methode sollte sich an den Eigenschaften des Zielproteins und der Verfügbarkeit geeigneter Antikörper oder Fluoreszenzfarbstoffe zur Markierung orientieren.

SUN- und KASH-Domänenproteine sind grundlegende Bestandteile von LINC-Komplexen, die in vielen eukaryotischen Systemen gut untersucht wurden. Ihr Vorkommen und ihre funktionelle Bedeutung in Apicomplexa-Parasiten sind jedoch noch immer wenig erforscht, obwohl es indirekte Hinweise auf ihre Existenz gibt. In Zusammenarbeit mit Mirjam Wagner untersucht diese Studie die subzelluläre Lokalisierung und funktionelle Rolle von TgSLP1, einem SUN-ähnlichen Protein, in *T. gondii* mittels SRM. Unsere Ergebnisse zeigen, dass TgSLP1 für die Aufrechterhaltung der Centrocone-Integrität und die Gewährleistung einer präzisen Kernsegregation während der Endodyogenie von entscheidender Bedeutung ist. Wir gehen davon aus, dass TgSLP1 Teil eines Apicomplexa-spezifischen LINC-Komplexes ist, der die Verbindung zwischen dem zweiteiligen Centrosom und den Centromeren vermittelt. Die Identifizierung eines potenziellen KASH-ähnlichen Bindungspartners bleibt jedoch eine offene Frage für zukünftige Forschungen.

Als obligat intrazellulärer Protozoon ist *Toxoplasma gondii* für seine Verbreitung und Invasion in Wirtszellen auf einen Aktin-basierten Gleitmechanismus angewiesen. Diese Prozesse werden durch einen konservierten Motilitätsapparat namens Glideosom erleichtert, der aus wesentlichen molekularen Komponenten besteht, darunter filamentöses Aktin (F-Aktin), Myosine, Glideosom-assoziierte Proteine (GAPs) und Glideosom-assoziierte

Konnektor-Motorkomplexe (GAC). Diese Komponenten vermitteln gemeinsam Krafterzeugung und -übertragung und ermöglichen so die Bewegung des Parasiten und das Eindringen in die Wirtszelle. Das lineare Modell war der vorherrschende Rahmen zur Erklärung der Motilität von *Toxoplasma gondii*. Jüngste Fortschritte bei bedingten Knockout-Strategien (KO), Mikroskopietechnologien und eine umfassende Überprüfung der vorhandenen Literatur legen jedoch die Notwendigkeit einer Neubewertung dieses Modells nahe, um es besser an neue experimentelle Erkenntnisse anzupassen.

SRM-Studien haben die Lokalisierung von F-Aktin, MyoA, GAC und MyoH im Zytosol von *Toxoplasma gondii* gezeigt. MyoA und GAP45 wurden im Raum zwischen der PM und IMC gefunden, während GAC, FRM1 und MyoH am Konoid lokalisiert und an der Gleitmotilität beteiligt waren. Darüber hinaus müssen das mögliche Vorhandensein von F-Aktin im PM-IMC-Raum und das dynamische Verhalten von FRM1 weiter untersucht werden. Basierend auf diesen Beobachtungen schlagen wir alternative hybride lineare Modelle für die Parasitenmotilität vor. Ein Modell legt nahe, dass der IMC durchlässig ist, sodass Aktin und MyoA seine offene Alveolarstruktur durchqueren können, was das Aktinrecycling erleichtert. Alternativ kann die Motilität aufgrund der Assoziation von FRM1 und MyoH mit Mikrotubuli ausschließlich durch mikrotubulibasierte Mechanismen gesteuert werden. Weitere Studien sind erforderlich, um die zugrunde liegenden Mechanismen aufzuklären und diese Hypothesen zu bestätigen.

8 Reference

Abu Samraa, N, Cheryl Myra Ethelwyn McCrindle, Barend Louis Penzhorn, and B Cenci-Goga. 2007. 'Seroprevalence of toxoplasmosis in sheep in South Africa', *Journal of the South African Veterinary Association*, 78: 116-20.

Adl, Sina M, Brian S Leander, Alastair GB Simpson, John M Archibald, O Roger Anderson, David Bass, Samuel S Bowser, Guy Brugerolle, Mark A Farmer, and Sergey Karpov. 2007. 'Diversity, nomenclature, and taxonomy of protists', *Systematic biology*, 56: 684-89.

Alexander, David L, Jeffrey Mital, Gary E Ward, Peter Bradley, and John C Boothroyd. 2005. 'Identification of the moving junction complex of Toxoplasma gondii: a collaboration between distinct secretory organelles', *PLoS pathogens*, 1: e17.

Alkema, Manon, Isaie J Reuling, Gerdie M de Jong, Kjerstin Lanke, Luc E Coffeng, Geert-Jan van Gemert, Marga van de Vegte-Bolmer, Quirijn de Mast, Reinout van Crevel, and Karen Ivinson. 2021. 'A randomized clinical trial to compare Plasmodium falciparum gametocytemia and infectivity after blood-stage or mosquito bite–induced controlled malaria infection', *The Journal of infectious diseases*, 224: 1257-65.

Andenmatten, N., S. Egarter, A. J. Jackson, N. Jullien, J. P. Herman, and M. Meissner. 2013a. 'Conditional genome engineering in Toxoplasma gondii uncovers alternative invasion mechanisms', *Nat Methods*, 10: 125-7.

Andenmatten, Nicole, Saskia Egarter, Allison J Jackson, Nicolas Jullien, Jean-Paul Herman, and Markus Meissner. 2013b. 'Conditional genome engineering in Toxoplasma gondii uncovers alternative invasion mechanisms', *Nature methods*, 10: 125-27.

Anderson-White, Brooke, Josh R Beck, Chun-Ti Chen, Markus Meissner, Peter J Bradley, and Marc-Jan Gubbels. 2012. 'Cytoskeleton assembly in Toxoplasma gondii cell division', *International review of cell and molecular biology*, 298: 1-31.

Andrianantoandro, Ernesto, and Thomas D Pollard. 2006. 'Mechanism of actin filament turnover by severing and nucleation at different concentrations of ADF/cofilin', *Molecular cell*, 24: 13-23.

Angrisano, Fiona, David T Riglar, Angelika Sturm, Jennifer C Volz, Michael J Delves, Elizabeth S Zuccala, Lynne Turnbull, Chaitali Dekiwadia, Maya A Olshina, and Danushka S Marapana. 2012. 'Spatial localisation of actin filaments across developmental stages of the malaria parasite', *PLoS One*, 7: e32188.

Attias, Márcia, Dirceu E Teixeira, Marlene Benchimol, Rossiane C Vommaro, Paulo Henrique Crepaldi, and Wanderley De Souza. 2020. 'The life-cycle of

Toxoplasma gondii reviewed using animations', *Parasites & vectors*, 13: 1-13.

Bargieri, Daniel, Vanessa Lagal, Nicole Andenmatten, Isabelle Tardieux, Markus Meissner, and Robert Menard. 2014. 'Host cell invasion by apicomplexan parasites: the junction conundrum', *PLoS pathogens*, 10: e1004273.

Bargieri, Daniel Y, Nicole Andenmatten, Vanessa Lagal, Sabine Thiberge, Jamie A Whitelaw, Isabelle Tardieux, Markus Meissner, and Robert Ménard. 2013. 'Apical membrane antigen 1 mediates apicomplexan parasite attachment but is dispensable for host cell invasion', *Nature communications*, 4: 2552.

Barylyuk, Konstantin, Ludek Koreny, Huiling Ke, Simon Butterworth, Oliver M Crook, Imen Lassadi, Vipul Gupta, Eelco Tromer, Tobias Mourier, and Tim J Stevens. 2020. 'A comprehensive subcellular atlas of the Toxoplasma proteome via hyperLOPIT provides spatial context for protein functions', *Cell host & microbe*, 28: 752-66. e9.

Baum, Jake, and Alan F Cowman. 2011. 'Revealing a parasite's invasive trick', *Science*, 333: 410-11.

Beck, Josh R, Allan L Chen, Elliot W Kim, and Peter J Bradley. 2014. 'RON5 is critical for organization and function of the Toxoplasma moving junction complex', *PLoS pathogens*, 10: e1004025.

Bergman, Lawrence W, Karine Kaiser, Hisashi Fujioka, Isabelle Coppens, Thomas M Daly, Sarah Fox, Kai Matuschewski, Victor Nussenzweig, and Stefan HI Kappe. 2003. 'Myosin A tail domain interacting protein (MTIP) localizes to the inner membrane complex of Plasmodium sporozoites', *Journal of cell science*, 116: 39-49.

Bertiaux, E., A. C. Balestra, L. Bournonville, V. Louvel, B. Maco, D. Soldati-Favre, M. Brochet, P. Guichard, and V. Hamel. 2021. 'Expansion microscopy provides new insights into the cytoskeleton of malaria parasites including the conservation of a conoid', *PLoS Biol*, 19: e3001020.

Besteiro, Sébastien, Adeline Michelin, Joël Poncet, Jean-François Dubremetz, and Maryse Lebrun. 2009. 'Export of a Toxoplasma gondii rhoptry neck protein complex at the host cell membrane to form the moving junction during invasion', *PLoS pathogens*, 5: e1000309.

Betzig, Eric, George H Patterson, Rachid Sougrat, O Wolf Lindwasser, Scott Olenych, Juan S Bonifacino, Michael W Davidson, Jennifer Lippincott-Schwartz, and Harald F Hess. 2006. 'Imaging intracellular fluorescent proteins at nanometer resolution', *Science*, 313: 1642-45.

Bichet, Marion, Candie Joly, Ahmed Hadj Henni, Thomas Guilbert, Marie Xémard, Vincent Tafani, Vanessa Lagal, Guillaume Charras, and Isabelle Tardieux. 2014. 'The toxoplasma-host cell junction is anchored to the cell cortex to sustain parasite invasive force', *BMC biology*, 12: 1-21.

Bisio, Hugo, Matteo Lunghi, Mathieu Brochet, and Dominique Soldati-Favre. 2019. 'Phosphatidic acid governs natural egress in Toxoplasma gondii via a guanylate cyclase receptor platform', *Nature microbiology*, 4: 420-28.

Bisio, Hugo, and Dominique Soldati-Favre. 2019. 'Signaling cascades governing entry into and exit from host cells by Toxoplasma gondii', *Annual Review of Microbiology*, 73: 579-99.

Black, Michael W, and John C Boothroyd. 2000. 'Lytic cycle of Toxoplasma gondii', *Microbiology and molecular biology reviews*, 64: 607-23.

Bolotin, Alexander, Benoit Quinquis, Alexei Sorokin, and S Dusko Ehrlich. 2005. 'Clustered regularly interspaced short palindrome repeats (CRISPRs) have spacers of extrachromosomal origin', *Microbiology*, 151: 2551-61.

Bookwalter, Carol S, Anne Kelsen, Jacqueline M Leung, Gary E Ward, and Kathleen M Trybus. 2014. 'A Toxoplasma gondii class XIV myosin, expressed in Sf9 cells with a parasite co-chaperone, requires two light chains for fast motility', *Journal of Biological Chemistry*, 289: 30832-41.

Boothroyd, John C, and Jean-Francois Dubremetz. 2008. 'Kiss and spit: the dual roles of Toxoplasma rhoptries', *Nature Reviews Microbiology*, 6: 79-88.

Boothroyd, John C, and Michael E Grigg. 2002. 'Population biology of Toxoplasma gondii and its relevance to human infection: do different strains cause different disease?', *Current opinion in microbiology*, 5: 438-42.

Bosch, Jürgen, Stewart Turley, Thomas M Daly, Stephen M Bogh, Michelle L Villasmil, Claudia Roach, Na Zhou, Joanne M Morrisey, Akhil B Vaidya, and Lawrence W Bergman. 2006. 'Structure of the MTIP–MyoA complex, a key component of the malaria parasite invasion motor', *Proceedings of the National Academy of Sciences*, 103: 4852-57.

Bottanelli, Francesca, Emil B Kromann, Edward S Allgeyer, Roman S Erdmann, Stephanie Wood Baguley, George Sirinakis, Alanna Schepartz, David Baddeley, Derek K Toomre, and James E Rothman. 2016. 'Two-colour live-cell nanoscale imaging of intracellular targets', *Nature communications*, 7: 10778.

Boucher, Lauren E, and Jürgen Bosch. 2015. 'The apicomplexan glideosome and adhesins–structures and function', *Journal of Structural Biology*, 190: 93-114.

Branon, Tess C, Justin A Bosch, Ariana D Sanchez, Namrata D Udeshi, Tanya Svinkina, Steven A Carr, Jessica L Feldman, Norbert Perrimon, and Alice Y Ting. 2018. 'Efficient proximity labeling in living cells and organisms with TurboID', *Nature biotechnology*, 36: 880-87.

Brown, Kevin M, Shaojun Long, and L David Sibley. 2018. 'Conditional knockdown of proteins using auxin-inducible degron (AID) fusions in Toxoplasma gondii', *Bio-protocol*, 8: e2728-e28.

Bullen, Hayley E, Yonggen Jia, Yoshiki Yamaryo-Botté, Hugo Bisio, Ou Zhang, Natacha Klages Jemelin, Jean-Baptiste Marq, Vern Carruthers, Cyrille Y

Botté, and Dominique Soldati-Favre. 2016. 'Phosphatidic acid-mediated signaling regulates microneme secretion in Toxoplasma', *Cell host & microbe*, 19: 349-60.

Burg, J Lawrence, DALIA Perelman, LLOYD H Kasper, PATRICIA L Ware, and JC Boothroyd. 1988. 'Molecular analysis of the gene encoding the major surface antigen of Toxoplasma gondii', *Journal of immunology (Baltimore, Md.: 1950)*, 141: 3584-91.

Caldas, Lucio Ayres, and Wanderley De Souza. 2018. 'A window to Toxoplasma gondii egress', *Pathogens*, 7: 69.

Carruthers, Vern B. 2019. 'Interrupting Toxoplasma's Regularly Scheduled Program of Egress', *Trends in Parasitology*, 35: 338-40.

Carruthers, Vern B, Olivia K Giddings, and L David Sibley. 1999. 'Secretion of micronemal proteins is associated with Toxoplasma invasion of host cells', *Cellular microbiology*, 1: 225-35.

Carruthers, Vern, and John C Boothroyd. 2007. 'Pulling together: an integrated model of Toxoplasma cell invasion', *Current opinion in microbiology*, 10: 83-89.

Chang, Jae Byum, Fei Chen, Young Gyu Yoon, Erica E Jung, Hazen Babcock, Jeong Seuk Kang, Shoh Asano, Ho Jun Suk, Nikita Pak, and Paul W Tillberg. 2017. 'Iterative expansion microscopy', *Nature methods*.

Chapman, H David, John R Barta, Damer Blake, Arthur Gruber, Mark Jenkins, Nicholas C Smith, Xun Suo, and Fiona M Tomley. 2013. 'A selective review of advances in coccidiosis research', *Advances in parasitology*, 83: 93-171.

Chen, Chun-Ti, and Marc-Jan Gubbels. 2015. 'Apicomplexan cell cycle flexibility: centrosome controls the clutch', *Trends in Parasitology*, 31: 229-30.

———. 2019. 'TgCep250 is dynamically processed through the division cycle and is essential for structural integrity of the Toxoplasma centrosome', *Molecular biology of the cell*, 30: 1160-69.

Chen, Jingjing, Jennifer M Gardner, Zulin Yu, Sarah E Smith, Sean McKinney, Brian D Slaughter, Jay R Unruh, and Sue L Jaspersen. 2019. 'Yeast centrosome components form a noncanonical LINC complex at the nuclear envelope insertion site', *Journal of Cell Biology*, 218: 1478-90.

Chozinski, T. J., A. R. Halpern, H. Okawa, H. J. Kim, G. J. Tremel, R. O. Wong, and J. C. Vaughan. 2016. 'Expansion microscopy with conventional antibodies and fluorescent proteins', *Nat Methods*, 13: 485-8.

Courjol, Flavie, and Mathieu Gissot. 2018. 'A coiled-coil protein is required for coordination of karyokinesis and cytokinesis in Toxoplasma gondii', *Cellular microbiology*, 20: e12832.

Cova, Marta Mendonça, Mauld H Lamarque, and Maryse Lebrun. 2022. 'How apicomplexa parasites secrete and build their invasion machinery', *Annual Review of Microbiology*, 76: 619-40.

Cox, Frank EG. 2002. 'History of human parasitology', *Clinical microbiology reviews*, 15: 595-612.

Crisp, Melissa, Qian Liu, Kyle Roux, JB Rattner, Catherine Shanahan, Brian Burke, Phillip D Stahl, and Didier Hodzic. 2006. 'Coupling of the nucleus and cytoplasm: role of the LINC complex', *The Journal of cell biology*, 172: 41-53.

Cyrklaff, Marek, Mikhail Kudryashev, Andrew Leis, Kevin Leonard, Wolfgang Baumeister, Robert Menard, Markus Meissner, and Friedrich Frischknecht. 2007. 'Cryoelectron tomography reveals periodic material at the inner side of subpellicular microtubules in apicomplexan parasites', *The Journal of experimental medicine*, 204: 1281-87.

Daher, Wassim, Fabienne Plattner, Marie-France Carlier, and Dominique Soldati-Favre. 2010. 'Concerted action of two formins in gliding motility and host cell invasion by Toxoplasma gondii', *PLoS pathogens*, 6: e1001132.

Dardé, Marie-Laure. 2004. 'Genetic analysis of the diversity in Toxoplasma gondii', *Annali dell'Istituto superiore di sanita*, 40: 57-63.

Das, Sujaan, Leandro Lemgruber, Chwen L Tay, Jake Baum, and Markus Meissner. 2017. 'Multiple essential functions of Plasmodium falciparum actin-1 during malaria blood-stage development', *BMC biology*, 15: 1-16.

Das, Sujaan, Johannes Felix Stortz, Markus Meissner, and Javier Periz. 2021. 'The multiple functions of actin in apicomplexan parasites', *Cellular microbiology*, 23: e13345.

Del Rosario, Mario, Javier Periz, Georgios Pavlou, Oliver Lyth, Fernanda Latorre-Barragan, Sujaan Das, Gurman S Pall, Johannes Felix Stortz, Leandro Lemgruber, and Jamie A Whitelaw. 2019. 'Apicomplexan F-actin is required for efficient nuclear entry during host cell invasion', *EMBO reports*, 20: e48896.

Deng, Huifang, Rachel Cummins, Gereon Schares, Chiara Trevisan, Heidi Enemark, Helga Waap, Jelena Srbljanovic, Olgica Djurkovic-Djakovic, Sara Monteiro Pires, and Joke WB van der Giessen. 2021. 'Mathematical modelling of Toxoplasma gondii transmission: A systematic review', *Food and waterborne parasitology*, 22: e00102.

Dobrowolski, Janice M, Ingrid R Niesman, and L David Sibley. 1997. 'Actin in the parasite Toxoplasma gondii is encoded by a single copy gene, ACT1 and exists primarily in a globular form', *Cell motility and the cytoskeleton*, 37: 253-62.

Dominguez, Roberto. 2004. 'Actin-binding proteins–a unifying hypothesis', *Trends in biochemical sciences*, 29: 572-78.

Dominguez, Roberto, and Kenneth C Holmes. 2011. 'Actin structure and function', *Annual review of biophysics*, 40: 169-86.

Donald, Robert GK, and David S Roos. 1994. 'Homologous recombination and gene replacement at the dihydrofolate reductase-thymidylate synthase

locus in Toxoplasma gondii', *Molecular and biochemical parasitology*, 63: 243-53.

Dos Santos Pacheco, N., and D. Soldati-Favre. 2021a. 'Coupling Auxin-Inducible Degron System with Ultrastructure Expansion Microscopy to Accelerate the Discovery of Gene Function in Toxoplasma gondii', *Methods Mol Biol*, 2369: 121-37.

Dos Santos Pacheco, Nicolas, Lorenzo Brusini, Romuald Haase, Nicolò Tosetti, Bohumil Maco, Mathieu Brochet, Oscar Vadas, and Dominique Soldati-Favre. 2022. 'Conoid extrusion regulates glideosome assembly to control motility and invasion in Apicomplexa', *Nature microbiology*, 7: 1777-90.

Dos Santos Pacheco, Nicolas, and Dominique Soldati-Favre. 2021b. 'Coupling auxin-inducible degron system with ultrastructure expansion microscopy to accelerate the discovery of gene function in Toxoplasma gondii', *Parasite Genomics: Methods and Protocols*: 121-37.

Douglas, Ross G, Robert W Moon, and Friedrich Frischknecht. 2024. 'Cytoskeleton organization in formation and motility of apicomplexan parasites', *Annual Review of Microbiology*, 78.

Dubey, Jitender Prakask. 2016. *Toxoplasmosis of animals and humans* (CRC press).

Dubey, JP, DS Lindsay, and CA106833 Speer. 1998. 'Structures of Toxoplasma gondii tachyzoites, bradyzoites, and sporozoites and biology and development of tissue cysts', *Clinical microbiology reviews*, 11: 267-99.

Dubochet, Jacques. 2012. 'Cryo-EM—the first thirty years', *Journal of microscopy*, 245: 221-24.

Dubois, David J, and Dominique Soldati-Favre. 2019. 'Biogenesis and secretion of micronemes in Toxoplasma gondii', *Cellular microbiology*, 21: e13018.

Dubremetz, Jean François. 2007. 'Rhoptries are major players in Toxoplasma gondii invasion and host cell interaction', *Cellular microbiology*, 9: 841-48.

Egarter, S., N. Andenmatten, A. J. Jackson, J. A. Whitelaw, G. Pall, J. A. Black, D. J. Ferguson, I. Tardieux, A. Mogilner, and M. Meissner. 2014. 'The toxoplasma Acto-MyoA motor complex is important but not essential for gliding motility and host cell invasion', *PLoS One*, 9: e91819.

Eggeling, Christian, Katrin I Willig, Steffen J Sahl, and Stefan W Hell. 2015. 'Lens-based fluorescence nanoscopy', *Quarterly reviews of biophysics*, 48: 178-243.

Farrell, Megan, and Marc-Jan Gubbels. 2014. 'The T oxoplasma gondii kinetochore is required for centrosome association with the centrocone (spindle pole)', *Cellular microbiology*, 16: 78-94.

Ferguson, David JP. 2009. 'Toxoplasma gondii: 1908-2008, homage to Nicolle, Manceaux and Splendore', *Memorias do Instituto Oswaldo Cruz*, 104: 133-48.

Fiedler, K, C Hülsse, W Straube, and V Briese. 1999. 'Toxoplasmosis-antibody seroprevalence in Mecklenburg-Western Pomerania', *Zentralblatt fur Gynakologie*, 121: 239-43.

Francia, Maria E, and Boris Striepen. 2014. 'Cell division in apicomplexan parasites', *Nature Reviews Microbiology*, 12: 125-36.

Frenal, K., J. F. Dubremetz, M. Lebrun, and D. Soldati-Favre. 2017. 'Gliding motility powers invasion and egress in Apicomplexa', *Nat Rev Microbiol*, 15: 645-60.

Frénal, Karine, Jean-François Dubremetz, Maryse Lebrun, and Dominique Soldati-Favre. 2017. 'Gliding motility powers invasion and egress in Apicomplexa', *Nature Reviews Microbiology*, 15: 645-60.

Frénal, Karine, Valérie Polonais, Jean-Baptiste Marq, Rolf Stratmann, Julien Limenitakis, and Dominique Soldati-Favre. 2010. 'Functional dissection of the apicomplexan glideosome molecular architecture', *Cell host & microbe*, 8: 343-57.

Frenkel, JK, JP Dubey, and Nancy L Miller. 1970. 'Toxoplasma gondii in cats: fecal stages identified as coccidian oocysts', *Science*, 167: 893-96.

Freppel, Wesley, David JP Ferguson, Karen Shapiro, Jitender P Dubey, Pierre-Henri Puech, and Aurélien Dumètre. 2019. 'Structure, composition, and roles of the Toxoplasma gondii oocyst and sporocyst walls', *The Cell Surface*, 5: 100016.

Fridolfsson, Heidi N, and Daniel A Starr. 2010. 'Kinesin-1 and dynein at the nuclear envelope mediate the bidirectional migrations of nuclei', *Journal of Cell Biology*, 191: 115-28.

Fuentes, Isabel, Jose M Rubio, Carmen Ramírez, and Jorge Alvar. 2001. 'Genotypic characterization of Toxoplasma gondii strains associated with human toxoplasmosis in Spain: direct analysis from clinical samples', *Journal of clinical microbiology*, 39: 1566-70.

Gajria, Bindu, Amit Bahl, John Brestelli, Jennifer Dommer, Steve Fischer, Xin Gao, Mark Heiges, John Iodice, Jessica C Kissinger, and Aaron J Mackey. 2007. 'ToxoDB: an integrated Toxoplasma gondii database resource', *Nucleic acids research*, 36: D553-D56.

Galbraith, Catherine G, and James A Galbraith. 2011. 'Super-resolution microscopy at a glance', *Journal of cell science*, 124: 1607-11.

Galkin, Vitold E, Albina Orlova, Dmitri S Kudryashov, Alexander Solodukhin, Emil Reisler, Gunnar F Schröder, and Edward H Egelman. 2011. 'Remodeling of actin filaments by ADF/cofilin proteins', *Proceedings of the National Academy of Sciences*, 108: 20568-72.

Gaskins, Elizabeth, Stacey Gilk, Nicolette DeVore, Tara Mann, Gary Ward, and Con Beckers. 2004. 'Identification of the membrane receptor of a class XIV myosin in Toxoplasma gondii', *The Journal of cell biology*, 165: 383-93.

Geuze, Hans J, Jan W Slot, Peter A van der Ley, and RC Scheffer. 1981. 'Use of colloidal gold particles in double-labeling immunoelectron microscopy of ultrathin frozen tissue sections', *Journal of Cell Biology*, 89: 653-65.

Gilk, Stacey D, Elizabeth Gaskins, Gary E Ward, and Con JM Beckers. 2009. 'GAP45 phosphorylation controls assembly of the Toxoplasma myosin XIV complex', *Eukaryotic cell*, 8: 190-96.

Gissot, Mathieu. 2022. 'Toxoplasma gondii: Asexual Cycle in the Intermediate Host.' in, *Lifecycles of Pathogenic Protists in Humans* (Springer).

Gissot, Mathieu, Robert Walker, Stephane Delhaye, Ludovic Huot, David Hot, and Stanislas Tomavo. 2012. 'Toxoplasma gondii chromodomain protein 1 binds to heterochromatin and colocalises with centromeres and telomeres at the nuclear periphery', *PLoS One*, 7: e32671.

Gordon, Jennifer L, and L David Sibley. 2005. 'Comparative genome analysis reveals a conserved family of actin-like proteins in apicomplexan parasites', *BMC genomics*, 6: 1-13.

Göttfert, Fabian, Tino Pleiner, Jörn Heine, Volker Westphal, Dirk Görlich, Steffen J Sahl, and Stefan W Hell. 2017. 'Strong signal increase in STED fluorescence microscopy by imaging regions of subdiffraction extent', *Proceedings of the National Academy of Sciences*, 114: 2125-30.

Göttfert, Fabian, Christian A Wurm, Veronika Mueller, Sebastian Berning, Volker C Cordes, Alf Honigmann, and Stefan W Hell. 2013. 'Coaligned dual-channel STED nanoscopy and molecular diffusion analysis at 20 nm resolution', *Biophysical journal*, 105: L01-L03.

Graindorge, Arnault, Karine Frénal, Damien Jacot, Julien Salamun, Jean Baptiste Marq, and Dominique Soldati-Favre. 2016. 'The conoid associated motor MyoH is indispensable for Toxoplasma gondii entry and exit from host cells', *PLoS pathogens*, 12: e1005388.

Gras, Simon, Allison Jackson, Stuart Woods, Gurman Pall, Jamie Whitelaw, Jacqueline M Leung, Gary E Ward, Craig W Roberts, and Markus Meissner. 2017. 'Parasites lacking the micronemal protein MIC2 are deficient in surface attachment and host cell egress, but remain virulent in vivo', *Wellcome open research*, 2.

Gras, Simon, Elena Jimenez-Ruiz, Christen M Klinger, Katja Schneider, Andreas Klingl, Leandro Lemgruber, and Markus Meissner. 2019. 'An endocytic-secretory cycle participates in Toxoplasma gondii in motility', *PLoS biology*, 17: e3000060.

Griffiths, Gareth, and John Milton Lucocq. 2014. 'Antibodies for immunolabeling by light and electron microscopy: not for the faint hearted', *Histochemistry and cell biology*, 142: 347-60.

Grigg, Michael E, Jyotsom Ganatra, John C Boothroyd, and Todd P Margolis. 2001. 'Unusual abundance of atypical strains associated with human ocular toxoplasmosis', *The Journal of infectious diseases*, 184: 633-39.

Gubbels, Marc-Jan, Margaret Lehmann, Mani Muthalagi, Maria E Jerome, Carrie F Brooks, Tomasz Szatanek, Jayme Flynn, Ben Parrot, Josh Radke, and Boris Striepen. 2008. 'Forward genetic analysis of the apicomplexan cell division cycle in Toxoplasma gondii', *PLoS pathogens*, 4: e36.

Gubbels, Marc-Jan, Shipra Vaishnava, Nico Boot, Jean-François Dubremetz, and Boris Striepen. 2006. 'A MORN-repeat protein is a dynamic component of the Toxoplasma gondii cell division apparatus', *Journal of cell science*, 119: 2236-45.

Gubbels, MJ, CD Keroack, S Dangoudoubiyam, HL Worliczek, AS Paul, C Bauwens, B Elsworth, K Engelberg, DK Howe, and I Coppens. 2020. "Fussing about fission: defining variety among mainstream and exotic apicomplexan cell division modes. Front Cell Infect Microbiol 10: 269." In.

Günay-Esiyok, Özlem, Ulrike Scheib, Matthias Noll, and Nishith Gupta. 2019. 'An unusual and vital protein with guanylate cyclase and P4-ATPase domains in a pathogenic protist', *Life Science Alliance*, 2.

Guo, Jinyu, Hui Yang, Chixiang Lu, Di Cui, Murong Zhao, Cun Li, Weihua Chen, Qian Yang, Zhijie Li, and Mingkun Chen. 2025. 'BOOST: a robust ten-fold expansion method on hour-scale', *Nature communications*, 16: 2107.

Gustafson, Paul V, Hilda D Agar, and Dorothy I Cramer. 1954. 'An electron microscope study of Toxoplasma'.

Gustafsson, Mats GL. 2000. 'Surpassing the lateral resolution limit by a factor of two using structured illumination microscopy', *Journal of microscopy*, 198: 82-87.

Hagan, Iain, and Mitsuhiro Yanagida. 1995. 'The product of the spindle formation gene sad1+ associates with the fission yeast spindle pole body and is essential for viability', *The Journal of cell biology*, 129: 1033-47.

Håkansson, Sebastian, Hiroshi Morisaki, John Heuser, and L David Sibley. 1999. 'Time-lapse video microscopy of gliding motility in Toxoplasma gondii reveals a novel, biphasic mechanism of cell locomotion', *Molecular biology of the cell*, 10: 3539-47.

Halpern, A. R., G. C. M. Alas, T. J. Chozinski, A. R. Paredez, and J. C. Vaughan. 2017. 'Hybrid Structured Illumination Expansion Microscopy Reveals Microbial Cytoskeleton Organization', *ACS Nano*, 11: 12677-86.

Hanssen, Eric, Chaitali Dekiwadia, David T Riglar, Melanie Rug, Leandro Lemgruber, Alan F Cowman, Marek Cyrklaff, Mikhail Kudryashev, Friedrich Frischknecht, and Jake Baum. 2013. 'Electron tomography of p lasmodium falciparum merozoites reveals core cellular events that underpin erythrocyte invasion', *Cellular microbiology*, 15: 1457-72.

Haque, Farhana, David J Lloyd, Dawn T Smallwood, Carolyn L Dent, Catherine M Shanahan, Andrew M Fry, Richard C Trembath, and Sue Shackleton. 2006. 'SUN1 interacts with nuclear lamin A and cytoplasmic nesprins to provide a

physical connection between the nuclear lamina and the cytoskeleton', *Molecular and cellular biology*, 26: 3738-51.

Harding, Clare R, Saskia Egarter, Matthew Gow, Elena Jiménez-Ruiz, David JP Ferguson, and Markus Meissner. 2016. 'Gliding associated proteins play essential roles during the formation of the inner membrane complex of Toxoplasma gondii', *PLoS pathogens*, 12: e1005403.

Hartmann, Jan, Ke Hu, Cynthia Y He, Laurence Pelletier, David S Roos, and Graham Warren. 2006. 'Golgi and centrosome cycles in Toxoplasma gondii'.

Hassan, Eman M, Banu Örmeci, Maria C DeRosa, Brent R Dixon, Syed A Sattar, and Asma Iqbal. 2021. 'A review of Cryptosporidium spp. and their detection in water', *Water Science and Technology*, 83: 1-25.

Hazards, EFSA Panel on Biological, Kostas Koutsoumanis, Ana Allende, Avelino Alvarez-Ordóñez, Declan Bolton, Sara Bover-Cid, Marianne Chemaly, Robert Davies, Alessandra De Cesare, and Lieve Herman. 2018. 'Public health risks associated with food-borne parasites', *EFSA journal*, 16: e05495.

Heaslip, Aoife T, Jacqueline M Leung, Kimberly L Carey, Federica Catti, David M Warshaw, Nicholas J Westwood, Bryan A Ballif, and Gary E Ward. 2010. 'A small-molecule inhibitor of T. gondii motility induces the posttranslational modification of myosin light chain-1 and inhibits myosin motor activity', *PLoS pathogens*, 6: e1000720.

Hell, Stefan W, and Jan Wichmann. 1994. 'Breaking the diffraction resolution limit by stimulated emission: stimulated-emission-depletion fluorescence microscopy', *Optics letters*, 19: 780-82.

Herm-Götz, Angelika, Carolina Agop-Nersesian, Sylvia Münter, Joshua S Grimley, Thomas J Wandless, Friedrich Frischknecht, and Markus Meissner. 2007. 'Rapid control of protein level in the apicomplexan Toxoplasma gondii', *Nature methods*, 4: 1003-05.

Herm-Götz, Angelika, Stefan Weiss, Rolf Stratmann, Setsuko Fujita-Becker, Christine Ruff, Edgar Meyhöfer, Thierry Soldati, Dietmar J Manstein, Michael A Geeves, and Dominique Soldati. 2002. 'Toxoplasma gondii myosin A and its light chain: a fast, single-headed, plus-end-directed motor', *The EMBO journal*.

Hildebrandt, A, JS Gray, and K-P Hunfeld. 2013. 'Human babesiosis in Europe: what clinicians need to know', *Infection*, 41: 1057-72.

Hill, Dolores, and Jitender P Dubey. 2002. 'Toxoplasma gondii: transmission, diagnosis and prevention', *Clinical microbiology and infection*, 8: 634-40.

Holland, Gary N. 1999. 'Reconsidering the pathogenesis of ocular toxoplasmosis', *American journal of ophthalmology*, 128: 502-05.

Honore, S, A Couvelard, YJ Garin, C Bedel, D Henin, ML Darde, and F Derouin. 2000. 'Genotyping of Toxoplasma gondii strains from immunocompromised patients', *Pathologie-biologie*, 48: 541-47.

Horn, Henning F. 2014. 'LINC complex proteins in development and disease', *Current topics in developmental biology*, 109: 287-321.

Howe, Daniel K, Stephanie Honoré, Francis Derouin, and L David Sibley. 1997. 'Determination of genotypes of Toxoplasma gondii strains isolated from patients with toxoplasmosis', *Journal of clinical microbiology*, 35: 1411-14.

Howe, Daniel K, and L David Sibley. 1995. 'Toxoplasma gondii comprises three clonal lineages: correlation of parasite genotype with human disease', *Journal of infectious diseases*, 172: 1561-66.

Hu, Ke, Jeff Johnson, Laurence Florens, Martin Fraunholz, Sapna Suravajjala, Camille DiLullo, John Yates, David S Roos, and John M Murray. 2006. 'Cytoskeletal components of an invasion machine—the apical complex of Toxoplasma gondii', *PLoS pathogens*, 2: e13.

Hung, Yu-Fu, Qu Chen, Isa Pires, Peter B Rosenthal, and Inari Kursula. 2022. 'Structure of Toxoplasma gondii glideosome-associated connector suggests a role as an elastic element in actomyosin force generation for gliding motility', *bioRxiv*: 2022.12. 09.519741.

Hutchison, WM. 1965. 'Experimental transmission of Toxoplasma gondii', *Nature*, 206: 961-62.

Huynh, My-Hang, and Vern B Carruthers. 2006. 'Toxoplasma MIC2 is a major determinant of invasion and virulence', *PLoS pathogens*, 2: e84.

Jacobs, Leon, Jack S Remington, and Marjorie L Melton. 1960. 'The resistance of the encysted form of Toxoplasma gondii', *The Journal of parasitology*, 46: 11-21.

Jacot, Damien, Nicolò Tosetti, Isa Pires, Jessica Stock, Arnault Graindorge, Yu-Fu Hung, Huijong Han, Rita Tewari, Inari Kursula, and Dominique Soldati-Favre. 2016. 'An apicomplexan actin-binding protein serves as a connector and lipid sensor to coordinate motility and invasion', *Cell host & microbe*, 20: 731-43.

Jewett, Travis J, and L David Sibley. 2003. 'Aldolase forms a bridge between cell surface adhesins and the actin cytoskeleton in apicomplexan parasites', *Molecular cell*, 11: 885-94.

Jones, JL, and JP Dubey. 2010. 'Waterborne toxoplasmosis–recent developments', *Experimental parasitology*, 124: 10-25.

Jones, Philip, David Binns, Hsin-Yu Chang, Matthew Fraser, Weizhong Li, Craig McAnulla, Hamish McWilliam, John Maslen, Alex Mitchell, and Gift Nuka. 2014. 'InterProScan 5: genome-scale protein function classification', *Bioinformatics*, 30: 1236-40.

Jullien, Nicolas, François Sampieri, Alain Enjalbert, and Jean-Paul Herman. 2003. 'Regulation of Cre recombinase by ligand-induced complementation of inactive fragments', *Nucleic acids research*, 31: e131-e31.

Kafsack, Björn FC, Janethe DO Pena, Isabelle Coppens, Sandeep Ravindran, John C Boothroyd, and Vern B Carruthers. 2009. 'Rapid membrane disruption by

a perforin-like protein facilitates parasite exit from host cells', *Science*, 323: 530-33.

Kan, Andrey, Yan-Hong Tan, Fiona Angrisano, Eric Hanssen, Kelly L Rogers, Lachlan Whitehead, Vanessa P Mollard, Anton Cozijnsen, Michael J Delves, and Simon Crawford. 2014. 'Quantitative analysis of P lasmodium ookinete motion in three dimensions suggests a critical role for cell shape in the biomechanics of malaria parasite gliding motility', *Cellular microbiology*, 16: 734-50.

Kato, Kentaro. 2018. 'How does Toxoplama gondii invade host cells?', *Journal of Veterinary Medical Science*, 80: 1702-06.

Katsumata, Kazuhiro, Eriko Nishi, Sadia Afrin, Kaoru Narusawa, and Ayumu Yamamoto. 2017. 'Position matters: multiple functions of LINC-dependent chromosome positioning during meiosis', *Current genetics*, 63: 1037-52.

Kim, Dae In, Samuel C Jensen, Kyle A Noble, Birendra Kc, Kenneth H Roux, Khatereh Motamedchaboki, and Kyle J Roux. 2016. 'An improved smaller biotin ligase for BioID proximity labeling', *Molecular biology of the cell*, 27: 1188-96.

Konstantinovic, Neda, Hélène Guegan, Tijana Stäjner, Sorya Belaz, and Florence Robert-Gangneux. 2019. 'Treatment of toxoplasmosis: Current options and future perspectives', *Food and waterborne parasitology*, 15: e00036.

Koreny, Ludek, Mohammad Zeeshan, Konstantin Barylyuk, Eelco C Tromer, Jolien JE van Hooff, Declan Brady, Huiling Ke, Sara Chelaghma, David JP Ferguson, and Laura Eme. 2021. 'Molecular characterization of the conoid complex in Toxoplasma reveals its conservation in all apicomplexans, including Plasmodium species', *PLoS biology*, 19: e3001081.

Kovar, David R, Elizabeth S Harris, Rachel Mahaffy, Henry N Higgs, and Thomas D Pollard. 2006. 'Control of the assembly of ATP-and ADP-actin by formins and profilin', *Cell*, 124: 423-35.

Kudyba, Heather M, David W Cobb, Joel Vega-Rodríguez, and Vasant Muralidharan. 2021. 'Some conditions apply: Systems for studying Plasmodium falciparum protein function', *PLoS pathogens*, 17: e1009442.

Kumar, Amit, Oscar Vadas, Nicolas Dos Santos Pacheco, Xu Zhang, Kin Chao, Nicolas Darvill, Helena Ø Rasmussen, Yingqi Xu, Gloria Meng-Hsuan Lin, and Fisentzos A Stylianou. 2023. 'Structural and regulatory insights into the glideosome-associated connector from Toxoplasma gondii', *Elife*, 12: e86049.

Kumpula, E-P, and Inari Kursula. 2015. 'Towards a molecular understanding of the apicomplexan actin motor: on a road to novel targets for malaria remedies?', *Structural Biology and Crystallization Communications*, 71: 500-13.

Kumpula, Esa-Pekka, Andrea J Lopez, Leila Tajedin, Huijong Han, and Inari Kursula. 2019. 'Atomic view into Plasmodium actin polymerization, ATP hydrolysis, and fragmentation', *PLoS biology*, 17: e3000315.

Kuo, Joe Chin-Hun, Marshall J Colville, Michelle R Sorkin, Jacky Lok Ka Kuo, Ling Ting Huang, Dana N Thornlow, Gwendolyn M Beacham, Gunther Hollopeter, Matthew P DeLisa, and Christopher A Alabi. 2024. 'Bio-orthogonal Glycan Imaging of Cultured Cells and Whole Animal C. elegans with Expansion Microscopy', *ACS Central Science*.

Kur, Jozef, Lucyna Holec-Gąsior, and Elżbieta Hiszczyńska-Sawicka. 2009. 'Current status of toxoplasmosis vaccine development', *Expert review of vaccines*, 8: 791-808.

Lamarque, Mauld, Sebastien Besteiro, Julien Papoin, Magali Roques, Brigitte Vulliez-Le Normand, Juliette Morlon-Guyot, Jean-François Dubremetz, Sylvain Fauquenoy, Stanislas Tomavo, and Bart W Faber. 2011. 'The RON2-AMA1 interaction is a critical step in moving junction-dependent invasion by apicomplexan parasites', *PLoS pathogens*, 7: e1001276.

Lamarque, Mauld H, Magali Roques, Marie Kong-Hap, Michelle L Tonkin, George Rugarabamu, Jean-Baptiste Marq, Diana M Penarete-Vargas, Martin J Boulanger, Dominique Soldati-Favre, and Maryse Lebrun. 2014. 'Plasticity and redundancy among AMA–RON pairs ensure host cell entry of Toxoplasma parasites', *Nature communications*, 5: 4098.

Laporte, Marine H, Nikolai Klena, Virginie Hamel, and Paul Guichard. 2022. 'Visualizing the native cellular organization by coupling cryofixation with expansion microscopy (Cryo-ExM)', *Nature methods*, 19: 216-22.

Lebrun, Maryse, Adeline Michelin, Hiba El Hajj, Joël Poncet, Peter J Bradley, Henri Vial, and Jean François Dubremetz. 2005. 'The rhoptry neck protein RON4 relocalizes at the moving junction during Toxoplasma gondii invasion', *Cellular microbiology*, 7: 1823-33.

Lee, Sung Haeng, and Roberto Dominguez. 2010. 'Regulation of actin cytoskeleton dynamics in cells', *Molecules and cells*, 29: 311-26.

Leung, Jacqueline M, Mark A Rould, Christoph Konradt, Christopher A Hunter, and Gary E Ward. 2014. 'Disruption of TgPHIL1 alters specific parameters of Toxoplasma gondii motility measured in a quantitative, three-dimensional live motility assay', *PLoS One*, 9: e85763.

Li, Wei, Janessa Grech, Johannes Felix Stortz, Matthew Gow, Javier Periz, Markus Meissner, and Elena Jimenez-Ruiz. 2022. 'A splitCas9 phenotypic screen in Toxoplasma gondii identifies proteins involved in host cell egress and invasion', *Nature microbiology*, 7: 882-95.

Long, Shaojun, Bryan Anthony, Lisa L Drewry, and L David Sibley. 2017. 'A conserved ankyrin repeat-containing protein regulates conoid stability, motility and cell invasion in Toxoplasma gondii', *Nature communications*, 8: 2236.

Lorestani, Alexander, Lilach Sheiner, Kevin Yang, Seth D Robertson, Nivedita Sahoo, Carrie F Brooks, David JP Ferguson, Boris Striepen, and Marc-Jan Gubbels. 2010. 'A Toxoplasma MORN1 null mutant undergoes repeated divisions but is defective in basal assembly, apicoplast division and cytokinesis', *PLoS One*, 5: e12302.

Lourido, Sebastian. 2019. 'Toxoplasma gondii'.

Lučić, Vladan, Friedrich Förster, and Wolfgang Baumeister. 2005. 'Structural studies by electron tomography: from cells to molecules', *Annu. Rev. Biochem.*, 74: 833-65.

M'Saad, Ons, and Joerg Bewersdorf. 2020. 'Light microscopy of proteins in their ultrastructural context', *Cold Spring Harbor Laboratory*.

Malone, Christian J, William D Fixsen, H Robert Horvitz, and Min Han. 1999. 'UNC-84 localizes to the nuclear envelope and is required for nuclear migration and anchoring during C. elegans development', *Development*, 126: 3171-81.

Malone, Christian J, Lisa Misner, Nathalie Le Bot, Miao-Chih Tsai, Jay M Campbell, Julie Ahringer, and John G White. 2003. 'The C. elegans hook protein, ZYG-12, mediates the essential attachment between the centrosome and nucleus', *Cell*, 115: 825-36.

Mann, Tara, and Con Beckers. 2001. 'Characterization of the subpellicular network, a filamentous membrane skeletal component in the parasite Toxoplasma gondii', *Molecular and biochemical parasitology*, 115: 257-68.

Martinez, Matthew, Shrawan Kumar Mageswaran, Amandine Guérin, William David Chen, Cameron Parker Thompson, Sabine Chavin, Dominique Soldati-Favre, Boris Striepen, and Yi-Wei Chang. 2023. 'Origin and arrangement of actin filaments for gliding motility in apicomplexan parasites revealed by cryo-electron tomography', *Nature communications*, 14: 4800.

McCoy, James M, Lachlan Whitehead, Giel G van Dooren, and Christopher J Tonkin. 2012. 'Tg CDPK3 regulates calcium-dependent egress of Toxoplasma gondii from host cells', *PLoS pathogens*, 8: e1003066.

McGough, Amy, Brian Pope, Wah Chiu, and Alan Weeds. 1997. 'Cofilin changes the twist of F-actin: implications for actin filament dynamics and cellular function', *The Journal of cell biology*, 138: 771-81.

McGregor, Alexandra Lynn, Chieh-Ren Hsia, and Jan Lammerding. 2016. 'Squish and squeeze—the nucleus as a physical barrier during migration in confined environments', *Current opinion in cell biology*, 40: 32-40.

Meissner, Markus, Susan Brecht, Hermann Bujard, and Dominique Soldati. 2001. 'Modulation of myosin A expression by a newly established tetracycline repressor-based inducible system in Toxoplasma gondii', *Nucleic acids research*, 29: e115-e15.

Meissner, Markus, Dirk Schlüter, and Dominique Soldati. 2002. 'Role of Toxoplasma gondii myosin A in powering parasite gliding and host cell invasion', *Science*, 298: 837-40.

Michel, Adam O, Alexander Mathis, and Marie-Pierre Ryser-Degiorgis. 2014. 'Babesia spp. in European wild ruminant species: parasite diversity and risk factors for infection', *Veterinary research*, 45: 1-11.

Molan, A, K Nosaka, M Hunter, and W Wang. 2019. 'Global status of Toxoplasma gondii infection: systematic review and prevalence snapshots', *Trop Biomed*, 36: 898-925.

Montoya, Jose G. 2002. 'Laboratory diagnosis of Toxoplasma gondii infection and toxoplasmosis', *The Journal of infectious diseases*, 185: S73-S82.

Morrison, David A. 2009. 'Evolution of the Apicomplexa: where are we now?', *Trends in Parasitology*, 25: 375-82.

Morrissette, Naomi S, and L David Sibley. 2002. 'Cytoskeleton of apicomplexan parasites', *Microbiology and molecular biology reviews*, 66: 21-38.

Moussaoui, Dihia, James P Robblee, Daniel Auguin, Elena B Krementsova, Silvia Haase, Thomas CA Blake, Jake Baum, Julien Robert-Paganin, Kathleen M Trybus, and Anne Houdusse. 2020. 'Full-length Plasmodium falciparum myosin A and essential light chain PfELC structures provide new anti-malarial targets', *Elife*, 9: e60581.

Munera Lopez, Jonathan, Isadonna F Tengganu, Jun Liu, John M Murray, Luisa F Arias Padilla, Ying Zhang, Peter T Brown, Laurence Florens, and Ke Hu. 2022. 'An apical protein, Pcr2, is required for persistent movement by the human parasite Toxoplasma gondii', *PLoS pathogens*, 18: e1010776.

Münter, Sylvia, Benedikt Sabass, Christine Selhuber-Unkel, Mikhail Kudryashev, Stephan Hegge, Ulrike Engel, Joachim P Spatz, Kai Matuschewski, Ulrich S Schwarz, and Friedrich Frischknecht. 2009. 'Plasmodium sporozoite motility is modulated by the turnover of discrete adhesion sites', *Cell host & microbe*, 6: 551-62.

Nagayasu, Eiji, Yu-chen Hwang, Jun Liu, John M Murray, and Ke Hu. 2016. 'Loss of a doublecortin (DCX) domain containing protein causes structural defects in a tubulin-based organelle of Toxoplasma gondii and impairs host cell invasion', *bioRxiv*: 069377.

Nebl, Thomas, Judith Helena Prieto, Eugene Kapp, Brian J Smith, Melanie J Williams, John R Yates 3rd, Alan F Cowman, and Christopher J Tonkin. 2011. 'Quantitative in vivo analyses reveal calcium-dependent phosphorylation sites and identifies a novel component of the Toxoplasma invasion motor complex', *PLoS pathogens*, 7: e1002222.

Neuhaus, Eva M, Heinz Horstmann, Wolfhard Almers, Markus Maniak, and Thierry Soldati. 1998. 'Ethane-freezing/methanol-fixation of cell monolayers: a procedure for improved preservation of structure and

antigenicity for light and electron microscopies', *Journal of Structural Biology*, 121: 326-42.
Nicolle, Charles. 1908. 'Sur une infection a corps de Leishman (on organismes voisons) du gondi', *CR Acad Sci*, 147: 736.
Nishi, Manami, Ke Hu, John M Murray, and David S Roos. 2008. 'Organellar dynamics during the cell cycle of Toxoplasma gondii', *Journal of cell science*, 121: 1559-68.
Norman, Roshan X, Yu-Chia Chen, Emma E Recchia, Jonathan Loi, Quincy Rosemarie, Sydney L Lesko, Smit Patel, Nathan Sherer, Motoki Takaku, and Mark E Burkard. 2024. 'One step 4× and 12× 3D-ExM enables robust super-resolution microscopy of nanoscale cellular structures', *Journal of Cell Biology*, 224: e202407116.
Nwaneshiudu, Adaobi, Christiane Kuschal, Fernanda H Sakamoto, R Rox Anderson, Kathryn Schwarzenberger, and Roger C Young. 2012. 'Introduction to confocal microscopy', *Journal of Investigative Dermatology*, 132: 1-5.
O'Leary, Jennifer K, Roy D Sleator, and Brigid Lucey. 2021. 'Cryptosporidium spp. diagnosis and research in the 21st century', *Food and waterborne parasitology*, 24: e00131.
Odenwald, Johanna, Bernardo Gabiatti, Silke Braune, Siqi Shen, Martin Zoltner, and Susanne Kramer. 2023. 'Beyond BioID: Streptavidin outcompetes antibody fluorescence signals in protein localization and readily visualises targets evading immunofluorescence detection', *bioRxiv*: 2023.12. 01.569576.
Oliveira Souza, Rodolpho Ornitz, Chunlin Yang, and Gustavo Arrizabalaga. 2024. 'Myosin A and F-Actin play a critical role in mitochondrial dynamics and inheritance in Toxoplasma gondii', *PLoS pathogens*, 20: e1012127.
Opsteegh, Marieke, Titia M Kortbeek, Arie H Havelaar, and Joke WB van der Giessen. 2015. 'Intervention strategies to reduce human Toxoplasma gondii disease burden', *Clinical infectious diseases*, 60: 101-07.
Oracz, Joanna, Volker Westphal, Czesław Radzewicz, Steffen J Sahl, and Stefan W Hell. 2017. 'Photobleaching in STED nanoscopy and its dependence on the photon flux applied for reversible silencing of the fluorophore', *Scientific reports*, 7: 11354.
Oza, Pranav, Sue L Jaspersen, Adriana Miele, Job Dekker, and Craig L Peterson. 2009. 'Mechanisms that regulate localization of a DNA double-strand break to the nuclear periphery', *Genes & development*, 23: 912-27.
Pacheco, Nicolas Dos Santos, Nicolò Tosetti, Ludek Koreny, Ross F Waller, and Dominique Soldati-Favre. 2020. 'Evolution, composition, assembly, and function of the conoid in Apicomplexa', *Trends in Parasitology*, 36: 688-704.
Padmakumar, VC, Thorsten Libotte, Wenshu Lu, Hafida Zaim, Sabu Abraham, Angelika A Noegel, Josef Gotzmann, Roland Foisner, and Iakowos

Karakesisoglou. 2005. 'The inner nuclear membrane protein Sun1 mediates the anchorage of Nesprin-2 to the nuclear envelope', *Journal of cell science*, 118: 3419-30.

Panza, Paolo, Julia Maier, Christian Schmees, Ulrich Rothbauer, and Christian Söllner. 2015. 'Live imaging of endogenous protein dynamics in zebrafish using chromobodies', *Development*, 142: 1879-84.

Patterson, Kristin, Ari B Molofsky, Christina Robinson, Shelley Acosta, Courtney Cater, and Janice A Fischer. 2004. 'The functions of Klarsicht and nuclear lamin in developmentally regulated nuclear migrations of photoreceptor cells in the Drosophila eye', *Molecular biology of the cell*, 15: 600-10.

Paul, Aditya S, and Thomas D Pollard. 2009. 'Review of the mechanism of processive actin filament elongation by formins', *Cell motility and the cytoskeleton*, 66: 606-17.

Pavlou, G., B. Touquet, L. Vigetti, P. Renesto, A. Bougdour, D. Debarre, M. Balland, and I. Tardieux. 2020. 'Coupling Polar Adhesion with Traction, Spring, and Torque Forces Allows High-Speed Helical Migration of the Protozoan Parasite Toxoplasma', *ACS Nano*, 14: 7121-39.

Periz, J., J. Whitelaw, C. Harding, S. Gras, M. I. Del Rosario Minina, F. Latorre-Barragan, L. Lemgruber, M. A. Reimer, R. Insall, A. Heaslip, and M. Meissner. 2017. 'Toxoplasma gondii F-actin forms an extensive filamentous network required for material exchange and parasite maturation', *Elife*, 6.

Periz, Javier, Mario Del Rosario, Alexandra McStea, Simon Gras, Colin Loney, Lin Wang, Marisa L Martin-Fernandez, and Markus Meissner. 2019. 'A highly dynamic F-actin network regulates transport and recycling of micronemes in Toxoplasma gondii vacuoles', *Nature communications*, 10: 4183.

Pieperhoff, Manuela S, Gurman S Pall, Elena Jiménez-Ruiz, Sujaan Das, Carmen Melatti, Matthew Gow, Eleanor H Wong, Joanne Heng, Sylke Müller, and Michael J Blackman. 2015. 'Conditional U1 gene silencing in Toxoplasma gondii', *PLoS One*, 10: e0130356.

Piña, Ricardo, Alma I Santos-Díaz, Erika Orta-Salazar, Azucena Ruth Aguilar-Vazquez, Carola A Mantellero, Isabel Acosta-Galeana, Argel Estrada-Mondragon, Mara Prior-Gonzalez, Jadir Isai Martinez-Cruz, and Abraham Rosas-Arellano. 2022. 'Ten approaches that improve immunostaining: a review of the latest advances for the optimization of immunofluorescence', *International journal of molecular sciences*, 23: 1426.

Pinto-Ferreira, Fernanda, Eloiza Teles Caldart, Aline Kuhn Sbruzzi Pasquali, Regina Mitsuka-Breganó, Roberta Lemos Freire, and Italmar Teodorico Navarro. 2019. 'Patterns of transmission and sources of infection in outbreaks of human toxoplasmosis', *Emerging infectious diseases*, 25: 2177.

Pollard, Thomas D, and John A Cooper. 2009. 'Actin, a central player in cell shape and movement', *Science*, 326: 1208-12.

Portes, Juliana, Emile Barrias, Renata Travassos, Márcia Attias, and Wanderley de Souza. 2020. 'Toxoplasma gondii mechanisms of entry into host cells', *Frontiers in cellular and infection microbiology*, 10: 294.

Porto, AM, MM Amorim, IC Coelho, and Luiz Carlos Santos. 2008. 'Serologic profile of toxoplasmosis in pregnant women attended at a teaching-hospital in Recife', *Revista da Associacao Medica Brasileira (1992)*, 54: 242-48.

Pospich, Sabrina, Esa-Pekka Kumpula, Julian von der Ecken, Juha Vahokoski, Inari Kursula, and Stefan Raunser. 2017. 'Near-atomic structure of jasplakinolide-stabilized malaria parasite F-actin reveals the structural basis of filament instability', *Proceedings of the National Academy of Sciences*, 114: 10636-41.

Poulin, Robert. 2007. 'Evolutionary Ecology of Parasites', *Springer Netherlands*, 15: 342.

Pražák, Vojtech, Daven Vasishtan, Kay Grünewald, Ross G Douglas, and Josie L Ferreira. 2024. 'Molecular architecture of glideosome and nuclear F-actin in Plasmodium falciparum', *bioRxiv*: 2024.04. 22.590301.

Pruyne, David, Marie Evangelista, Changsong Yang, Erfei Bi, Sally Zigmond, Anthony Bretscher, and Charles Boone. 2002. 'Role of formins in actin assembly: nucleation and barbed-end association', *Science*, 297: 612-15.

Radke, Jay R, Boris Striepen, Michael N Guerini, Maria E Jerome, David S Roos, and Michael W White. 2001. 'Defining the cell cycle for the tachyzoite stage of Toxoplasma gondii', *Molecular and biochemical parasitology*, 115: 165-75.

Radke, Jay R, and Michael W White. 1998. 'A cell cycle model for the tachyzoite of Toxoplasma gondii using the Herpes simplex virus thymidine kinase', *Molecular and biochemical parasitology*, 94: 237-47.

Ren, Bingjian, Romuald Haase, Sharon Patray, Quynh Nguyen, Bohumil Maco, Nicolas Dos Santos Pacheco, Yi-Wei Chang, and Dominique Soldati-Favre. 2024. 'Architecture of the Toxoplasma gondii apical polar ring and its role in gliding motility and invasion', *Proceedings of the National Academy of Sciences*, 121: e2416602121.

Robert-Gangneux, Florence, and Marie-Laure Dardé. 2012. 'Epidemiology of and diagnostic strategies for toxoplasmosis', *Clinical microbiology reviews*, 25: 264-96.

Robert-Paganin, Julien, James P Robblee, Daniel Auguin, Thomas CA Blake, Carol S Bookwalter, Elena B Krementsova, Dihia Moussaoui, Michael J Previs, Guillaume Jousset, and Jake Baum. 2019. 'Plasmodium myosin A drives parasite invasion by an atypical force generating mechanism', *Nature communications*, 10: 3286.

Rodier, MH, J Berthonneau, A Bourgoin, G Giraudeau, G Agius, C Burucoa, A Hekpazo, and JL Jacquemin. 1995. 'Seroprevalences of Toxoplasma, malaria,

rubella, cytomegalovirus, HIV and treponemal infections among pregnant women in Cotonou, Republic of Benin', *Acta tropica*, 59: 271-77.

Roth, JURGEN, MOISE Bendayan, and LELIO Orci. 1978. 'Ultrastructural localization of intracellular antigens by the use of protein A-gold complex', *Journal of Histochemistry & Cytochemistry*, 26: 1074-81.

Rugarabamu, George, Jean-Baptiste Marq, Amandine Guérin, Maryse Lebrun, and Dominique Soldati-Favre. 2015. 'Distinct contribution of T oxoplasma gondii rhomboid proteases 4 and 5 to micronemal protein protease 1 activity during invasion', *Molecular microbiology*, 97: 244-62.

Rust, Michael J, Mark Bates, and Xiaowei Zhuang. 2006. 'Sub-diffraction-limit imaging by stochastic optical reconstruction microscopy (STORM)', *Nature methods*, 3: 793-96.

Sabin, Albert B, and Harry A Feldman. 1948. 'Dyes as microchemical indicators of a new immunity phenomenon affecting a protozoon parasite (Toxoplasma)', *Science*, 108: 660-63.

Sahl, Steffen J, Stefan W Hell, and Stefan Jakobs. 2017. 'Fluorescence nanoscopy in cell biology', *Nature reviews Molecular cell biology*, 18: 685-701.

Sahoo, Nivedita, Wandy Beatty, John Heuser, David Sept, and L David Sibley. 2006. 'Unusual kinetic and structural properties control rapid assembly and turnover of actin in the parasite Toxoplasma gondii', *Molecular biology of the cell*, 17: 895-906.

Saibil, Helen R. 2022. 'Cryo-EM in molecular and cellular biology', *Molecular cell*, 82: 274-84.

Sanchez, Syrian G, and Sébastien Besteiro. 2021. 'The pathogenicity and virulence of Toxoplasma gondii', *Virulence*, 12: 3095-114.

Sander, J. D., and J. K. Joung. 2014. 'CRISPR-Cas systems for editing, regulating and targeting genomes', *Nat Biotechnol*, 32: 347-55.

Sato, Aya, Berith Isaac, Carolyn M Phillips, Regina Rillo, Peter M Carlton, David J Wynne, Roshni A Kasad, and Abby F Dernburg. 2009. 'Cytoskeletal forces span the nuclear envelope to coordinate meiotic chromosome pairing and synapsis', *Cell*, 139: 907-19.

Sato, Shigeharu. 2011. 'The apicomplexan plastid and its evolution', *Cellular & Molecular Life Sciences Cmls*, 68: 1285-96.

Sattler, Julia Magdalena, Markus Ganter, Marion Hliscs, Kai Matuschewski, and Herwig Schüler. 2011. 'Actin regulation in the malaria parasite', *European journal of cell biology*, 90: 966-71.

Sauer, Brian. 1987. 'Functional expression of the cre-lox site-specific recombination system in the yeast Saccharomyces cerevisiae', *Molecular and cellular biology*.

Sauer, Brian, and Nancy Henderson. 1988. 'Site-specific DNA recombination in mammalian cells by the Cre recombinase of bacteriophage P1', *Proceedings of the National Academy of Sciences*, 85: 5166-70.

Schatten, Heide, L David Sibley, and Hans Ris. 2003. 'Structural evidence for actin-like filaments in Toxoplasma gondii using high-resolution low-voltage field emission scanning electron microscopy', *Microscopy and Microanalysis*, 9: 330-35.

Schermelleh, Lothar, Peter M Carlton, Sebastian Haase, Lin Shao, Lukman Winoto, Peter Kner, Brian Burke, M Cristina Cardoso, David A Agard, and Mats GL Gustafsson. 2008. 'Subdiffraction multicolor imaging of the nuclear periphery with 3D structured illumination microscopy', *Science*, 320: 1332-36.

Schermelleh, Lothar, Alexia Ferrand, Thomas Huser, Christian Eggeling, Markus Sauer, Oliver Biehlmaier, and Gregor PC Drummen. 2019. 'Super-resolution microscopy demystified', *Nature cell biology*, 21: 72-84.

Schindelin, Johannes, Ignacio Arganda-Carreras, Erwin Frise, Verena Kaynig, Mark Longair, Tobias Pietzsch, Stephan Preibisch, Curtis Rueden, Stephan Saalfeld, and Benjamin Schmid. 2012. 'Fiji: an open-source platform for biological-image analysis', *Nature methods*, 9: 676-82.

Schnell, Ulrike, Freark Dijk, Klaas A Sjollema, and Ben NG Giepmans. 2012. 'Immunolabeling artifacts and the need for live-cell imaging', *Nature methods*, 9: 152-58.

Schultz, Aric J, and Vern B Carruthers. 2018. 'Toxoplasma gondii LCAT primarily contributes to tachyzoite egress', *Msphere*, 3: 10.1128/mspheredirect. 00073-18.

Shaner, Nathan C, George H Patterson, and Michael W Davidson. 2007. 'Advances in fluorescent protein technology', *Journal of cell science*, 120: 4247-60.

Sheffield, Harley G, and Marjorie L Melton. 1968. 'The fine structure and reproduction of Toxoplasma gondii', *The Journal of parasitology*: 209-26.

———. 1970. 'Toxoplasma gondii: the oocyst, sporozoite, and infection of cultured cells', *Science*, 167: 892-93.

Shen, Bang, Kevin M Brown, Tobie D Lee, and L David Sibley. 2014. 'Efficient gene disruption in diverse strains of Toxoplasma gondii using CRISPR/CAS9', *Mbio*, 5: 10.1128/mbio. 01114-14.

Shen, Bang, Jeffrey S Buguliskis, Tobie D Lee, and L David Sibley. 2014. 'Functional analysis of rhomboid proteases during Toxoplasma invasion', *Mbio*, 5: 10.1128/mbio. 01795-14.

Sibley, L David. 2010. 'How apicomplexan parasites move in and out of cells', *Current opinion in biotechnology*, 21: 592-98.

Sibley, LD. 2004. 'Intracellular parasite invasion strategies', *Science*, 304: 248-53.

Skillman, Kristen M, Karthikeyan Diraviyam, Asis Khan, Keliang Tang, David Sept, and L David Sibley. 2011. 'Evolutionarily divergent, unstable filamentous actin is essential for gliding motility in apicomplexan parasites', *PLoS pathogens*, 7: e1002280.

Skotarczak, Bogumiła. 2016. 'The role of ticks in transmission cycle of Toxoplasma gondii', *Annals of Parasitology*, 62.

Slot, Jan W, and Hans J Geuze. 1981. 'Sizing of protein A-colloidal gold probes for immunoelectron microscopy', *The Journal of cell biology*, 90: 533-36.

———. 2007. 'Cryosectioning and immunolabeling', *Nature protocols*, 2: 2480-91.

Soldati, Dominique, Bernardo J Foth, and Alan F Cowman. 2004. 'Molecular and functional aspects of parasite invasion', *Trends in Parasitology*, 20: 567-74.

Soldati, Dominique, Kami Kim, Jennifer Kampmeier, Jean-Francois Dubremetz, and John C Boothroyd. 1995. 'Complementation of a Toxoplasma gondii ROP1 knock-out mutant using phleomycin selection', *Molecular and biochemical parasitology*, 74: 87-97.

Splendore, A. 1908. 'Un nuovo protozoa parassita deconigli incontrato nelle lesioni anatomiche d'une malattia che ricorda in molti punti il Kala-azar dell'uoma. Nota preliminare pel', *Rev Soc Sci Sao Paulo*, 3: 109-12.

Stadler, Rachel V, Shane R Nelson, David M Warshaw, and Gary E Ward. 2022. 'A circular zone of attachment to the extracellular matrix provides directionality to the motility of Toxoplasma gondii in 3D', *Elife*, 11: e85171.

Starr, Daniel A, and Min Han. 2002. 'Role of ANC-1 in tethering nuclei to the actin cytoskeleton', *Science*, 298: 406-09.

Stelzer, S, W Basso, J Benavides Silván, Luis M Ortega-Mora, P Maksimov, J Gethmann, FJ Conraths, and G Schares. 2019. 'Toxoplasma gondii infection and toxoplasmosis in farm animals: Risk factors and economic impact', *Food and waterborne parasitology*, 15: e00037.

Stortz, Johannes Felix, Mario Del Rosario, Mirko Singer, Jonathan M Wilkes, Markus Meissner, and Sujaan Das. 2019. 'Formin-2 drives polymerisation of actin filaments enabling segregation of apicoplasts and cytokinesis in Plasmodium falciparum', *Elife*, 8: e49030.

Striepen, Boris, Michael J Crawford, Michael K Shaw, Lewis G Tilney, Frank Seeber, and David S Roos. 2000. 'The plastid of Toxoplasma gondii is divided by association with the centrosomes', *The Journal of cell biology*, 151: 1423-34.

Striepen, Boris, Carly N Jordan, Sarah Reiff, and Giel G Van Dooren. 2007. 'Building the perfect parasite: cell division in apicomplexa', *PLoS pathogens*, 3: e78.

Suarez, Catherine, Gaëlle Lentini, Raghavendran Ramaswamy, Marjorie Maynadier, Eleonora Aquilini, Laurence Berry-Sterkers, Michael Cipriano, Allan L Chen, Peter Bradley, and Boris Striepen. 2019. 'A lipid-binding

protein mediates rhoptry discharge and invasion in Plasmodium falciparum and Toxoplasma gondii parasites', *Nature communications*, 10: 4041.

Suvorova, Elena S, Maria Francia, Boris Striepen, and Michael W White. 2015. 'A novel bipartite centrosome coordinates the apicomplexan cell cycle', *PLoS biology*, 13: e1002093.

Sweeney, Kristin R, Naomi S Morrissette, Stephanie LaChapelle, and Ira J Blader. 2010. 'Host cell invasion by Toxoplasma gondii is temporally regulated by the host microtubule cytoskeleton', *Eukaryotic cell*, 9: 1680-89.

Tanaka, Masahito, Takeomi Kikuchi, Hiroyuki Uno, Keisuke Okita, Toshiko Kitanishi-Yumura, and Shigehiko Yumura. 2017. 'Turnover and flow of the cell membrane for cell migration', *Scientific reports*, 7: 12970.

Tapley, Erin C, and Daniel A Starr. 2013. 'Connecting the nucleus to the cytoskeleton by SUN–KASH bridges across the nuclear envelope', *Current opinion in cell biology*, 25: 57-62.

Tardieux, Isabelle, and Jake Baum. 2016. 'Reassessing the mechanics of parasite motility and host-cell invasion', *Journal of Cell Biology*, 214: 507-15.

Tenter, Astrid M, Anja R Heckeroth, and Louis M Weiss. 2000. 'Toxoplasma gondii: from animals to humans', *International journal for parasitology*, 30: 1217-58.

Tokuyasu, KT. 1980. 'Immunochemistry on ultrathin frozen sections', *The Histochemical Journal*, 12: 381-403.

Tokuyasu, KTa. 1973. 'A technique for ultracryotomy of cell suspensions and tissues', *The Journal of cell biology*, 57: 551-65.

Tomasina, Ramiro, Fabiana C Gonzalez, Érica S Martins-Duarte, Philippe Bastin, Mathieu Gissot, and María E Francia. 2022. 'Separate to operate: the centriole-free inner core of the centrosome regulates the assembly of the intranuclear spindle in Toxoplasma gondii', *Mbio*, 13: e01859-22.

Tonkin, Michelle L, Magali Roques, Mauld H Lamarque, Martine Pugnière, Dominique Douguet, Joanna Crawford, Maryse Lebrun, and Martin J Boulanger. 2011. 'Host cell invasion by apicomplexan parasites: insights from the co-structure of AMA1 with a RON2 peptide', *Science*, 333: 463-67.

Tosetti, Nicolò, Nicolas Dos Santos Pacheco, Dominique Soldati-Favre, and Damien Jacot. 2019. 'Three F-actin assembly centers regulate organelle inheritance, cell-cell communication and motility in Toxoplasma gondii', *Elife*, 8: e42669.

Truckenbrodt, Sven, Manuel Maidorn, Dagmar Crzan, Hanna Wildhagen, Selda Kabatas, and Silvio O Rizzoli. 2018. 'X10 expansion microscopy enables 25-nm resolution on conventional microscopes', *EMBO reports*, 19: e45836.

Tyler, Jessica S, and John C Boothroyd. 2011. 'The C-terminus of Toxoplasma RON2 provides the crucial link between AMA1 and the host-associated invasion complex', *PLoS pathogens*, 7: e1001282.

Urban, Nicolai T, Katrin I Willig, Stefan W Hell, and U Valentin Nägerl. 2011. 'STED nanoscopy of actin dynamics in synapses deep inside living brain slices', *Biophysical journal*, 101: 1277-84.

Vahokoski, Juha, Saligram Prabhakar Bhargav, Ambroise Desfosses, Maria Andreadaki, Esa-Pekka Kumpula, Silvia Muñico Martinez, Alexander Ignatev, Simone Lepper, Friedrich Frischknecht, and Inga Siden-Kiamos. 2014. 'Structural differences explain diverse functions of Plasmodium actins', *PLoS pathogens*, 10: e1004091.

Van Poppel, Nicole FJ, Jelle Welagen, Rudy FJJ Duisters, Arno N Vermeulen, and Dick Schaap. 2006. 'Tight control of transcription in Toxoplasma gondii using an alternative tet repressor', *International journal for parasitology*, 36: 443-52.

Van Troys, Marleen, Lynn Huyck, Shirley Leyman, Stien Dhaese, Joël Vandekerkhove, and Christophe Ampe. 2008. 'Ins and outs of ADF/cofilin activity and regulation', *European journal of cell biology*, 87: 649-67.

Vartak, Supriya V, Hassan A Swarup, Vidya Gopalakrishnan, Vindya K Gopinatha, Virginie Ropars, Mridula Nambiar, Franklin John, Sharath Kumar S Kothanahally, Rupa Kumari, and Nitu Kumari. 2018. 'Autocyclized and oxidized forms of SCR 7 induce cancer cell death by inhibiting nonhomologous DNA end joining in a Ligase IV dependent manner', *The FEBS journal*, 285: 3959-76.

Venugopal, Kannan, and Sabrina Marion. 2018. 'Secretory organelle trafficking in Toxoplasma gondii: A long story for a short travel', *International Journal of Medical Microbiology*, 308: 751-60.

Vicidomini, Giuseppe, Gael Moneron, Kyu Y Han, Volker Westphal, Haisen Ta, Matthias Reuss, Johann Engelhardt, Christian Eggeling, and Stefan W Hell. 2011. 'Sharper low-power STED nanoscopy by time gating', *Nature methods*, 8: 571-73.

Vilcinskas, A. 2016. 'The role of epigenetics in host-parasite coevolution: lessons from the model host insects Galleria mellonella and Tribolium castaneum', *Zoology (Jena)*, 119: 273-80.

Wagner, Mirjam. 2023. 'A Potential LINC Complex: The SUN-like Protein TgSLP1 Plays an Essential Role in Cell Division in the Apicomplexan Parasite Toxoplasma Gondii', Universitätsbibliothek der Ludwig-Maximilians-Universität.

Wagner, Mirjam, Yuan Song, Elena Jiménez-Ruiz, Sonja Härtle, and Markus Meissner. 2023. 'The SUN-like protein TgSLP1 is essential for nuclear division in the apicomplexan parasite Toxoplasma gondii', *Journal of cell science*, 136.

Wang, Jin-Lei, Si-Yang Huang, Michael S Behnke, Kai Chen, Bang Shen, and Xing-Quan Zhu. 2016. 'The past, present, and future of genetic manipulation in Toxoplasma gondii', *Trends in Parasitology*, 32: 542-53.

Wang, Shuoshuo, Elizabeth Stoops, Unnikannan Cp, Barak Markus, Adriana Reuveny, Elly Ordan, and Talila Volk. 2018. 'Mechanotransduction via the LINC complex regulates DNA replication in myonuclei', *Journal of Cell Biology*, 217: 2005-18.

Wegel, Eva, Antonia Göhler, B Christoffer Lagerholm, Alan Wainman, Stephan Uphoff, Rainer Kaufmann, and Ian M Dobbie. 2016. 'Imaging cellular structures in super-resolution with SIM, STED and Localisation Microscopy: A practical comparison', *Scientific reports*, 6: 27290.

Weinman, David, and Anne H Chandler. 1954. 'Toxoplasmosis in Swine and Rodents. Reciprocal Oral Infection and Potential Human Hazard', *Proceedings of the Society for Experimental Biology and Medicine*, 87: 211-16.

Wen, Gang, Volker Leen, Taoufik Rohand, Markus Sauer, and Johan Hofkens. 2023. 'Current progress in expansion microscopy: chemical strategies and applications', *Chemical Reviews*, 123: 3299-323.

Wesseling, John G, Mari A Smits, and John GG Schoenmakers. 1988. 'Extremely diverged actin proteins in Plasmodium falciparum', *Molecular and biochemical parasitology*, 30: 143-53.

Wetzel, DM, S Håkansson, K Hu, D Roos, and LD Sibley. 2003. 'Actin filament polymerization regulates gliding motility by apicomplexan parasites', *Molecular biology of the cell*, 14: 396-406.

Whitelaw, Jamie Adam. 2017. 'The dynamic nature and functions of actin in Toxoplasma gondii', University of Glasgow.

Woglar, Alexander, Marie Pierron, Fabian Zacharias Schneider, Keshav Jha, Coralie Busso, and Pierre Gönczy. 2022. 'Molecular architecture of the C. elegans centriole', *PLoS biology*, 20: e3001784.

Wolf, Abner, David Cowen, and Beryl Paige. 1939. 'Human toxoplasmosis: occurrence in infants as an encephalomyelitis verification by transmission to animals', *Science*, 89: 226-27.

Xiao, Jianchun, and Robert H Yolken. 2015. 'Strain hypothesis of Toxoplasma gondii infection on the outcome of human diseases', *Acta physiologica*, 213: 828-45.

Yadav, Vikas, and Kaustuv Sanyal. 2018. 'Sad1 spatiotemporally regulates kinetochore clustering to ensure high-fidelity chromosome segregation in the human fungal pathogen Cryptococcus neoformans', *Msphere*, 3: 10.1128/msphere. 00190-18.

Yasuda, T, K Yagita, T Nakamura, and T Endo. 1988. 'Immunocytochemical localization of actin in Toxoplasma gondii', *Parasitology research*, 75: 107-13.

Yee, Michelle, Tobias Walther, Friedrich Frischknecht, and Ross G Douglas. 2022. 'Divergent Plasmodium actin residues are essential for filament

localization, mosquito salivary gland invasion and malaria transmission', *PLoS pathogens*, 18: e1010779.

Youssefi, MR, AA Sefidgar, A Mostafazadeh, and S Mahdavi Omran. 2007. 'Serologic evaluation of toxoplasmosis in matrimonial women in Babol, Iran', *Pakistan Journal of Biological Sciences: PJBS*, 10: 1550-52.

Zhang, Xiaochang, Kai Lei, Xiaobing Yuan, Xiaohui Wu, Yuan Zhuang, Tian Xu, Rener Xu, and Min Han. 2009. 'SUN1/2 and Syne/Nesprin-1/2 complexes connect centrosome to the nucleus during neurogenesis and neuronal migration in mice', *Neuron*, 64: 173-87.

Zhen, Yen-Yi, Thorsten Libotte, Martina Munck, Angelika A Noegel, and Elena Korenbaum. 2002. 'NUANCE, a giant protein connecting the nucleus and actin cytoskeleton', *Journal of cell science*, 115: 3207-22.

Zhou, Kang, Melissa M Rolls, David H Hall, Christian J Malone, and Wendy Hanna-Rose. 2009. 'A ZYG-12–dynein interaction at the nuclear envelope defines cytoskeletal architecture in the C. elegans gonad', *Journal of Cell Biology*, 186: 229-41.

Zwettler, Fabian U, Sebastian Reinhard, Davide Gambarotto, Toby DM Bell, Virginie Hamel, Paul Guichard, and Markus Sauer. 2020. 'Molecular resolution imaging by post-labeling expansion single-molecule localization microscopy (Ex-SMLM)', *Nature communications*, 11: 3388.

9 Acknowledgement

Studying abroad alone as a PhD is not an easy thing. Therefore, I would like to sincerely thank all my supervisors, colleagues, family members and friends who have given me support and help in my studies and life. Without you, I wouldn't be who I am now.

I am very grateful to Prof. Dr. Markus Meissner for offering me the opportunity to work and study in experimental parasitology. He is a respectable scientist with profound knowledge and novel ideas; he is a responsible supervisor who pays attention to every subject and gives students ample learning opportunities, encouragement and financial support; he is also a kind person, full of humor (although sometimes dry humor), and treats everyone equally. I benefited a lot from working with him.

Many thanks to Dr. Francisco Javier Coloma Periz for supervising me in my daily work. He is a very dedicated and serious researcher, involved in many research projects and has been committed to applying new research techniques. He is a very responsible supervisor; no matter how stupid my questions were, he taught me patiently and helped me to solve my problems. He played a great role in my transformation from a novice with weak foundation to an almost qualified doctoral student.

Thanks to Dr. Elena Jiménez-Ruiz and Dr. Simon Gras, who always offer advice and help to everyone and take on lab responsibilities like sorting. Thanks to Dr. Wei Li and Dr. Miriam Rafajlovic who not only help me with experiments, but also cares about me in life from beginning to end. Thanks Dr. Mirko Singer and Dr. Sujaan Das, although I haven't been with you for a long time, they are excellent scientist worth learning from; in particular, Mirko’s ‘100,000 questions’ at the lab meeting are still fresh in my memory.

ACKNOWLEDGEMENT

Thanks to all my colleague in experimental parasitology. Thanks to PeiPei Qin, Janessa Grech, Mirjam Wagner, Matthew Gow, Julia von Knoerzer-Suckow, Maresa Watzlowik, Ella Schadt, Thrishla Kumar, Catherine Graue and Vitoria Catschor dos Santos, they are very friendly and nice persons, and I am really happy to have them here.

Thanks to Marzena Broniszewska for management of the laboratory. Thanks to Angelika Derschum and Adelheid Ackermann for all the administrative work. Thanks to Kathrin Simon for the waste disposal.

Thanks for salary supporting from China Scholarship Council (CSC) and the help of embassy staff. This allows Chinese students like me to study abroad.

Many thanks to my parents Feng Liu and Weijun Song. Although we are more than 8,000 kilometers apart, you will always be my strongest support. Thanks my dearest friends Jiaqi Jiang, Meng Lv, Yijing Qu, Zhen Wang, Jiaming Dan and Wei Wei. Love overcomes all difficulties and will last forever.

Thanks to Dr. Francisco Javier Periz Coloma and Dr. Whitelaw Jamie Adam again for the (un)published figures and schematics that been cited in this thesis.

As a non-native English speaker, I hereby declare that this thesis was written by myself, but an artificial intelligence tool was used to polish and correct the grammar and spelling issues of the article.